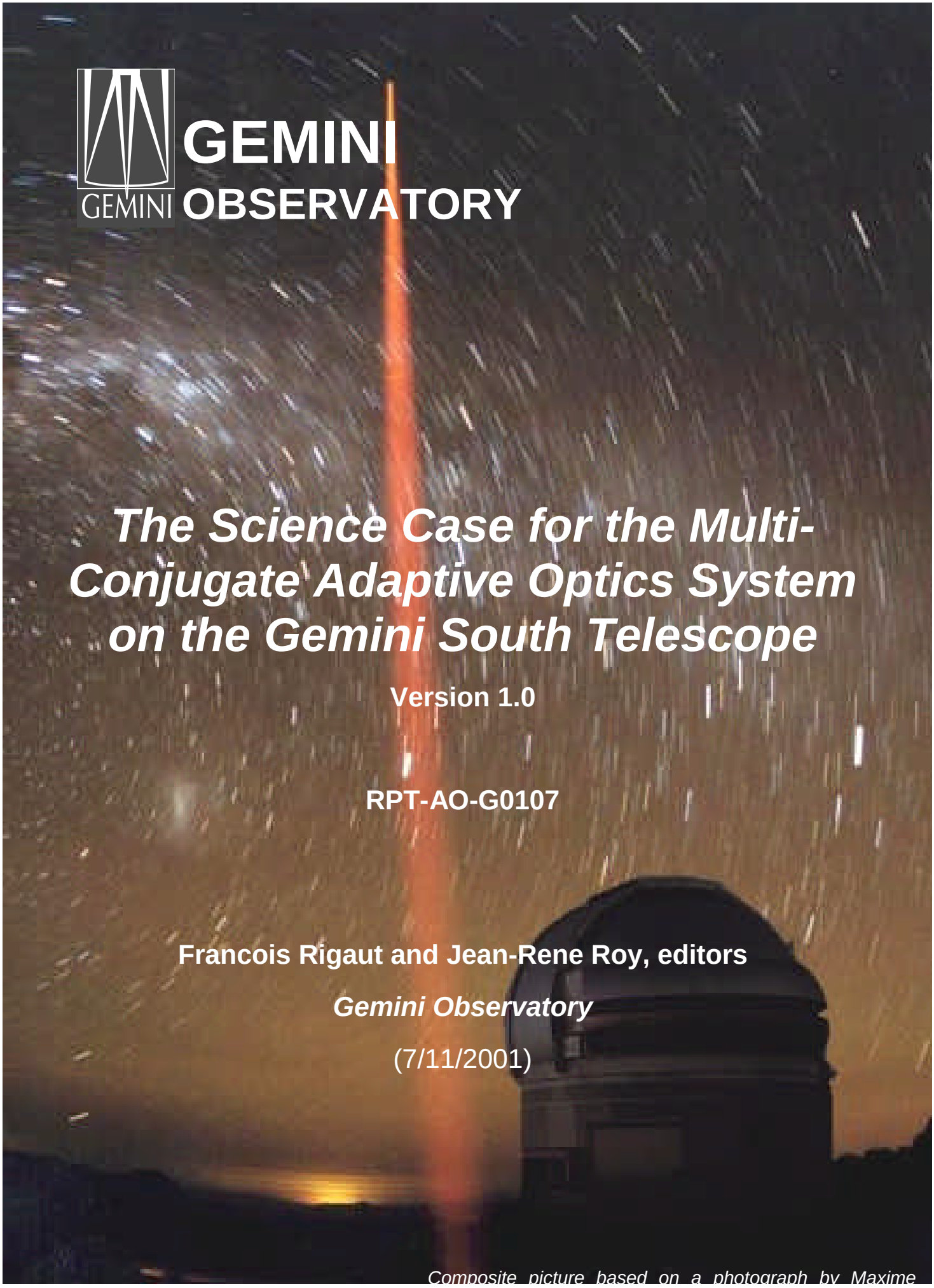

GEMINI OBSERVATORY

The Science Case for the Multi-Conjugate Adaptive Optics System on the Gemini South Telescope

Version 1.0

RPT-AO-G0107

Francois Rigaut and Jean-Rene Roy, editors

Gemini Observatory

(7/11/2001)

Composite picture based on a photograph by Maxime

Foreword

The Science Case for Multi-Conjugate Adaptive Optics on the Gemini South Telescope is a document presenting the range of science that will be enabled once an innovative and powerful adaptive optics system is implemented on the Gemini South Telescope. This text not only offers a description of the advantages that exquisite image quality over a field of view of 2 arcminutes provided by MCAO technology will give, but also presents several programs of research that the astronomers of the Gemini communities intend to carry out once the MCAO system is in place.

The MCAO Science Case is the work of many astronomers from all the Gemini communities. It is the product of many discussions and exchanges, repeated calculations, and countless modeling runs on computers. These fed into a successful workshop that brought together 45 astronomers at the Center for Adaptive Optics in October 2000 to discuss MCAO and its potential.

Many individuals have contributed to refining the MCAO science case, and several participants of the workshop produced written MCAO "proposals". However, the completion of this MCAO Science Case document would not have been possible without the help of key individuals. We wish to thank in particular Simon Morris (Herzberg Institute of Astrophysics and Durham University) and Patrick Roche (Oxford University) for their enthusiastic commitment and relentless efforts in helping us to put together the main elements of the MCAO Science Case document. We also thank Ivan Baldry (Anglo-Australian Observatory), Chip Kobulnicky (University of Wisconsin) and Eric Steinbring (Center for Adaptive Optics) who provided key quantitative inputs through the entire process. Andre Gehz (UCLA), Inger Jorgensen (Gemini Observatory) and Roger Davies (University of Durham) have made many helpful comments on an earlier draft version of this document.

The MCAO Science Case is a work in progress. This text must be viewed as a live document. The present document is an upgraded version from the science cases presented at the MCAO Conceptual Design Review in May 2000. In the same vein, we plan to review and to revise the present version following the MCAO Preliminary Design Review and the assessment by the Gemini Science Committee and the Gemini Board, which will take place later this year. The aim is to use each step to develop a stronger science case. The next edition will include detailed feasibility studies for the various scientific programs proposed here, with target selection and field centering done taking into account the availability and properties of tip/tilt stars in each science field. We wish to get as close as possible to a set of true MCAO proposals for Gemini South.

The organization of the MCAO Science Case is as follows. Chapter One is an introduction to the science context in which MCAO emerged; this chapter sets out the thinking process leading to the definition of a fully developed science case. Chapter Two presents the limitations of "classical" adaptive optics, i.e. the technique of using only one guide star, natural or laser; the principles of MCAO are then reviewed in the context of the key advantages over the classical approach. The science case for MCAO is developed in the successive chapters. Chapter Three is devoted to a single

astrophysical theme: the exploration of the distribution of stellar masses in the Milky Way and its evolution through time and as a function of environment. Chapter Four discusses several observing programs on nearby galaxies to be conducted with MCAO. Chapter Five is a detailed assessment of the research aiming at understanding the formation and early evolution of galaxies by the study of the structure, dynamics and chemistry of distant galaxies as enabled by MCAO imaging and spectroscopy.

The MCAO program is supported by the Gemini Observatory, which is operated by the Association of Universities for Research in Astronomy, Inc. under a cooperative agreement with the NSF on behalf of the Gemini partnership: the National Science Foundation (United States), the Particle Physics and Astronomy Research Council (United Kingdom), the National Research Council (Canada), CONICYT (Chile), the Australian National Research Council (Australian), CNPq (Brazil) and CONICET (Argentina).

Jean-Rene Roy

Associate Director Gemini North

Francois Rigaut

Gemini Adaptive Optics Program Scientist

TABLE OF CONTENTS

CHAPTER 1

INTRODUCTION

1.1 An historical perspective

The history of astronomy is a fascinating record of the fruitful alliance between contemporary technologies and the minds of astronomers of all epochs to better understand the universe. This story dates back to the Stone Age where our prehistoric ancestors started following the cyclical motions of the brighter heavenly bodies and used animal bones as calculators for recording natural phenomena (Marshak 1971). The megalithic monuments of Western Europe, Stonehenge and Callanish for example, represent a heroic achievement of prehistoric technology and science. The next step came with Greek science when powerful new mathematical and practical tools were invented to measure the size of the Earth and the distances to the Moon and the Sun; this brilliant epoch in the history of civilization reached its apogee in the few centuries after 600 B.C. Islamic scientists astronomers expanded this fine tradition of measurements much further with a more systematic approach to fulfill the needs of navigation and time keeping during the first centuries of the 2nd millennium. Not only did they devised a sophisticated mathematical framework, but they also designed and built a whole range of instruments to measure time, angles and distances exploiting the best precision achievable with the human eye, an effort that culminated in the remarkable observatory, institute and research enterprise of Tycho Brahe at Uranienborg on the island of Hven in Renaissance Denmark in the late 16th century.

Then from the early 1600 to the present day, three major revolutions marked the history of optical astronomy. The first one, as we all well know took place, in 1609: Galileo Galilei, following up on ideas of the Dutch optician Hans Lippershey, built the first telescope to reveal stunning new views of our Moon, Sun, planets and Milky Way. The second revolution happened at the end of the 19th and through the 20th centuries: it was the development of powerful new detectors that multiplied our efficiencies at gathering light by factors of hundreds and thousands, starting from the primitive photographic plates of a hundred years ago to the superbly performing arrays of CCDs of today delivering quantum efficiencies close to 100%. The third revolution, we claim, is adaptive optics, the technology for correcting in real time wavefront distortions introduced by the earth's atmosphere (Tyson 1991; Hardy 1998; Roddier 1999). Adaptive optics works best in the near-infrared domain (0.8 to 3 microns), where it can provide diffraction limited images. Originally proposed by Horace W. Babcock (1953), the first trials on telescopes started only in the 1970's and the first common users systems were implemented at ESO and the CFHT in the early 1990s. For example, the systems now used on the Gemini North and the Keck telescopes deliver images comparable or finer than WFPC2 and NICMOS on the Hubble Space Telescope. This achievement is stunning.

AO offers a tremendous science potential, especially when building and implementation costs of a ground-based system are compared to investments for a space facility. Although the scientific exploitation of AO corrected images is limited now to regions relatively close to bright reference

objects (V < 17) and fields of view of about 10-20 arcsec, the possibility of doing sub-arcsec astrophysics with the ground-based telescopes is triggering a change of paradigm in our approach of observing from the ground. The AO capability is only now fully being implemented on telescopes with the completion of the first generation of instruments to be fed by AO systems.

The full potential of adaptive optics will be realized with Multi-conjugate Adaptive Optics, a technology allowing tomographic evaluation of the whole column of atmosphere through which the light traveled, and which will produce high and stable Strehl ratios over fields of several arcmin (cf. Chapter Two). Furthermore, the use of a small constellation of laser guide stars across the field of view will eliminate most of the cone effects and will increase the sky coverage by an order of magnitude.

The Gemini Observatory is proposing to build a MCAO system for the Gemini South Telescope on Cerro Pachon in Chile. The design and building of a MCAO system is one of the boldest enterprises of contemporary ground-based astronomy. It is mobilizing the efforts of important segments of the international laser community to develop a Sodium laser delivering sufficient power to the 90 km sodium atom layer, and to design the challenging opto-mechanical module with its complex control systems.

In this document, we present the Science Case for MCAO. This multi million dollars program is a non-conventional approach to dramatically improve telescope performance in order to achieve our science goals. Not surprisingly, it presents some risks. Also the decision to invest large amount of resources to develop MCAO may mean that these resources will not be available to build two or three more conventional instruments. A choice is to be made between the science programs that we wish to pursue with Gemini South. In the light of the competition with other large ground-based telescopes and with new capabilities in space (SIRTF, SOFIA and NGST), one must try to exploit the niches where we can deliver the most rapidly the most important science with the best investing strategy of money and human resources. Our purpose is to show that the science that MCAO will allow us to do on the Gemini South Telescope in 2005 and later is unique.

Following the April 1999 Hilo Workshop on the Cerro Pachon Adaptive Optics capability, the Gemini AO team, in close consultation with the Gemini Project Scientists Team, the Instrumentation Forum and the Gemini Science Committee put together a four phase Adaptive Optics Program for the Gemini Telescopes:

1. Providing diffraction limited imaging by the implementation of early Adaptive Optics capability, using the University of Hawaii Hokupa'a/Quirc system on Gemini North until the facility AO system, Altair, becomes available in mid 2002. Altair, an altitude conjugate AO system will then replace Hokupa'a-36 and be capable of feeding all Gemini instruments on the Mauna Kea Telescope.
2. Increasing sky coverage for AO imaging by upgrading the Altair AO system with a 10 W Laser Guide star mounted on the MK Gemini Telescope.
3. Implementing AO on Gemini South to increase sky coverage by giving access to the southern hemisphere. A first step of this effort may include an upgraded Hokupa'a (85

correction elements, instead of 36), together with an experimental low-power off-the-shelf laser guide star capability for early use at Cerro Pachon.

4. Increasing the corrected AO field size to ~2 arcmin with an advanced Multi-Conjugate Adaptive Optics System for Cerro Pachon.

Already, we have seen the resolving power of modern 8 - 10 m telescopes increased by a factor of 10 with the use of adaptive optics systems. However, both natural guide star AO systems or the more complex "all-sky" laser guide star systems are still limited in field of view, which limits their science applications. The typical corrected field of view[1] in J band for a high-order AO system like Keck II is about 20'' in radius. The gain of MCAO over classical adaptive optics is quite dramatic as the simulation in Figure 1.1 illustrates.

1.1.1 MCAO as part of the Gemini Development program

The Gemini South Telescope equipped with multiconjugate adaptive optics can lead ground-based astronomy into the next decades with unmatched capabilities for its community years before the launch of NGST and, importantly, positions Gemini to be an ideal spectroscopic complement for it. Furthermore, the knowledge learned in implementing this multiconjugate adaptive optics is a crucial step to the next generation of extremely large (30 m and more) ground-based telescopes.

With MCAO technology and before NGST, the power of an 8 m telescope with low infrared background that can image near diffraction limited fields ~2 arcmin across will be realized. What are the drivers for a multi-conjugate adaptive optics system on a ground-based telescope?

1.1.1.1 MCAO Gives the Gemini Community Early Access to NGST-Type Science

Gemini-South is one of the latest large telescopes to have its adaptive optics systems defined. A summary of the adaptive optics capabilities that will become available in the next five years is listed in Table 1.1. It is evident that by the time the system is implemented, high-Strehl adaptive optics systems will be common on large telescopes. In the ~10 year time frame, Gemini will compete with the large optical interferometers and NGST. The VLTI, Keck, and LBT interferometers will obtain greater angular resolutions although with a limited sensitivity and field. NGST will dramatically outperform ground-based telescopes in IR wavelengths ($\lambda \geq 10$ μm) due to the decrease in sky brightness. However, at near-infrared wavelengths, ground-based observatories remain competitive when working at resolutions sufficient to work between OH lines. In this regime Gemini can, with an MCAO system, exploit the diffraction-limited resolutions over a similar field size as NGST with a multi-object spectrograph. This should give Gemini a 5 year advantage if the MCAO system and a multi-object spectrograph are delivered in the expected time frame, during which Gemini, equipped with an MCAO system and proper instrumentation (IRMOS, multiple IFUs and/or an imager) will produce NGST-type science.

[1] Here the corrected field-of-view is defined as the field angle at which the Strehl drops by a factor of 2 due to angular anisoplanatism.

Even after the successful launch of NGST, science programs requiring high spectral resolutions (R>10,000) are likely to remain limited to the ground (see Figure 1.2).

1.1.1.2 MCAO provides a natural intermediate step between current ground based facilities and 30 - 100 m class telescopes.

Telescopes as large as 30 - 100 m need very high order multiconjugate AO systems. The Gemini MCAO will prove the concept and allow smoother transition into the 30 – 100 m telescope era.

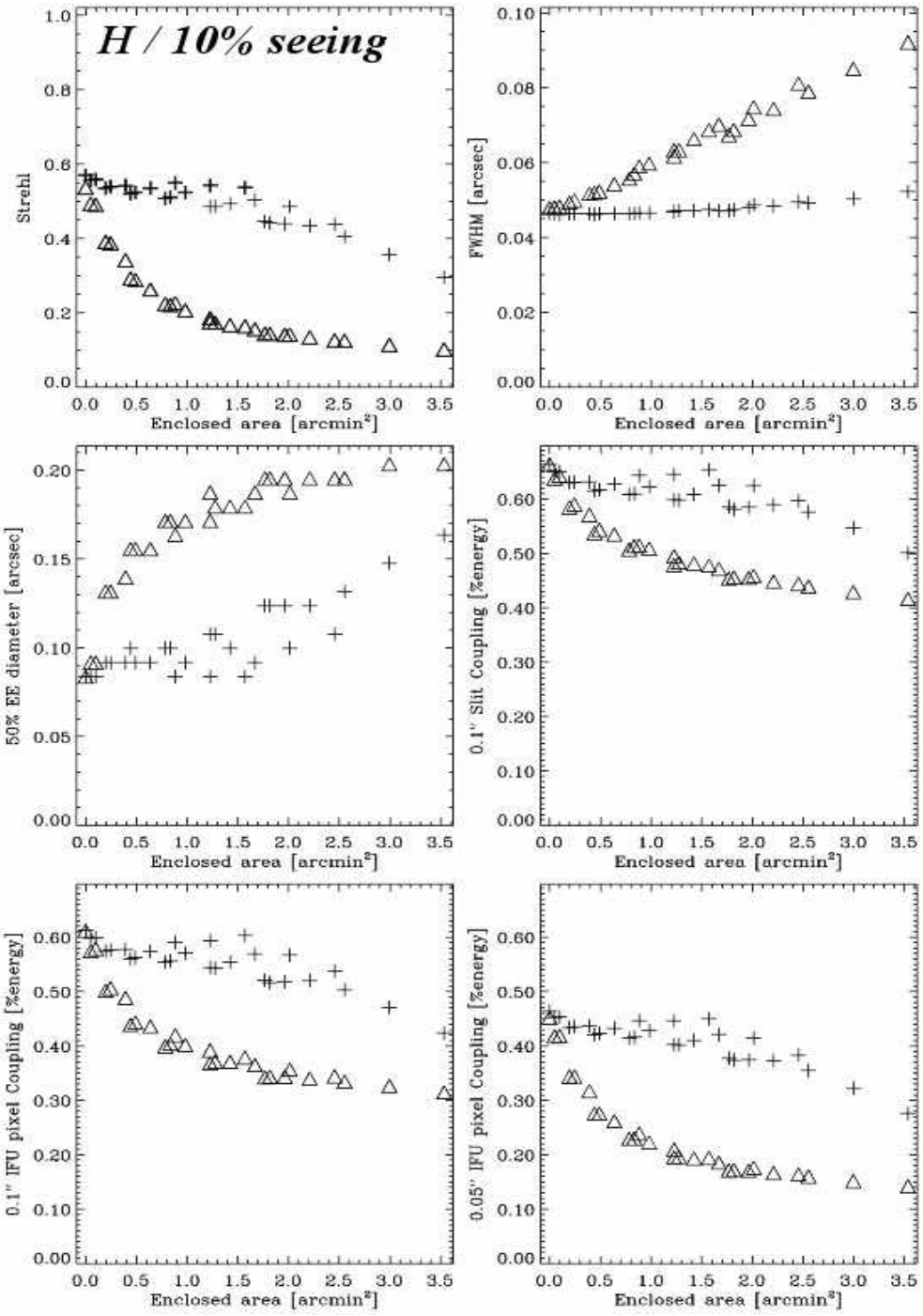

Facility	AOS	Schedule (tentative)	$SR_{2.2mm}$	Limiting Magnitude	2.2 mm Sky Cov.[2]	Focal-plane Instruments (Schedule)
Keck-II	Keck II AO Facility	NGS: Now LGS: 2000	0.8	NGS: 13 LGS: 18	0.4% 19%	NIRC2 (Now) (1024^2 InSb) NIRSPEC (Now) (1024^2 InSb, R-2000-25000)
Gemini-N	Hokupaa 36-element CS	NGS: Now	0.3	NGS: 16	2%	QUIRC (Now) (1024^2 HgCdTe)
Subaru	37-element CS	NGS: 2000?	0.3	NGS: 16	2%	CIAO (?) (Coronographic Imager) IRCS (?) (Spectrograph)
MMT	adaptive M2	NGS: 2000 LGS:?	0.7	NGS:~13 LGS:17-18	0.4% 19%	?
VLT	NAOS	NGS: 2001 LGS: 2003?	0.7	NGS: ~13	0.4%	CONICA (1999) (1024^2 InSb)
Gemini-N	Altair	NGS: 2001 LGS: 2002	0.65	NGS: 13 LGS: 18	1.5% 19%	NIRI (2000) GNIRS (2002/3)
VLT	MACAO 36-element CS	NGS: 2002	0.3	NGS: 16	2%	SINFONI (2001) (IFU spectrograph)
LBT	adaptive M2?	2002-2003	?	?	?	?
Gemini-S	MCAO	End of 2005	0.8	LGS: 18/20	50%	IRMOS (2003) Deployable IFUs (?)

Fig. 1.1. Comparison of H-band performance of classical AO and MCAO for 10 percentile seeing.

Table 1.1 - Summary of Adaptive Optics Facilities on 8-10 m telescopes

1.2 Implementation of the Gemini Observatory Science Plan

To undertake a Science Program exemplified by the three selected science themes described in this document, Gemini is developing with its broad community a comprehensive science and instrumentation development plan.

[2] Sky coverage is the percentage of the sky in which one would achieve 'high' performance from the AOS. The Galactic models of Bahcall and Soneira (1984) were used for the North Galactic Pole. The guide star-science target separation is taken to be 30'' in the NGS case and 60'' in the LGS case. Note that in the case of Altair-NGS the allowable separation was increased by a factor of 2 (diameter) to account for its altitude conjugated design.

MCAO is a key element of this program. We will need a new imager and a wide field infrared spectrograph to fully exploit the one to 2 arcmin field corrected by MCAO.

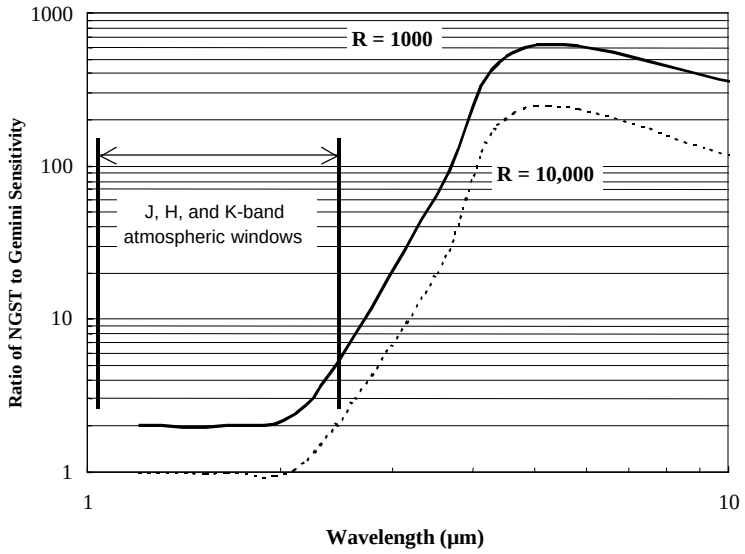

Fig. 1.2 – Relative signal to noise of NGST/Gemini assuming a signal to noise ratio of 10 and 4000 sec integrations on a point source. This comparison assumes moderate adaptive optics compensation, operation between OH emission lines, and spectral resolutions of R=1000 and R=10,000, as denoted on the plot. Note how sensitivity Gemini is expected to be compared to NGST in the astrophysically important 1 – 2.5 µm atmospheric windows.

To define the science goals that will be pursued with this increased AO capability, the Gemini Observatory organized a MCAO Science Workshop in the autumn 2000, with the co-sponsorship of the Center for Adaptive Optics, following the recommendations of the Gemini Science Committee, the Project Scientists team and of the Instrumentation Forum.

1.3 Goals of the Santa Cruz MCAO Science Case Workshop

The goal of this workshop was *"to explore the scientific opportunities for MCAO, quantify its advantages over current and planned conventional AO systems for a comprehensive set of science cases, and derive the MCAO instruments requirements".*

1.3.1 Description

To ensure the maximum efficiency in the workshop discussions, the number of participants was restricted to about 45. To make sure that the debates remained focused, the attendees were requested to come to the workshop with science case proposals. The Workshop took place at the Center for Adaptive Optics of the University of California, Santa Cruz, on October 23-25, 2000. About 45 astronomers and engineers from almost every Gemini partner countries participated in the three-day meeting. Most of the discussions took place around the themes of the global star formation history in the Milky Way, nearby galaxies and distant universe. The three teams addressing each one of these themes were coordinated by Pat Roche/Steve Strom (Milky Way), Bob Schommer/Taft Armandroff/Tod Lauer (nearby galaxies) and Simon Morris/Simon Lilly (distant galaxies).

The workshop discussions had been prepared by several weeks of simulations and modeling work by Ivan Baldry/Keith Taylor (Anglo-Australian Observatory), Chip Kobulnicky

(University of Wisconsin) and Eric Steinbring (Center for Adaptive Optics) led by Francois Rigaut and the three teams leaders.

1.3.1.1 Participants

Scientifc Organizing Committee: Francois Rigaut, Jean-Rene Roy, Robert Schommer, Pat Roche, Simon Morris, Taft Armandroff, Steve Strom, Jerry Nelson and Michael Bolte

Local Organizing Ccommittee: Paula Towle, Jennifer Purcell and Michael Bolte

Modelers: Ivan Baldry, Chip Kobulnicky and Eric Steinbring

Workshop participants:

Name	Institute	e-mail	W.Group
Taft Armandroff	NOAO, US	armand@noao.edu	II
Ivan Baldry	AAO, Australia	baldry@aaoepp.aao.gov.au	IV
Michael Bolte	UCSC, US	bolte@ucolick.edu	II
Bernhard Brandl	Cornell, US	brandl@astrosun.tn.corne	II
Julian Christou	UCSC, US	christou@ucolick.edu	IV
Mark Chun	Gemini	mchun@gemini.edu	II,
Gary da Costa	Mount Stromlo, ANU, Australia	gdc@mso.anu.edu.au	II
Tim Davidge	HIA, Canada	Tim.Davidge@nrc.ca	II
Roger Davies	University of Durham, UK	Roger.Davies@durham.ac.u	III
Rene Doyon	University of Montreal, Canada	doyon@astro.umontreal.ed	II
Mike Edmunds	University of Wales, UK	Mike.Edmunds@astro.cf.ac	II
Brent Ellerbroek	Gemini	bellerbroek@gemini.edu	IV
Doug Geisler	University of Conception, Chile	doug@kukita.cfm.educ.cl	II
P. Guhathakurta	UCSC, US	raja@ucolick.edu	III
Peter Hasting	UK	prh@roe.ac.uk	IV
Roger Haynes	AAO, Australia	rh@aaoepp.aao.gov.au	IV
Markus Kissler	ESO, Europe	mkissler@eso.org	II?
Chip Kobulnicky	University of Wisconsin, US	chip@astro.wisc.edu	IV
David Koo	UCSC, US	koo@ucolick.edu	III
Tod Lauer	NOAO, US	tlauer@noao.edu	II
Simon Lilly	HIA, Canada	lilly@astro.utoronto.ca	III
Peter McGregor	Canberra, Australia	peter@mso.anu.edu.au	II
Michael Meyer	University of Arizona, US	mmeyer@as.arizona.edu	I
Joe Miller	UCSC, US	miller@ucolick.edu	III
Dante Minniti	Universitad Catolica, Chile	dante@astro.puc.cl	II
Simon Morris	HIA, Canada	Simon.Morris@nrc.ca	III
Jerry Nelson	UCSC, US	jnelson@ucolick.edu	?
Celine d'Orgeville	Gemini	cdorgeville@gemini.edu	IV
Magnus Paterson	ROE, UK	mjp@roe.ac.uk	IV
Drew Phillips	UCSC, US	phillips@ucolick.edu	II
Phil Puxley	Gemini	ppuxley@gemini.edu	I
A. Quirrenbach	UCSD, US (TBC)	qui@cassir.ucsd.edu	I
Harvey Richer	University of BC, Canada	richer@astro.ubc.ca	I
Doug Richstone	University of Michigan, US	dor@electra.astro.lsa.umich.edu	II
Francois Rigaut	Gemini	frigaut@gemini.edu	IV
Pat Roche	Oxford, UK	pfr@astro.ox.ac.uk	I
Jean-Rene Roy	Gemini	jrroy@gemini.edu	IV
Basilio Santiago	UFRGS, Brasil		II
Ethan Schreier	STScI, US	ejs@stsci.edu	II
Ray Sharples	University of Durham, UK	r.m.sharples@durham.ac.uk	II
Doug Simons	Gemini	dsimons@gemini.edu	I
Eric Steinbring	UCSC, US	steinb@ucolick.edu	IV
Thaisa Storchi-Bergmann	UFRGS, Brasil	thaisa@if.ufrgs.br	III
Keith Taylor	Caltech, US	kt@astro.caltech.edu	?
Gillian Wright	ROE, UK	gsw@roe.ac.uk	III
Howard Yee	University of Toronto, Ca	hyee@astro.utoronto.ca	III

1.4 Perspectives from the MCAO Science Workshop

In the wake of numerous exchanges between the Gemini AO scientists and the team of the Gemini Project Scientists, the Santa Cruz workshop participants were asked to consider their science program in the light of the following MCAO imager and spectrograph basic characteristics.

1.4.1 Reference strawman instrumentation for MCAO

MCAO by itself cannot produce data. It stabilizes the beam and restores the diffraction limit of the telescope. Therefore it has to come with a suite of instruments, designed from requirements derived from the science cases. Efficient utilization of the MCAO system will depend upon the availability of a large field infrared multi-object spectrograph (IRMOS) and a near-IR imager with complementary design characteristics. Both instruments should be matched to the F/32 output beam of the MCAO system, and must provide diffraction-limited image quality over the field of view. Such instruments would yield unique scientific capabilities before the launch of NGST sometimes around 2010. The IRMOS would remain competitive with NGST given sufficient spectral resolution.

1.4.2 Strawman Imager

Wavelength	1 - 2.5 μm
Field	80" x 80"
# pixels	4k x 4k
Sampling	0.02"

In addition, the following is desired:

- Low dark current (small pixels / narrow band imaging)
- Low and well characterized distortion (astrometric applications)
- Low and well characterized image aberrations
- Simple Spectral mode (cost issues)?

This instrument will most probably use bootable 2k x 2k arrays.

Note that this imager is slightly under-sampled in J band, but this is probably acceptable in a spirit of compromise to get the largest field exploitable at the output of MCAO.

1.4.3 Strawman MCAO Spectrograph

The current idea would be to have a multi-slit spectrograph, or more ambitiously, a system of deployable Integral Field Units (15-25), each of them with the following characteristics:

Wavelength	1 - 2.5 μm
Field per IFU	3 - 5"
Spatial sampling	0.1"
Spectral resolution (2 pixels)	5000-10000
Patrol Field	circular 2' diameter

In addition to this multiple IFU spectrograph, FLAMINGO-II, a multi slitlets spectrograph already being designed as a general user cryogenic near infrared spectrograph will be available. The latter will have a field of view of approximately 2.8 arcmin at F/34, which is adequate for MCAO (2 arcmin unvignetted field). The slit width can be as small as 0.1 arcsec.

The detailed science cases are presented in the following chapters. We did not attempt to explore all the programs that would use MCAO. Trade-offs are involved, and we felt that the design and performance of the MCAO and its instruments should be driven by the most significant science.

The imaging sciences cases are very numerous and demonstrate the unique capability of MCAO fed imagers to compete and/or complement the science programs done on space facilities like HST (WFPC2, ACS and NICMOS), SIRTF and SOFIA. In particular, astrometry to an accuracy of 1-2 milliarcsec per year (with observations spread over a few years) over fields of view of ~1 arcmin offers outstanding astrophysical potential to establish the distances to nearby objects, determining stellar system memberships and identifying binary systems.

Multi-object spectroscopy with a slitlet systems (e.g. FLAMINGO II) fed by MCAO can fulfill a broad range of key science objectives for the exploration of substellar objects, dense cluster of stars, various bodies in the Magellanic Clouds and distant galaxies.

Multi-deployable integral fields units (IFUs) are most desirable to determine the spectroscopic properties of distant galaxies (kinematics, metal abundances, star formation rate) and of super stellar clusters (age and chemistry, kinematics).

To put the MCAO capabilities in perspective, we note that the Advanced Camera System on HST will have a field of view of 202'' x 202'' with 0.05'' pixels. The Wide Field Camera 3 (WFC3) is designed to use as much field as possible on HST and will operate over the range 200 nm to 1800 nm. Thus science that needs HST optical may require MCAO infrared mosaicing.

References:

Babcock, H. W. 1953, *PASP*, 65, 229

Hardy, J. W. 1998, *Adaptive Optics for Astronomical Telescopes*, Oxford University Press

Marshak, R. 1971. *The Roots of Civilization*, McGraw-Hill

Roddier, F. 1999, *Adaptive Optics in Astronomy*, Cambridge University Press

Tyson, R.K. 1991, *Principles of Adaptive Optics*, Academic Press Inc.

CHAPTER 2

CLASSICAL AO LIMITATIONS, MCAO PRINCIPLES, AND WHY MCAO IS NEEDED

As a general introduction to multi-conjugate active optics (MCAO), we review the basic AO principles and we show how anisoplanatism affects the off-axis image quality in classical adaptive optics systems which use only one reference guide star to sample the atmosphere turbulence. The principles of MCAO are then presented and the specific parameters of the Gemini MCAO system will be defined.

2.1 Summary

By compensating the atmospheric turbulence in a three dimension (3-D) fashion, MCAO provides a uniform image quality ("diffraction-limited" in the near-IR) over a much wider field than classical AO; the field can reach one to two arcmin in diameter depending on the selected image quality (IQ) criterion. This is particularly important to tackle a number of astrophysical problems that require relatively wide field of view or very accurate photometry. MCAO also solves the cone effect associated with the use of laser guide stars. Furthermore, the average sky coverage in H band is approximately 50% over the whole sky.

2.2 Anisoplanatism, Cone effect and Sky coverage: The plague of Classical AO

Although it is a new technique, AO has been and is continuing to provide a harvest of new scientific results. All the major large telescopes have recognized its unique and innovating value. However, its wider application has been restricted because of several well-identified problems. We review these limitations.

2.1.1 Limited anisoplanatic angle

The wavefront sensors measures the phase perturbations integrated along the line of sight. The atmosphere is three-dimensional, and the perturbations occur everywhere between the telescope and the highest turbulent layers, typically at 10-15 km above any given site. In directions away from the guide star, the integrated phase perturbation differs because the beam is going through another part of the turbulence volume. If the compensation is the best at the guide star ("on-axis"), it degrades as soon as one looks off-axis. Of course, how fast this degradation happens depends on a number of parameters, such as the vertical distribution of turbulence (the so called C_n^2 profile), the wavelength and the order of the AO system (i.e. how many modes are corrected). For low to medium order systems currently in operation, in locations such as the Chilean sites or Mauna Kea, typical values for the isoplanatic angle (defined here as the angle from the guide star at which the Strehl ratio has fallen by 50% with respect to its value at the guide star) are 20" in J band, 30" in H and 40" in K band; this angle gets even smaller for the new

generation of higher order systems on current large telescopes. The isoplanatic angle varies as $\lambda^{1.2}$ and as the airmass$^{1.6}$.

The images below (Fig. 2.1) present an example of anisoplanatism. These two images are extracted from a 35" x 35" K band image taken with the infrared camera KIR and the AO system PUEO at the Canada-France-Hawaii Telescope. They are separated by approximately 30" (center to center). The difference is striking: Airy rings are almost completely gone in the image further away from the guide star; the loss in Strehl is of a factor of 2 (47% left image; 24% right image) and the FWHM goes from 0.140" to 0.185". This is a typical result for an object at airmass = 1.8, for the few period statistics that we have, and illustrates the importance of resolution and Strehl ratio. For this sort of imaging programs (which probably represents most of the stellar population studies), not only is the Strehl ratio important to increase the signal to noise ratio, but also is angular resolution, that plays a crucial role in crowded field.

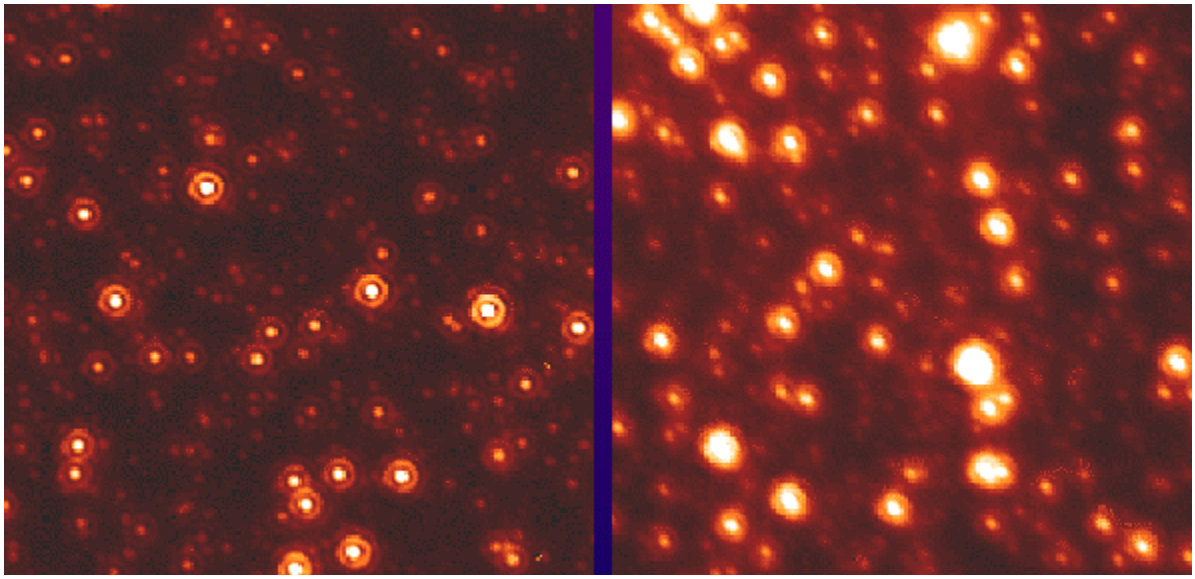

Fig. 2.1. AO images obtained at CFHT with PUEO/KIR illustrating the problem of anisoplanatism. The sub-fields shown are separated by 30" (center to center). Each field is approximately 7"x7".

2.1.2 Sky coverage

AO compensation can solely be obtained in the vicinity of relatively bright stars (R ~ 15). Only 5% of the sky is accessible for diffraction limited imaging with AO while assuming an acceptable degradation of the compensation performance. This severe limitation has led to the idea of using Laser Guide Stars (LGSs). To date, the most promising laser guide star concept uses the fluorescence of sodium atoms in the mesosphere, a layer well known to atmospheric scientists and which lies between 90 and 100 km above see level. This concept has been validated by a few experiments, for example at Calar Alto in Spain and at Lick Observatory, where researchers have achieved closed AO loop imaging using sodium beacons.

2.1.3 Cone effect

However, LGSs do not come without limitations. The major one is that, the source being at a finite range, the return beam does not probe exactly the same volume as the beam coming from an astronomical object at infinity. One can easily visualize that this geometrical effect will be more severe when the telescope diameter increases. Typically, the cone effect induces a Strehl ratio loss of 50% at 1 micron on an 8-m telescope and for a typical Chile or Mauna Kea vertical turbulence profile. This is a major limitation for current large telescope, where it also prevents the extension of laser guide star AO into the visible part of the spectrum. LGS AO, and its large associated increase in sky coverage, remains therefore unachievable with the next generation of giant telescopes, unless the cone effect problem is solved.

2.2 ... and MCAO, the cure

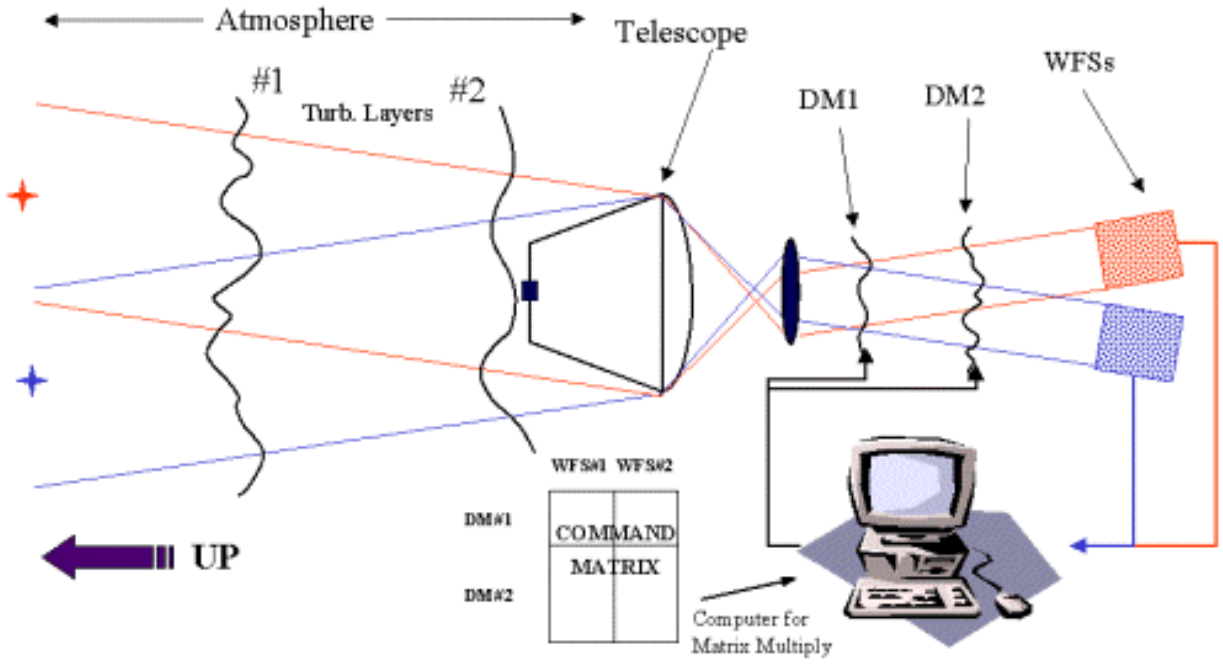

Fig. 2.2. The MCAO concept; see the text for a complete description.

MCAO solves all of the three above limitations. By using several guide stars and several deformable mirrors, image compensation can be achieved uniformly over fields significantly larger than the natural isoplanatic patch. The MCAO technique can use natural or laser guide stars indifferently. The very essence of MCAO - by probing and correcting a large turbulent volume of the atmosphere - also eliminates the cone effect when using *several* laser guide stars. MCAO increases the compensation performance of current 8-m telescopes and opens the full potential of the application of LGS AO on giant telescopes (30-50 m). The wide MCAO field (over ~1 arcmin at the diffraction limit in the current design of the Gemini MCAO) forces us into new scientific territory which the Santa Cruz MCAO Science Case workshop has explored and which is described in the next chapters of this document.

Fig. 2.2 shows a sketch of a MCAO system. Two wavefront sensors (WFSs) are sensing two off-axis guide stars. Perturbations at different altitudes are then seen with different shifts between the two sensors. The information from both sensors is processed by a central processing unit, which feeds them to a reconstructor that computes the command to apply to a set of deformable mirrors which minimize the WFS error signal. The 3D turbulence content is never explicitly reconstructed in this process, avoiding the extreme sensitivity to noise of the latter techniques. MCAO's sensitivity to noise is actually very similar to classical AO; this has the happy consequence that the guide star brightness requirements are the same (i.e. laser power). A collection of more complete articles on the MCAO principles, limitation and performance can be found in the Gemini AO archives for the reader who wishes to explore this in more detail. Table 2.1 lists the main characteristics of the Gemini MCAO system. More details on the instrument itself and on the expected performance are also available on the Gemini web site.

Table 2.1: MCAO System Parameters

DM conjugate ranges	0, 4.5 and 9 km
DM Orders	16, 16 and 8 actuators across the pupil
Guide Star geometry	(0,0) and (+/-42.5,+/-42.5) arcsecs (LGS)
WFS Orders	16 by 16 (LGS); Tip-tilt (NGS)
LGS Laser Power	Equivalent to 125 PDEs/cm2/s at WFS
Launch Telescope	Behind the telescope secondary, 45cm diameter
NGS magnitudes	3 times 19 (for 50% Strehl reduction in H)
Control bandwidths	33Hz (LGS); 0-90Hz (NGS)
Control algorithms	Decoupled control of the LGS and NGS modes

2.3 The Gemini MCAO Performance

The following deals with the performance of the planned Gemini MCAO system, in terms of sensitivities, image quality and sky coverage. Most of these performance metrics are compared to what would be achieved with Classical Laser Guide Star AO (CAO), with a single deformable mirror, wave front sensor and guide star). Some sensitivity comparisons with HST/NICMOS and NGST are also given.

Summary:

- MCAO performance is very uniform over a 1 square arcmin field, both in terms of Strehl ratios and more general PSF characteristics.

- Images are basically diffraction-limited, in term of FWHM, over the full 1 square arcmin field of view, even for the faintest NGS considered here.
- Strehl ratios, under median seeing conditions (r_0=16.5 cm at 550nm), vary from 45% to 80% in the 1-2.5 micron range and 0-30 degrees zenith angles, with relative uniformity (relative Strehl ratio standard deviation) from +/-1.5 to 6%.
- The Strehl ratio degrades "gracefully" outside the 1 square arcmin central field. The useable field with Strehl ratio above 50% of the peak value corresponds to a full 2 arcmin field in H and K bands, and approximately 1.5 arcmin at J.
- Three natural guide stars (NGS) are needed to get the best compensation from the MCAO system. Fortunately, the magnitude limits (R ~ 19) correspond to useful values for sky coverage (~15% at the galactic pole and over 70% at 30^o galactic latitude), even when degrading effects such as sky background noise and windshake jitter are taken into account.
- The overall performance is a weak function of the exact match between the deformable mirror conjugation altitudes and the locations of the dominant turbulent layers.
- Under median seeing conditions, MCAO brings a 1.5 to 1.7 mag sensitivity gain over the 1-2.5 micron range on point sources with respect to seeing limited imaging. Gains with respect to HST/NICMOS, under the same conditions, are 0.3 (J) and 1.2 (K) mag.
- For high spectral resolution spectroscopy, MCAO feeding a spectrograph will have the same sensitivity as NGST, ensuring a competitive niche for this instrument after the NGST launch.
- Multiplex gains with respect to CAO are 10 x to 20 x in spectroscopic coverage.

2.3.1 MCAO Performance

We explore further the MCAO performance in terms of Strehl ratio, PSF behavior across the field, and image motion.

2.3.1.1 Strehl, FWHM and encircled energy versus field of view

The Strehl ratio[3] defines the level of image quality achieved. Hence it will impact the science that we will be able to carry out with instruments fed by the MCAO system.

Under a continuous atmospheric turbulence profile, MCAO significantly reduces, but does not eliminate the effect of anisoplanatism on AO system performance. The mean Strehl ratio decreases with increasing field-of-view, if the guide star and deformable mirror configurations are held constant. The relative variability of the Strehl ratio over the field will also increase. Table 2.2 illustrates these trends as computed for the median Cerro Pachon turbulence profile and the Gemini MCAO baseline wavefront sensor/deformable mirror configuration, but without including the effects of wavefront sensor measurement noise or servo lag. The field of view used for performance evaluation is a square from 51.5 to 68.5 arcsec in width, and the five laser guide

[3] The Strehl ratio is the ratio of the peak intensity of the image to the peak intensity of the airy pattern (both image being normalized in total intensity). A Strehl ratio of 1 means that the image is perfectly diffraction limited.

stars are located at the center and corners of the field. The RMS variability of the Strehl increases fairly rapidly with increasing field-of-view size, approximately by a factor of 1.5 for every increment of 8.5 arcsec of the field. The field-averaged Strehl ratios also begin to degrade more rapidly as the width of the field is pushed beyond 60 arcsec. This reduction in Strehl takes place across the entire field and is not restricted to the edges. All these effects become somewhat more

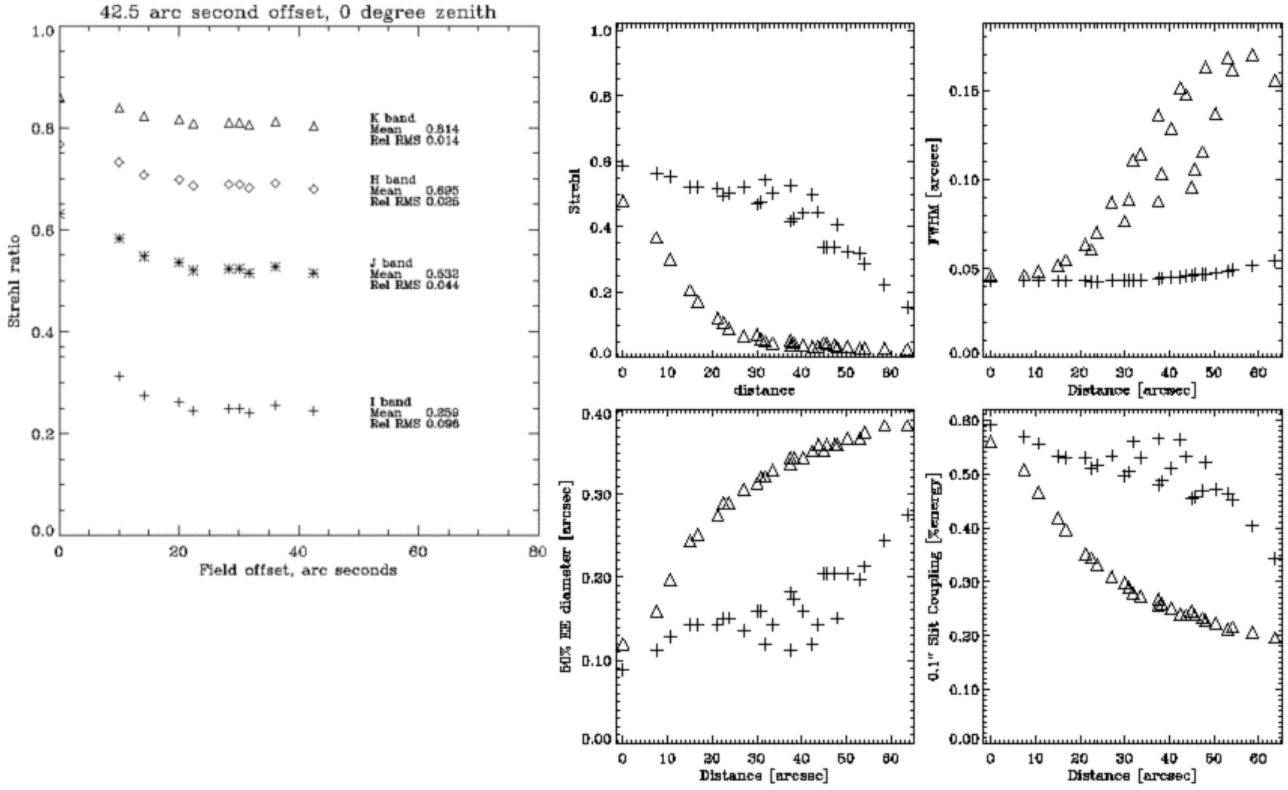

Fig. 2.3.. Left: Strehl ratio versus distance from center field at I, J, H and K bands, for the Gemini MCAO with a minimum variance estimator (BLE Code). Right: Strehl ratio, FWHM, Encircled Energy and fraction of flux coupled though a slit of 0.1" versus the distance from the field center for the Gemini MCAO system (crosses) and a Classical LGS AO system of similar order (triangles, Least square estimator, FR code).

pronounced when LGS WFS noise and servo lag are included in the calculations. A one square arcmin field appears to be a soft upper bound on MCAO capability at Cerro Pachon, if using three deformable mirrors and 5 LGSs. A comparison of the corrected field-of-views for MCAO and conventional AO will be presented later in this chapter.

Fig. 2.3 shows how the Strehl ratio varies in the field of view for several wavelength bands. No noise is included, only the error relative to the atmosphere (fitting, servo lag, anisoplanatism). The right hand panel of the figure shows an example of Strehl (upper left), FWHM (upper right), 50% encircled energy diameter (bottom left) and percentage of light coupled through a spectrograph slit (bottom right), versus the field position for a system equivalent to the Gemini South baseline system, with realistic noise factors included.

A more complete set of performance results is found on
http://www.gemini.edu/sciops/instruments/adaptiveOptics/MCAOPerformance.html

Table 2.2: Overall MCAO Strehl ratios (in %) derived from the MCAO error budget (includes all error sources)

Wavelength	Zenith	30 degrees	45 degrees
850 nm	4	2	0.5
1.25 μm	22	16	8
1.65 μm	42	35	23
2.20 μm	61	55	44

2.3.1.2 PSF characteristics

The PSF can be formally split into two components: one corresponding to errors in the high order modes controlled by the laser guide stars wavefront sensors and another corresponding to global image motion. The latter is exclusively related to modes controlled by using the tip-tilt NGS wavefront sensors.

High Order Modes

The high order modes are the primary culprits for the well-known core/halo PSF shape (see Fig. 2.4). To the first order (for a Strehl ratio > 20% and if one assume small image motion residuals), the percentage of energy encircled in the diffraction limited component of the image is proportional to the Strehl ratio. For a telescope with a small central obstruction like Gemini, the fraction of energy in the central peak of a perfect diffraction pattern is 82%. The energy in a diaphragm of diameter 2.44 λ/D is 82% of the total energy in the diffraction image, and the energy in a diaphragm of diameter λ/D is 50%. These numbers, multiplied by the Strehl ratio of the actual short exposure images (determined by the high order LGS-controlled loop), can be used as guidelines in signal-to-noise (SNR) estimates.

The halo has characteristics that vary with wavelength and quality of compensation, noise, etc, and it cannot be described simply in an analytical fashion. Its width varies between the seeing width and some fraction (0.25-0.3) of this quantity, being relatively smaller at shorter wavelengths. It is worth noting that in all the AO simulations carried out by us at the Gemini Observatory, the halo seems to have a less detrimental effect than for actual images taken with lower order systems on 3.6-m telescopes. This may be because the contrast in width between halo and core is larger for an 8-m telescope, the diffraction limit being twice smaller. This contributes to increase the halo/core contrast by a factor of ~ 5. Moreover, the Strehl ratios planned for the Gemini South Telescope MCAO system are slightly higher than those achieved with most AO systems on smaller telescopes, increasing further this contrast.

The spatial standard deviation of the Strehl ratio is of the order of 2.5% in H band at zenith for the MCAO baseline. These fluctuations are expected to be quite stable within +/- 1%, so that a first order correction on the photometry could reach this level of accuracy.

Image Motion

The effect of the NGS-controlled modes on the image is solely to convolve the average high order PSF component with a 2-D gaussian profile. A simulation code has been developed at the Gemini Observatory to estimate this effect. For example, with four m ~ 19 stars, tip and tilt vary from approximately 10 to 16 milliarsec (mas) within the central 1 square arcmin. It is important to note that this residual image motion will induce an elongation of the image, similar but smaller to what is observed in a one-star compensation system. The amplitude and direction of the elongation depends on location in the field, the relative brightness and location of the NGSs, and the $C_n^2(h)$ and wind profile.

The PSF core broadening caused by the residual image motion does not throw energy very far into the halo wings, as is the case for the imperfectly compensated high order modes. For an equivalent reduction in Strehl, the effective loss in resolution, 50% encircled energy, or slit throughput is therefore more benign. For instance, the 50% Strehl ratio loss that we adopt as an arbitrary criteria to estimate sky coverage is equivalent to a broadening of the time-averaged PSF by ~ 40 mas in the H band; this corresponds to an increase of the FWHM from 43 mas (diffraction limit) to 58 mas. The impact on the encircled energy depends on the wavelength. For spectrographs, however, whose pixel elements will probably not resolve the width of the diffraction core, the impact of this effect is moderate.

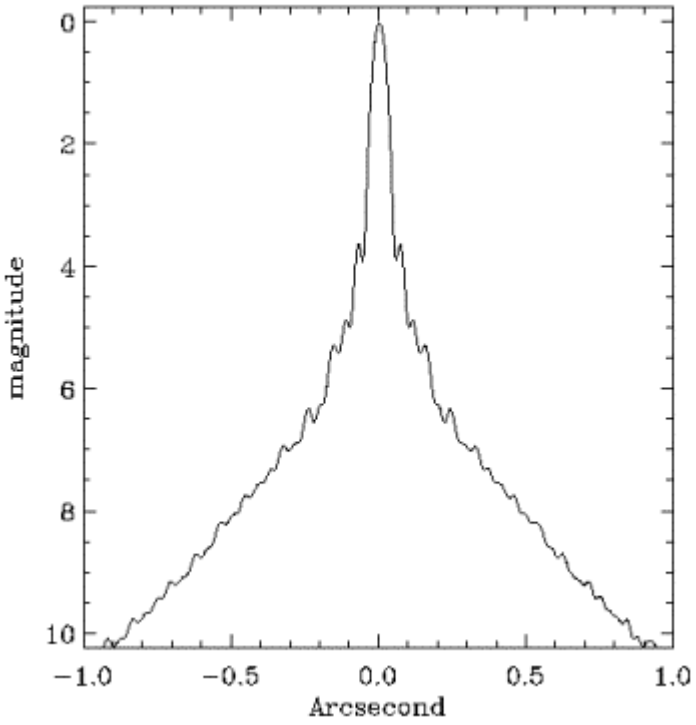

Fig. 2.4. Log of the cross section of a typical H band MCAO/CAO point spread function, showing the core and the halo. Only atmospheric residuals are considered (no telescope nor instrument aberrations included).

2.4 NGS Magnitude Limits

The performance of the low-order NGS loop may be determined using modal control. At present we have developed at the Gemini Observatory numerical codes and performed analyses to evaluate and optimize (a) the residual mean-square error in each NGS-controlled mode, and (b) the overall residual field-averaged phase variance. The statistics of the residual tip/tilt jitter at each point in the field of view can be computed from the statistics of the residual errors in the

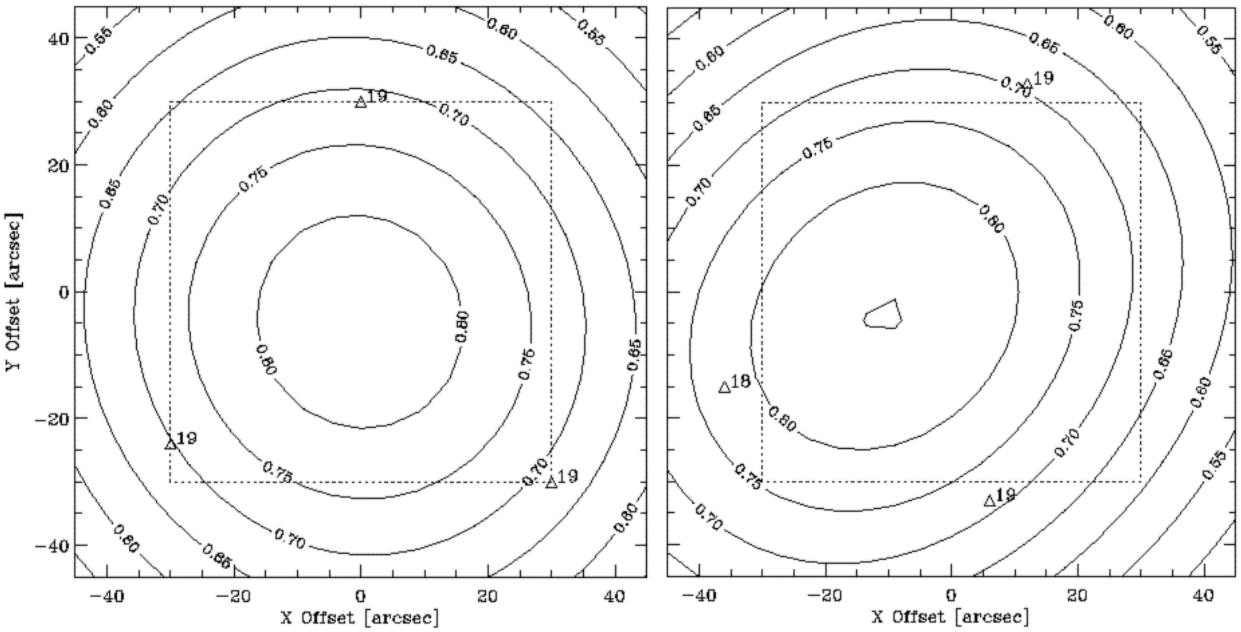

Fig. 2.5 : Strehl ratio reductions in H band due to noise and servo lag errors in the NGS loop for two sample guide star constellations. The curves are iso-Strehl contours. The NGS locations and magnitudes are indicated by the annotated triangles. The smaller square is the 1 arcminute field.

NGS-controlled modes, and the corresponding Strehl ratio reduction determined. Fig. 2.5 illustrates sample results for triangular constellations of three m ~ 18 - 19 NGSs. The NGS WFS noise model used for these results assumes quadrant detector APD tip/tilt sensors. No sharpening of the NGS image on the quadrant detector by the adaptive optics is included, which is a conservative assumption, even if the tip/tilt sensing is performed in the visible.

Fig. 2.5 shows that the Strehl ratio reduction due to the errors in the NGS-controlled tilt and tilt anisoplanatism modes is not uniform across the field of view. For imaging instruments, we expect that the nature of the non-uniformity may be determined and taken into account in the post-processing, based upon the statistics of the residual tip/tilt errors measured by the NGS WFSs. For spectroscopy, the reduction in Strehl ratio due to this residual image motion should have a negligible effect, since moderate amounts of tip/tilt jitter will broaden the central core of the PSF; there will be little reduction in the fraction of PSF energy coupled through the slit which will be about 0.1 arcsec in width.

A simpler, scalar indication of the performance of the NGS loop is the overall Strehl ratio corresponding to the residual field-averaged phase variance in the NGS-controlled modes. For a

fixed observing scenario and set of AO system parameters, this Strehl will be a function of (i) the magnitudes and locations of the three NGS, (ii) the sky background, and (iii) the disturbance spectrum for windshake-induced tip/tilt jitter. A reasonable definition of the NGS magnitude limit for MCAO is the value yielding to a field-averaged Strehl ratio reduction of 0.5 in H band.

Fig. 2.6 illustrates the field-averaged Strehl ratio in H band for the NGS loop with a sample NGS constellation and two different sets of values for sky background and telescope windshake. The NGS constellation consists of three stars of equal magnitude located at the corners of an equilateral triangle with a base of 0.87 arcmin that is centered within the 1 square arcmin field-of-view. The limiting NGS magnitude is about 20.3 for the optimistic case of an 80% sky background (for Mauna Kea), and no windshake-induced jitter. The limiting magnitude falls to about 19.1 for the more representative case of a 50% sky background and the "typical windshake" disturbance spectrum specified for the Gemini North Telescope. MCAO does not appear to be dramatically more or less sensitive to these error sources than conventional LGS AO. A more detailed investigation will be carried out as more accurate estimates/measurements of windshake at Cerro Pachon become available.

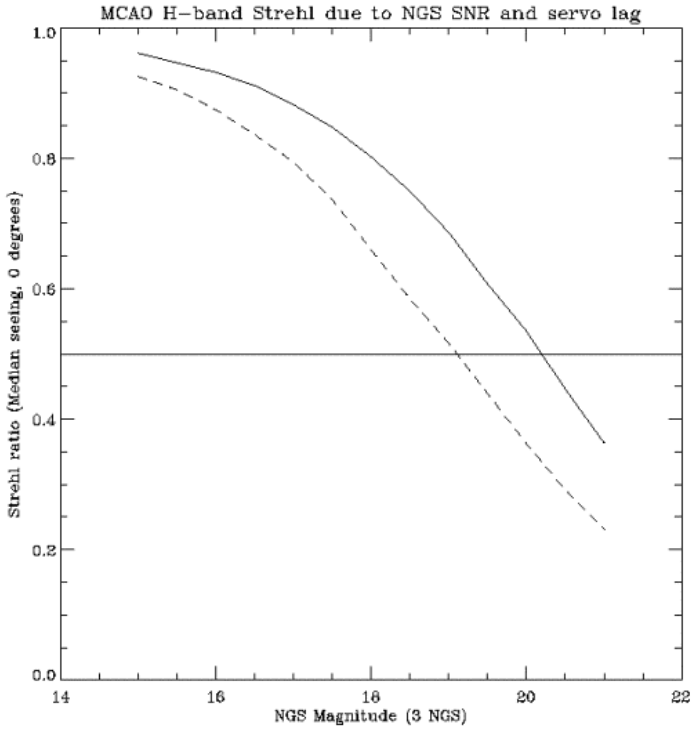

Figure 2.6. Field-averaged Strehl ratios in H band for the NGS loop as a function of NGS magnitude for median seeing, a 0 degree zenith angle, and a triangular guide star constellation with a base of 0.87 arcmin. Solid: No windshake jitter, 80% sky background (dark sky). Dashed: Typical Mauna Kea jitter, 50% sky background (grey sky).

The effect of a less favorable constellation geometry on the NGS magnitude limits has also been explored. Reducing the base of the equilateral triangle from 0.87 to 0.43 arcmin degrades the magnitude limit from 19.1 to about 18.4. Displacing the equilateral triangle from the center to one side of the 1 arcmin field increases the limit by a further 0.2. Additional results, illustrating the impact of the constellation geometry upon the performance of the NGS control loop, can be provided by Brent Ellerbroek and Francois Rigaut of the Gemini Observatory. Based upon these calculations, we have specified a limiting magnitude of 19 and a minimum triangle area of 0.25 square arcmin (corresponding to an equilateral triangle with base 0.75 arcmin) for the sky coverage estimates presented below.

2.5 MCAO gains and sensitivity compared to CAO and space-based instruments

Because of the complexity and increased costs of building a MCAO system, it is useful to understand the gains achieved by MCAO with respect to a CAO system, and also to performance without any AO correction.

2.5.1 Point source sensitivities

Table 2.3. Limiting sensitivities for MCAO/AO and no AO at CP, HST, and NGST.

	No AO	**MCAO**	**HST**	**NGST**
		Telescope		
Diameter [cm]	800	800	240	800[4]
	Throughputs (τ_{ATM} = 0.92; τ_{TEL} = 0.8; τ_{AOS} = 0.75; τ_{INST} = 0.6)			
τ_{TOTAL}	0.44	0.33	0.48	0.48
	Background [mag/arcsec^2 (Jy/arcsec^2)]			
λ = 2.1 μm (K'), R~5	13.8(2e-3)	13.8(2e-3)	16.9(1.1e-4)	20.3(5e-6)
λ = 1.25 μm / R~5	16.2(5.5e-4)	16.2(5.5e-4)	20.9(7e-6)	20.9(7e-6)
λ = 2.1 μm / R~10k	17.1(1e-4)	17.1(1e-4)	16.9(1.1e-4)	20.3(5e-6)
λ = 1.25 μm / R~10k	18.0(1e-4)	18.0(1e-4)	20.9(7e-6)	20.9(7e-6)
	Instrument (N_{dark} = 0.01 e-/s ; N_{read} = 15 e-)			
Pixel size	0.2''	*1/2D*	*1/2D*	*1/2D*
Longest Integration Time [sec]				
R=5	120	120	1000	1000
R=10000	4000	4000	1000	1000
		PSF		
Fraction of energy in 2x2 pixels				
2.1μm	0.5	0.4	0.3	0.4
1.25μm	0.5	0.2	0.25	0.25
	Limiting magnitudes, 5σ, 3600sec, aperture = 2x2pixels			
R~5 [Vega magnitude(nJy)]				
2.1 m**m (K')**	**23.2(370)**	**24.9(76)**	**23.7(230)**	**28.0(4.4)**
1.25 m**m (J)**	**24.8(190)**	**26.3(50)**	**26.0(66)**	**28.6(6.0)**
R~10000 [Vega magnitude(mJy)]				
2.1 m**m (K')**	**20.4(4.8)**	**20.3(4.8)**	**17.2(92)**	**20.1(6.1)**
1.25 m**m (J)**	**21.3(4.7)**	**20.5(9.7)**	**17.9(107)**	**20.5(9.7)**

[4] At the time we did these calculation, the baseline was still 8-m. The current 6.5-m baseline makes MCAO even more competitive, but estimations were not revised for the PDR.

Table 2.3 presents the limiting fluxes of a ground-based telescope with MCAO/AO or without AO at Cerro Pachon, the Hubble Space telescope with NICMOS, and the yardstick NGST. We list the 5-sigma, 1 hour limiting magnitudes for spectral resolutions of R=5 (broad band imaging) and R=10,000 ("between-the-OH-lines" spectroscopy). The backgrounds were taken from either the expected sky backgrounds for Gemini, the NICMOS manual, and from Gillett & Mountain (1997). The encircled energy fraction in the central 2 x 2 pixels is from simulated PSFs for the MCAO, NICMOS NIC2 growth curves (HST Instrument Science Report NICMOS-99-007), or estimated - in the case of NGST ("NGST science instrument capability report", Dec 29, 1999). We reconfirm the results of Gillett and Mountain that, at low resolutions, NGST has a significant advantage (2.5 - 3 magnitudes), while at high spectral resolutions, there is no SNR advantage. At these spectral resolutions, detector noise is important and the Gemini advantage arises from the lower cosmic ray flux and hence fewer frame readouts. In broadband imaging at 2.2 microns, MCAO has a 1.2-1.7 magnitude advantage over NICMOS and the no AO cases respectively. This gain is sizeable, especially when coupled with the increased field of view over which there is good Strehl ratio. Note that, at high spectral resolution, the no-AO case has a fainter limiting magnitude than MCAO, but this is through a slit 12 times larger (i.e. a 2 pixel slit width); this assumes there is no fine structure.

2.5.2 Sky coverage

Table 2.4 summarizes the sky coverage for classical LGS AO (CAO) and MCAO, for two galactic latitudes and the three near-infrared bands.

CAO / MCAO S.C. [%]	b=90^o	b=30^o
J	7 / 12	21 / 67
H	16 / 14	44 / 69
K	35 / 24	74 / 82

Table 2.4. **Classical AO and MCAO sky coverage**

The assumptions behind the MCAO and CAO sky coverage computations are described in section 3.4.3. For both cases, the sky coverage is computed as the fraction of the sky within which the Strehl ratio loss is < 50% with respect with the noiseless performance -on bright stars-. For instance, for the MCAO system, with a K band Strehl ratio of 60% under median seeing (r_0=16.5cm at 550nm), a Strehl ≥ 30% will be achieved over 24% of the sky at galactic pole latitudes. This table shows that the requirements for 3 tip-tilt NGS does not impact the sky coverage compared to classical LGS AO. CAO shows some gain at high galactic latitude for the longest wavelengths, but MCAO regains its advantage at shortest wavelengths where it recovers larger sky coverage at low galactic latitudes. Overall, there is only a moderate advantage for MCAO. The fact that MCAO is less wavelength dependent can be viewed as more easily enabling multi-wavelength imaging, a requisite for any program that need color-color or just J-K diagnostics.

2.5.3 Field of view multiplex gain

Table 2.5 shows that, for programs that need larger fields of view, MCAO provides a 10-20 multiplex gain compared to CAO. Such a large gain enables science programs that were not tractable previously - because of the time required to complete -. MCAO simply increases efficiency, e.g. which can be translated into more time spent on the object(s). This of course requires that the multiplex gain can be exploited, i.e. there should be a sufficient number of relevant objects in the correct field and adequate instrumentation to exploit this field (cf. Appendices 2 and 3).

Table 2.5 MCAO and CAO compensated surface area

	J	H	K
MCAO FoV Diameter [arcsec]	90	110	120
CAO FoV Diameter [arcsec]	20	30	40
Area gain	20	13	9

We note that the multiplexing gain is not simply a matter of doing CAO science faster: the field covered by MCAO enables new opportunities. In particular, for some science programs, the information is spread over a wide area (1-2 arcmin), and the science goal can only be achieved by imaging the entire object (e.g. microlensing of dense clusters, image reconstruction of lensed objects in gravitational arc systems, spatial evolution of star formation regions in nearby galaxies). For this type of objects, the probability to have enough guide stars to cover the entire object is equal to the CAO sky coverage to the n-th power, n being the number of field needed to cover the object with adequate image quality. For example, mosaicing a field with Strehl > $S_{peak}/2$ at 1.65 microns that is 1 arcmin in diameter requires four CAO fields. Using the numbers in Table 2.5, the probability that there will be guide stars in each of these fields is less than 4% at 30 degrees galactic latitude and considerably less than 1% at the galactic pole.

2.5.4 Uniform PSF

This feature is unique to MCAO. Although 0.1 magnitude error or better can be achieved in some cases on fields of 10-30” with CAO (cf. Davidge, private communication), a uniform PSF will vastly improve the accuracy of the image/spectra analysis. The study carried out in the frame of the science case on nearby and distant galaxies (cf. simulations presented in chapter 4) quantitatively illustrate this gain[1]. A uniform PSF is often mentioned as the biggest gain of MCAO.

[1] to be precise, the additional scatter in the CAO results for the stellar population case is due primarily to SNR loss in the CAO image. In the distant galaxy morphology study, however, errors of 25-50% are found on e.g. half light radii by mismatching the CAO PSF on and off-axis.

More generally, it is the experience of AO users that data reduction is a critical problem, because of (1) the lack of proper and simultaneous PSF calibration, and (2) of PSF spatial variability over the field. For some programs (e.g. stellar population, sparse to moderately crowded field), a PSF can be found in the field itself, by definition, however small the field is. For the majority of the wide field programs (high Z clusters, galaxy morphology/evolution, YSOs, solar system, ISM), this is not the case. Having a large, uniform field goes a long way toward solving this problem: if a star is present in the field of view (1 arcmin x 1 arcmin), it can be used for the whole uniform field. Since, by definition there are three m < 19 stars to serve as tip-tilt guide stars in a 2 arcmin diameter field, the probability of having at least one in the central 1 square arcmin field is high (60%).

Having full understanding of the capabilities and limitations of the proposed MCAO system on the Gemini South Telescope, we are now ready to explore the science programs that are enabled by MCAO. This exploration is the subject of the next three chapters. We will address successively the new frontiers we wish to touch for a deeper understanding of the formation and evolution of star formation in our Galaxy, the Milky Way (Chapter three), nearby galaxies (Chapter four) and distant galaxies (Chapter five).

2.6 Reference papers on MCAO:

"Principles, Performance and Limitations of Multi-Conjugate Adaptive Optics", F.Rigaut, B.L.Ellerbroek & R.Flicker, *Proc SPIE 4007*, p 1022-1031

“Scaling Multi-conjugate adaptive optics performance estimates to extremely large telescopes”, B.L.Ellerbroek & F.Rigaut, *Proc SPIE 4007*, p 1088-1099

"Comparison of multi-conjugate adaptive optics configurations and control algorithms for the Gemini 8-m telescope", R.Flicker, F.J.Rigaut & B.L.Ellerbroek, *Proc SPIE 4007*, p 1032

“Methods for correcting tilt anisoplanatism in laser guide star based multi-conjugate adaptive optics systems”, B.L.Ellerbroek & F.Rigaut, submitted to JOSA A.

CHAPTER 3

THE EVOLUTION OF THE MASS FUNCTION OF STARS IN THE MILKY WAY AND THE MAGELLANIC CLOUDS.

3.1 Summary

MCAO on Gemini South will provide dramatic new opportunities to probe the stellar mass function in stellar clusters, ranging from sites of current star-formation to old globular clusters. With MCAO, we propose to explore the behaviour of the global mass distribution of stars in relatively dense environments of the Milky Way Galaxy and the Magellanic Clouds. The prime observations will require deep imaging in the J, H and K bands and in some narrow near-infrared bands, followed up by multi-slit and IFU spectroscopy. Near-infrared photometry is ideal for probing the substellar mass function, and MCAO on Gemini will permit determination of the populations of brown dwarf and planetary mass objects in young, nearby clusters. Sub-stellar populations will also be measured in intermediate age clusters and in some of the most luminous super stellar clusters in the Milky Way and the Magellanic Clouds. Observations of globular clusters will allow us to probe the mass function and stellar mass limit over a large range of ages and metallicities. Spectroscopy will be used to establish spectral types, gravities and metallicity for subsets of the photometric samples spanning a range of metallicities, ages and environments.

A particularly exciting aspect of MCAO is the potential to use high precision astrometric measurements (at milli-arcsec levels) on relatively nearby Galactic clusters to ascertain cluster membership and to infer kinematical and dynamical properties (1 km/s at 1kpc is about 0.2 mas per yr). This capability is unique to MCAO and is a powerful new weapon for Galactic studies. This astrometric precision, at least for relative measurements, will be similar to those achieved by Hipparchos, but at much fainter levels.

The people who made substantial contributions to the Milky Way science case are:

Bernhard Brandl (Cornell, USA)
Dennis Crabtree (HIA, Canada)
Peter McGregor (Australian National University, Australia)
Michael Meyer (Steward Observatory, USA)
Phil Puxley (Gemini Observatory)
Harvey Richer (University British Columbia, Canada)
Pat Roche (Oxford University) – Group Leader
Jean-Rene Roy (Gemini Observatory)
Doug Simons (Gemini Observatory)

Several other individuals passed through the room and contributed comments, or provided e-mail input after the conference. On the proposed science programs described below, a few key people

are listed as PI and collaborators, but all present at the workshop provided feedback and insight. Pat Roche, Harvey Richer, Bernhard Brandl and Jean-Rene Roy put together the text of this chapter.

3.2 Background science

Determination of the global mass distribution of stars, and in particular, the initial mass function (IMF) of stars is a fundamental endeavour of modern astrophysics. Because stars evolve with time and are subject to a variety of environmental effects, the shape of this distribution changes over time; it may be truncated at both upper and lower ends of the mass spectrum and the slope of the distribution may become flatter or steeper. Understanding this evolution is fundamental to an understanding of the Galactic stellar populations. Ultimately, we wish to understand the processes and timescales for star formation, including how it can be triggered, and whether the trigger affects the mass function, the origin of massive and low-mass stars, and the evolution of disks.

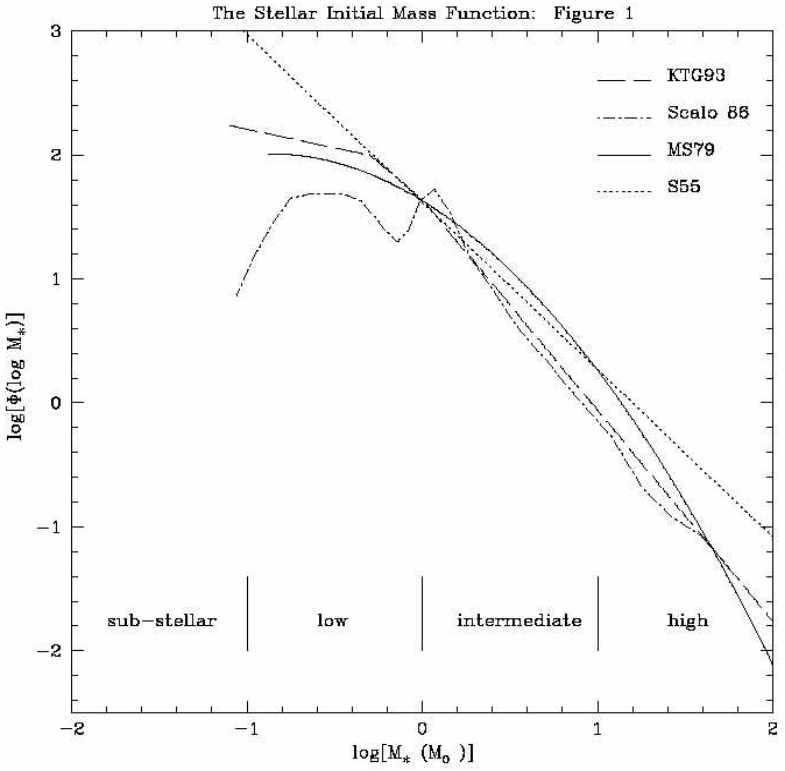

Fig. 3.1. Comparison of theoretical IMF curves from the literature – the IMF are from Kroupa et al (1993), Scalo (1986), Miller & Scalo (1979) and Salpeter (1955) -, illustrating the uncertainty in the slope at sub-stellar

Whilst the phenomena associated with star-formation have been mapped out by infrared, sub-mm and radio observations, the details of the process itself are still poorly understood. Why do some regions appear to preferentially form low-mass stars? What determines the fragmentation masses of the molecular clouds, and the stellar mass spectrum? How do circumstellar disks evolve and depend upon the stellar mass and their environment?

We wish to establish the Mass Function as a function of metallicity and provide answers to some fundamental questions, including: what is the mass and luminosity of the stars at the bottom of the H-burning sequence? How does it differ at different Z? Does it change with different stellar densities? Is it dependent upon the temperature and pressure of the gas? To do this, we need to look at star clusters spanning a range of ages and environments, including active star-forming regions, open clusters and globular clusters.

3.3 Proposed Observations

3.3.1 The Orion Nebula – a detailed study of a nearby massive star formation region

We propose deep imaging in J, H and K to identify all stellar objects, brown dwarfs and planetary mass objects in the central region of the Orion nebula cluster down to about 1 Jupiter mass. This will require photometry to J~26 and H, and K to ~25 mag over a field of ~6 x 6 arcmin^2. Orion is a particularly favorable target as the dense backdrop of the Orion Molecular Cloud limits contamination from background stars, while its relative proximity to the Earth (~450pc) means that few foreground objects will be included in the sample. There is good evidence that essentially all of the stars have formed within the last 2-million years, leading to a relatively well-understood population (e.g. Hillenbrand 1997). These young objects are much more luminous than old field stars of comparable mass identified through the SLOAN, DENIS and 2MASS surveys (by factors of 10^3 or more; Burrows et al 1997). A rich variety of phenomena associated with star formation have been detected in Orion, including proplyds, Herbig-Haro objects, wind shocks and ionization fronts (e.g. Bally et al 2000). All of these will undoubtedly show interesting diagnostic structures at the spatial resolutions available with Adaptive Optics on Gemini (e.g. Patience et al 2000; Ghez 2000; Macintosh & Ghez 2000) and would provide extremely interesting additional data from a deep photometric survey.

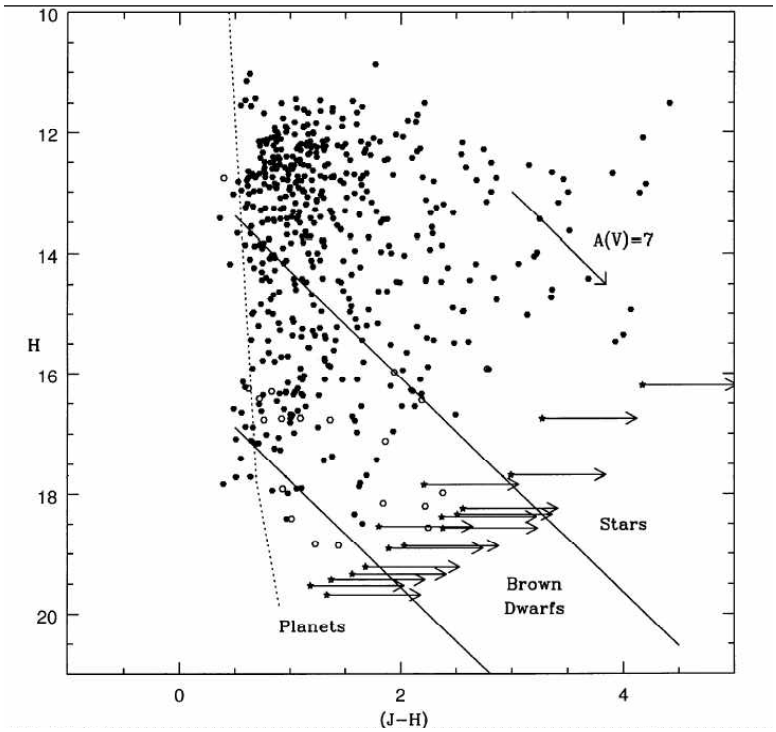

Figure 3.2: H magnitude plotted against (J-H) colour index for Orion point sources. The dotted line indicates the zero-reddening track for 1 Myr objects, while the approximate boundaries between stars, brown dwarfs and planetary mass objects are indicated (from Lucas & Roche 2000).

Observations of the central 25 arcmin^2 have revealed >600 point sources down to J magnitudes of ~20, of which about one third are below the hydrogen-burning limit, and a couple of percent are below the deuterium burning limit (Lucas & Roche 2000). The form of the mass function at these low masses is currently not well defined, but there is an indication that it probably is falling slowly at M ~10 M_{jup}. Identification of a turnover corresponding to the fragmentation limit of the molecular cloud is an important goal. In the center of the cluster, the bright nebular background, which has structure on all spatial scales, limits the sensitivity for detection of faint point sources. AO on Gemini, increases the contrast of the point sources, and substantially improves detectivity over seeing-limited observations (it should be possible to reach 1 Jupiter mass in >1 hr at H). We therefore wish to use MCAO to

conduct a deep census of the stellar population in Orion to determine the mass function from 0.001 to 10 $M_{\odot}$.

Contamination from field stars is believed to be small in the surveys conducted to date, but as the limiting fluxes become fainter, contamination from both foreground and background stars will increase. The potential for high quality astrometry with MCAO provides a new means of identifying contaminating field stars. In Orion, the cluster motions are predominately along the line of sight, so large transverse motions may indicate contaminating sources. (The proper motion at the distance of Orion is 0.5 mas per yr for a transverse velocity of 1 km/s). Monitoring over even a few years will provide important data on cluster membership and can also be used to identify binary systems. The core of the cluster is concentrated in the central 2 arcmin, but it is important to survey a much larger area to search for changes in stellar population in different regions. The sensitivity for deep surveys is also higher outside the central core as the nebular background is much fainter (> 25 arcmin^2). An MCAO system delivering as large a field as possible, commensurate with good sampling is required. The photometric precision required for object characterization is particularly high (~0.05 mag) at K ~ 25; however astrometry will probably drive the requirements.

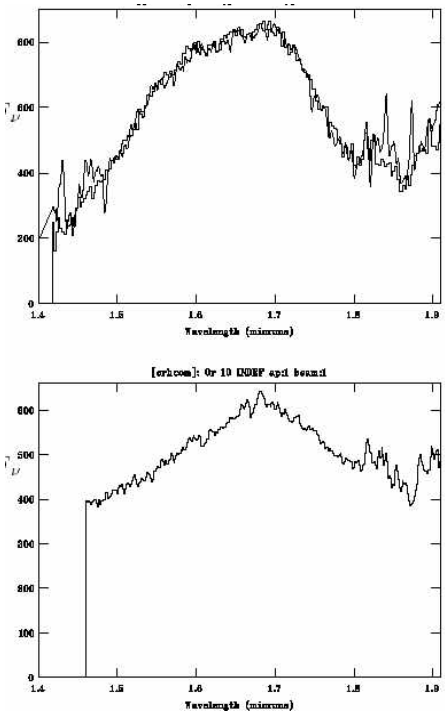

Fig. 3.3. Composite H band spectrum of low-mass candidates in the Orion cluster (bottom) compared to a field brown dwarf DBD0205-1159. Note the pronounced triangular profile in the Orion spectrum (from Lucas et al 2001).

Observations in the K band can be more difficult to interpret because of the possible effects of circumstellar dust emission and the increased likelihood of contamination from background stars. However, K fluxes will be required to give good estimates of the luminosity and may help identify particularly young objects, which are most likely to have excess emission at 2 microns.

Spectroscopy of the faint low luminosity candidates is difficult with existing IR spectrometers, but will become feasible for a large sample once multi-object IR spectrographs fed by AO-corrected images are available. The available low-resolution, low-signal-to-noise ratio observations do however indicate that follow-up spectroscopy will be rewarding. Low-mass brown dwarfs in the Orion cluster display markedly different water band profiles in the H band compared to older, field brown dwarfs (Lucas et al 2001). The triangular profiles seen in the Orion objects are probably due to the lower surface gravities and higher-temperatures (and consequent freedom from dust in the circumstellar envelopes). Higher resolution spectra should reveal some weak atomic lines as well as additional molecular bands that will probe the temperature and gravity (M/R) through detailed stellar atmosphere analysis. Models predict that the 2.2μm NaI line and the 2.3μm CO band heads weaken with decreasing gravity, and this appears to be borne out by the available spectra. Resolving powers of ~ 3000 in the J, H and K bands are required to measure and quantify the

weak atomic and molecular bands and resolve the atmospheric OH absorption lines. Slitlets are probably preferable for spectroscopy of the compact objects, though IFUs will give a better handle on the background, and will be much more suited for observations of proplyds and wind shocks.

Objects near the deuterium-burning limit in Orion with typical extinctions of A_V <5 mag have H~ 18 mag. Spectra with a S/N of 30 can be obtained in an exposure >1 hr, depending upon the nebular background. In several hours it will be possible to measure objects below 10 Jupiter masses.

Ten fields will sample the core of the cluster, with typically tens of brown dwarfs in each setting. There are lots of potential Wave Front Sensor guide stars in Orion, but saturation of the brightest stars may limit sensitivity in some regions.

3.3.2 Stellar and sub-stellar population variations in star-forming regions

Whilst Orion is the obvious starting point for a detailed investigation of a young star-forming region, it is vital to extend the observations to other examples, so that we can investigate the universality or otherwise of the bottom of the mass function. Does it depend on environmental factors, such as mass of the parent cloud or the metallicity?

Table 3.1. Masses of stars in young embedded clusters (column 6 label: read "kpc", not "pc")

Table 1: Ratios of High– to Low–Mass Stars for Young Embedded Clusters

Name	N_	Age	A_V–limit	$R_{grid/low}$	D(pc)	ρ_(pc^{-3}) [1]	T_{gas} [2]
NGC2024 [a]	72	3×10^5 yr	18.9^m	0.24 ± 0.14	0.5	2000–5000	50K
Ophiuchus [b]	32	3×10^5 yr	19.3^m	0.1 ± 0.04	0.5	500–1500	20K
L1495 [c]	27	3×10^5 yr	5.0^m	0.13 ± 0.05	1.0	15–45	10K
OMC–2 [d]	107	1×10^6 yr	5.0^m	0.07 ± 0.04	1.0	200–1000	50K
BD+40°4124 [e]	32	3×10^5 yr	20.0^m	0.45 ± 0.15	0.34	800–3000	30K
R Cr A [f]	45	1×10^6 yr	40.0^m	0.25 ± 0.07	0.5	500–1500	15K
ONC [g]	133	3×10^5 yr	2.0^m	0.07 ± 0.02	1.0	10,000	50K
Mon R2 [h]	115	1×10^6 yr	11.0^m	0.14 ± 0.10	0.8	1000–3000	35K
IC 348 [i]	73	2×10^6 yr	5.0^m	0.18 ± 0.06	1.0	100–700	12K

[1] Averaged over a region of r _ 0.3 pc.
[2] Inferred from NH_3 measurements when available.
[a] Meyer et al. (1999).
[b] Strom et al. (1995); Greene & Meyer (1995).
[c] Strom & Strom (1994); Luhman & Rieke (1997).
[d] Jones et al. (1994); Hillenbrand et al. (1997).
[e] Hillenbrand et al., 1995.
[f] Wilking et al. (1997); Wilking & Meyer (in prep).
[g] Hillenbrand (1997).
[h] Carpenter et al. (1997).
[i] Luhman et al. (1998); Herbig (1998).

These questions can only be answered by extending the program to other active star formation regions. The current position is summarized in Table 3.1, taken from Meyer et al. 2000. Most detailed studies to date have concentrated on northern hemisphere clusters. The southern

hemisphere has many rich clusters, including the nearby objects such as Ophiuchus, Corona Australis and Chamaeleon, which are extended over many arcmin.

The astrometric precision offered by MCAO will be even more important here, as the potential contamination from foreground and background objects is more severe than towards Orion.

3.3.3 Open Clusters

Open clusters provide snapshots of the effects of stellar and dynamical evolution over a range of ages and metallicities. Cluster membership of candidate objects can be determined from proper motion measurements derived from relative astrometry, so that relatively nearby clusters are the preferred targets. JHK photometry will yield the cluster mass function to the bottom of the H-

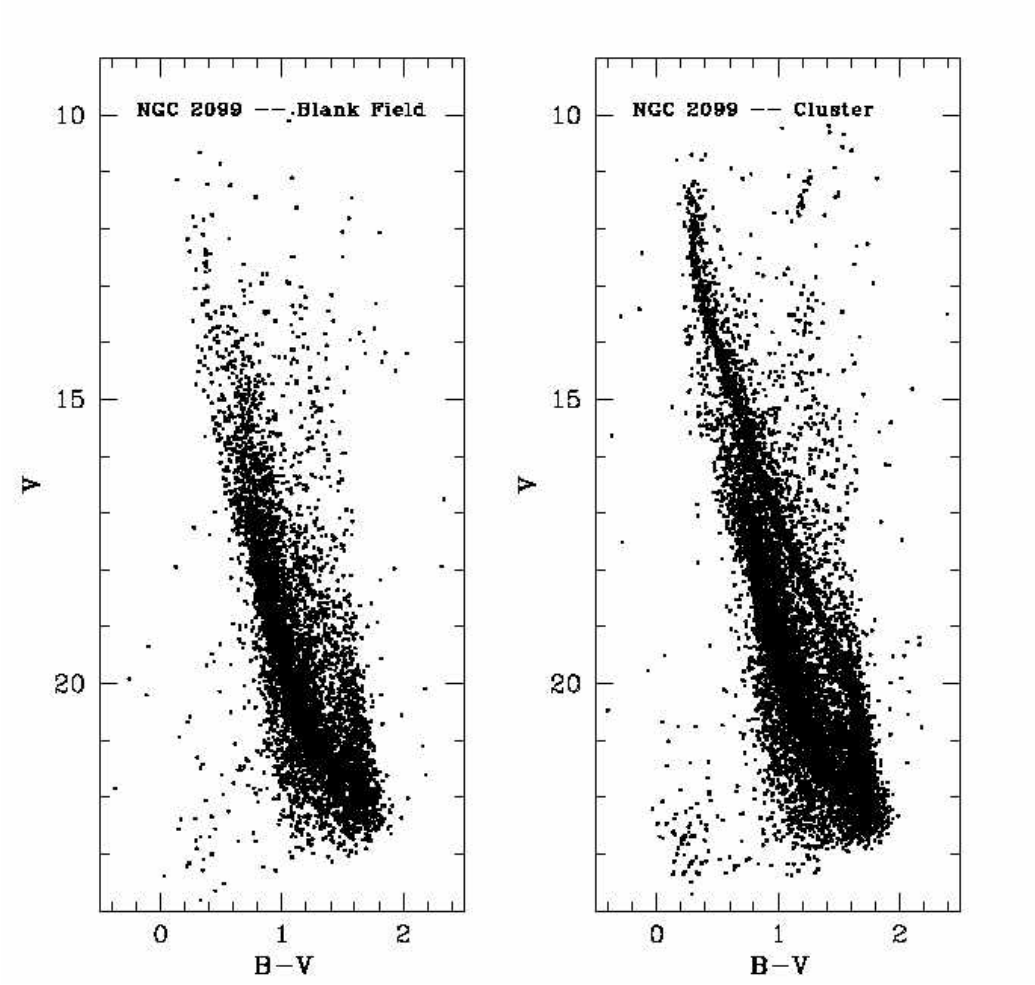

Fig. 3.4. Colour magnitude diagram for NGC 2099 (right) compared to a background field (left). Note that structure in the background field near (B-V)= 1.7 and 22.5< V < 20 blends with the bottom of the main sequence in the cluster field and prevents identification of low mass objects (From Kalirai et al 2001).

burning sequence and the end of the white dwarf cooling sequence to provide an independent age determination. Dynamical evolution can be studied from the variation in mass function with cluster radius and clues to the initial-final (i.e. precursor-white dwarf) mass relation for stars

gained from the masses of the white dwarfs. This relationship is a critical input datum for chemical evolution studies of galaxies and is currently only poorly constrained by data.

The foundation of the age scale in astrophysics is the fit of stellar evolution models to the main sequence turnoff in clusters. There are other techniques of age measurement such as solar oscillations and nucleocosmochronology but the applicability of these techniques is rather restrictive. The termination of the white dwarf cooling sequence in a cluster offers an approach that is largely independent of the physics of the turnoff method. Until recently it has been difficult to apply the technique; the cooling sequence ends at intrinsically faint magnitudes even for young clusters and contamination by stellar and extragalactic interlopers has always raised questions about the cooling ages determined for open clusters.

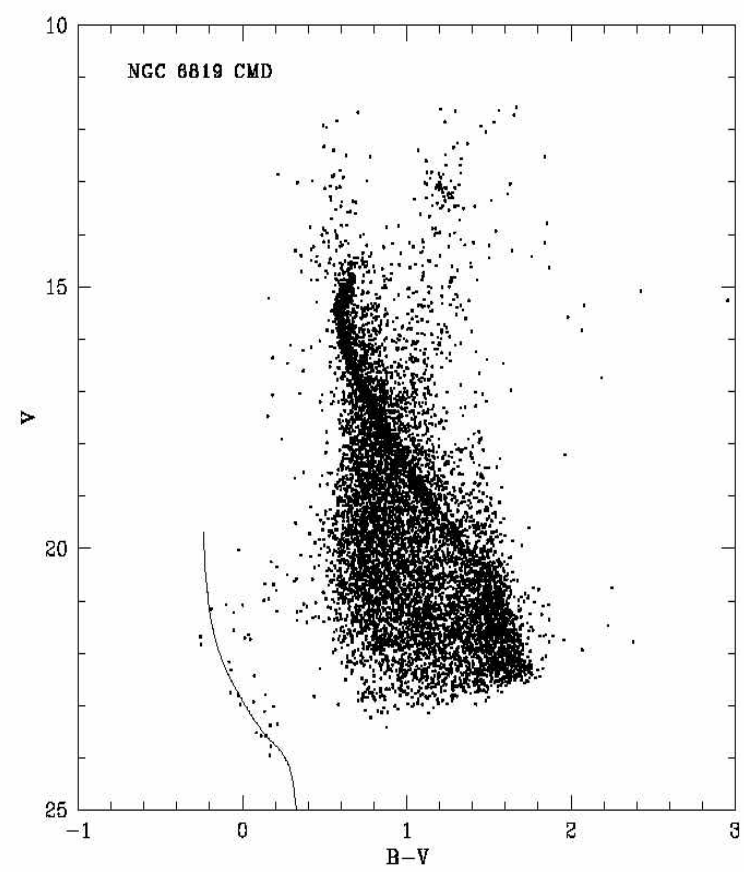

Fig. 3.5. Colour-magnitude diagram for the moderately old (2.5 Gyr) open cluster, NGC 6819. The solid line is a cooling track for a 0.7 $M_{\odot}$ white dwarf. This rich cluster has a number of white dwarf candidates, but there is likely to be significant contamination from blue compact galaxies; proper motion measurements will identify the bona-fide cluster objects (From Kalirai et al 2001).

White dwarfs cool at a well-determined rate so that their temperature can be used as a kind of cosmic clock. The universe is not old enough for white dwarfs to have faded into invisibility so that every white dwarf ever formed in the universe is still potentially observable.

In the ideal case, it would be possible to estimate the age of an open cluster with 3 different techniques: from the cluster turn-off, the turn-on, and the end of the white dwarf cooling sequence. However such systems are very rare as the very young clusters which still having sufficient stars just turning on to the main sequence will normally not have produced a large population of white dwarfs.

The difficulty is in relating this temperature directly to an age. However, the physics of white dwarf cooling, while having its own complexities, is much simpler than that of main sequence stars. Hence the temperature of a white dwarf is a potentially powerful and accurate age indicator.

In the environment of a star cluster, the white dwarf cooling sequence will terminate when the first white dwarf to form in the cluster is reached. The total age of this object is the cooling time of the white dwarf plus the main sequence lifetime of its progenitor. As the cluster ages, the latter lifetime becomes less important so that the white dwarf cooling time itself becomes a good estimate of the cluster age. As a test of this technique, the first part of this project would be to measure the white dwarf cooling age in a number of rich open star clusters and compare the derived age with that determined from the traditional main sequence turnoff technique.

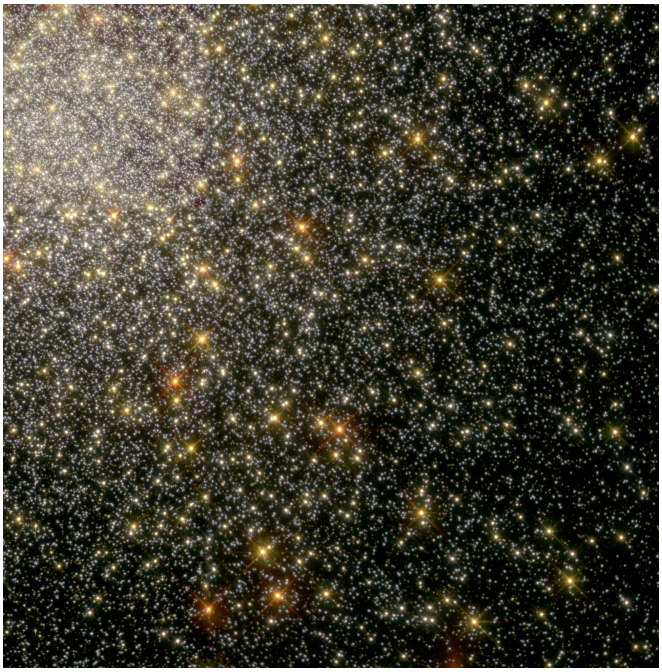

Fig. 3.6. HST image of NGC 104 showing the extreme density in the core of the cluster (From Gilliland et al 2000).

In order to have sufficient number of stars in a relatively small area, it will be necessary to choose rich clusters and to observe in multiple fields within each one. Proper motion measurements permit distinguishing white dwarfs from distant star-forming blue galaxies. The clusters in the sample should cover a range in ages to provide a detailed comparison between turn-off and white dwarf ages.

Table 3.2 lists 6 clusters, which cover a large spread of ages, and which are suggested for this program.

Table 3.2. Young stellar clusters

Cluster	Age (Myr)	Distance Modulus
NGC 6405	94	8.4
NGC 2516	110	8.1
NGC 3532	310	8.4
NGC 3680	1200	9.9
NGC 6253	5000	10.9
Coll 261	9000	11.7

3.3.4 Mass Function in nearby Globular Clusters over a range of Metal Abundances

In order to probe the mass function and sub-stellar limit in metal-poor objects, a program of deep JHK imaging will be needed, reaching down to the end of the population-II main sequence, in a number of globular clusters. Measurements of proper motions are essential here in order to identify cluster members and permit removal of field stars. Theory predicts that the mass of the bottom of the hydrogen-burning main sequence is a function of metal abundance and that this limit rises from 0.08 M? in stars with ~solar metallicity to 0.11 M? in low-metallicity objects. This can be tested by determination of the mass function in globular clusters, and searching for the break in the main sequence slope. In turn, this will provide important clues to the number of brown dwarfs formed in the early universe. In a globular cluster, these objects are faint, crowded and red (late-type M stars with M_J ~ 13 and M_K ~11). The uniformity of the point-spread function delivered by MCAO will be very important in enabling accurate photometry.

Observations of five globular clusters are required to cover fully the metallicity range from [m/H] near solar down to –2.0 within a true distance modulus = 14; the 5 southern globular clusters listed below are the suggested targets.

With a mean distance modulus ~ 12.5, exposures to reach the bottom of the main sequence will need to reach J = 26.5 and K = 24.5. Depending on the crowding, this should be possible in exposures of ~1hr. With 16 fields required in each cluster, and 5 clusters, the whole program would require > 300 hours plus overheads and calibrations.

Table 3.3. Sample of southern globular clusters to be observed with MCAO

Cluster	[m/H]	Distance Modulus
NGC6553	-0.34	13.7
NGC104	-0.76	13.3
NGC6121	-1.20	11.7
NGC6752	-1.56	13.0
NGC6397	-1.95	11.8

The globular cluster parameters of Table 3.3 are taken from Harris (1996).

3.3.5 Young Stellar Super-Clusters

Super star clusters dominate the star formation in starburst galaxies, and have almost certainly been very important in the star formation history of the Milky Way. They are compact, dense regions with large numbers of newly-formed stars with luminosities equivalent to many tens or hundreds of O-type stars. Understanding the stellar populations in these massive star-forming regions, and in particular the interplay between high- and low-mass star-formation, is a key goal.

This requires a wide field-of-view with a high and constant Strehl ratio, permitting deep JHK broadband imaging and photometry of stars ranging from massive O-type stars to objects below the hydrogen-burning limit. The challenge is to measure these faint populations in the face of severe crowding, compounded in some cases by extinction and contamination from background and foreground stars.

The best analogue to these extreme star-forming clusters known in the Milky Way is NGC 3603, at a distance of ~7 kpc from the sun, and the 30 Doradus region in the Large Magellanic Cloud. Far less well understood are the luminous stellar clusters that have been identified within ~100 pc of the Galactic Centre. These too are vigorous sites of star formation that appear to have substantial numbers of Wolf-Rayet stars. They are much less crowded than NGC 3603 or 30 Dor, but are very important in understanding recent star formation in the nucleus of the Milky Way. A number of other star formation regions in the Large and Small Magellanic Clouds will also be studied. At these distances, proper motion measurements are unlikely to be useful for establishment of cluster membership; nearby comparison fields will give estimates of the field star populations in lines of sight similar to the target clusters. Diffraction-limited observations in the H band yield spatial resolutions of 0.002pc (350 AU) in NGC 3603 to 0.016pc in the SMC, so that many stars will be blended, and statistical techniques will be required to quantify the low mass populations. Measurements in narrow-band filters (CO, Brγ etc) will also give information on the stellar population as well as on their interplay with the surrounding gas.

Fig. 3.7. Three colour image of NGC 3603 composed from Js (blue), H (green), and Ks (red) taken with ISAAC at the VLT. The field-of-view is 3.4¢´ 3.4¢ (Brandl et al 1999).

NGC 3603 has been studied in the near-infrared under excellent (0.4 arcsec) natural seeing conditions (Brandl et al 1999). Allowing for contamination on a statistical basis, leaves more than 1200 cluster members within a 33 arcsec radius of the cluster core to J ~ 21mag, and down to ~0.1 $M_?$.

In 30 Dor the situation is less clear: while Sirianni et al (2000) found a flattening of the IMF below 2 M_o in their WFPC2 data, observations with HST/NICMOS (Zinnecker et al 2001) do not suggest a significant flattening toward lower masses. MCAO operating in the near-infrared with higher sensitivity to low-mass stars than WFPC2 and better angular resolution than NICMOS will be able to provide a final answer to this key question.

Because of the severe crowding, spectroscopy with slits will suffer badly from confusion. Measurements with IFUs are likely to be the optimum approach, with increased contiguous coverage generally preferred to a set of smaller deployable IFUs across the field. Spectroscopy (R> 3000) will be required to determine the ages and masses of the stars.

Table 3.4. Apparent K magnitudes of low and intermediate mass stars in some representative target young super stellar clusters.

Mass (Mo)	NGC 3603	LMC	SMC
0.1	19.2	23.5	24.0
0.4	17.1	21.5	22.0
1.0	16.6	21.0	21.5
2.0	15.9	20.3	20.8
4.0	14.8	19.2	19.7

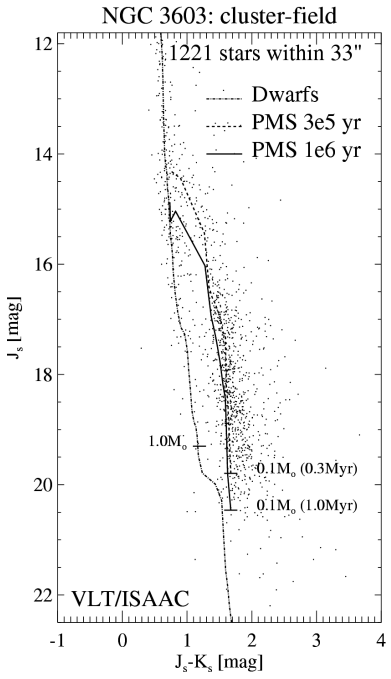

Fig. 3.8. Colour-Magnitude diagram for NGC3603 from Brandl et al (1999)

3.4 Instrument requirements

3.4.1 Imaging

All of these programs will benefit from relatively large fields of view. We wish to press for the largest feasible fields, with the proposed ~80 arcsec field near the minimum. The accuracy of astrometric measurements near the edges of the fields will need to be assessed; we are concerned that it may be lower there, and limit proper motion studies.

Good sampling of point sources will be a key requirement. We suggest that the pixel scale be set by the requirement for Nyquist sampling at H. This would lead to 1.5 pixels across the FWHM at J, and we need to understand the effects of confusion with faint stars and structured background in the crowded fields in order to assess the trade-off between sampling and field size. At K, contamination from foreground and background stars will become more problematic.

In some cases, large dynamic range will be needed in order to measure faint, low-mass objects in fields containing bright, massive stars. It would be desirable to implement read out (sampling) techniques which increase the dynamical range within one integration despite saturation on the brightest pixels.

MCAO should have a cleaner PSF and yield cleaner images than NICMOS/HST, although it will be less constant in time and will vary with field position and the guide star geometry. The very thin secondary mirror support spiders, which rotate on the sky as objects are tracked, lead to smaller diffraction spikes. In most fields, there will be a choice of many tip-tilt guide stars but the density may be too high for some targets?

IR wavefront sensors may be useful in some fields.

3.4.2 Spectroscopy

For the programs described here, where spectra will mostly be obtained of point sources, slitlets are probably preferred over IFUs for most fields.

For the case of Orion, there are ~800 objects brighter than K = 17 within the central 5 x 5 arcmin^2, leading to >100 potential targets per field. The resolving power required to measure and quantify gravity-sensitive spectral features is R~ 3000, with coverage across 0.2 microns per setting to measure e.g. the 2.21μm NaI line and the CO bandheads. In addition, R ≥ 3000 will enable the removal of atmospheric absorption lines. High sensitivity, coupled with good spectrum extraction from the complex background will be required to measure weak lines.

Observations of super stellar clusters, as well as extended sources such as proplyds and shocks in nearer clusters will require IFU spectroscopy.

3.5 Comparison with Conventional AO

The main benefits of MCAO compared to CAO arise in the increased astrometric precision and the complete coverage of the target clusters with uniform PSFs. If milli-arcsec astrometry becomes routinely practical with MCAO, it will revolutionize some areas of dynamics and kinematics in the Milky Way, and will provide a clear lead up to the micro-arcsec scale astrometric potential of GAIA when it is launched in 2012 (see http://astro.estec.esa.nl/SA-general/Projects/GAIA/gaia.html). GAIA is a photometric and astrometric satellite, operating in the optical, which will reach astrometric precisions of 4 micro-arcsec at V= 10mag, and 200 micro-arcsec at the limiting sensitivity near V= 20 mag. GAIA will reach higher precision than MCAO can offer, but it will be limited by interstellar extinction in many clusters.

The uniform PSFs across the cluster fields will be very important in maintaining uniform instrumental sensitivity and completeness, and will aid the application of deconvolution techniques in the crowded cores. The main effects on the data will be from the distributions of the stars and nebular backgrounds themselves, rather than artefacts induced by the instrumentation.

For the first time it will be possible to provide NIR images of extended objects or clusters with the same angular resolution as their optical WFPC2 counterpart, leading to a large number of direct comparisons and combinations over an extended wavelength range.

Large, deep surveys of dense regions – which are very difficult to schedule on a space observatory because of their time requirement – will be enabled by MCAO!

References:

Bally, J., O'Dell, C.R., & McCaughrean, M.J., 2000. AJ 119, 2919.

Brandl, B., et al. 1999. A&A 352, L69.

Burrows, A., et al. 1997. ApJ 491, 856.

Gilliland, R.L., et al. 2000. ApJ 545, L47.

Ghez, A. M. 2000, ``What can pre-main-sequence binary star populations tell us about formation mechanism?," Invited review in proceedings of IAU 200, eds B. Mathieu and H. Zinnecker

Harris, W.E., 1996, AJ, 112, 1487; + http://www.physun.mcmaster.ca/~harris/mwgc.dat

Hillenbrand, L.A., 1997. AJ 113, 1733.

Kalirai, J., 2001. AJ in press.

Kroupa, P., Toot, C.A., & Gilmore, G., 1993, MNRAS, 262, 545.

Lucas, P.W., & Roche P.F., 2000. MNRAS 314, 858.

Lucas, P.W., et al 2001. MNRAS Submitted.

Meyer, M.R., et al, 2000. Protostars & Planets IV, p121. University of Arizona Press.

Miller, G.E. & Scalo, J., 1979, ApJS, 41, 513.

Patience, J., Macintosh, B., Ghez, A. M. 2000, ``An Adaptive Optics Survey of the Trapezium with the Keck Telescope," BAAS, 197, 5202P

Salpeter, E.E., 1955, ApJ, 121, 161.

Scalo, J. 1986. Fundam. Comic. Physics, 11, 1.

Sirianni, M., et al 2000. ApJ 533, 203.

Zinnecker, H., et al 2001. IAU Symp. 207 (in press)

CHAPTER 4

HISTORY AND EVOLUTION OF STAR FORMATION IN NEARBY GALAXIES

4.1 Introduction

Nearby galaxies are unique in that they can be resolved into individual stars, and hence the study of these objects provides a fundamental step for understanding the properties of more distant systems. The stellar contents of Local Group systems have been resolved for over 75 years, starting with the pioneering works of Hubble, Baade and others. However, it is only recently by using ground-based telescopes that exploit the best sites, such as the CFHT, and space-based facilities, like the HST, that it has been possible to study individual stars in galaxies outside the Local Group. It is now possible to explore objects covering a diverse range of morphologies and environments are sampled. The ability to resolve stars in the Virgo cluster is of particular importance, as it is the nearest large cluster, and as such it provides an unprecedented laboratory for understanding clusters at larger redshifts.

Efforts to resolve galaxies are limited at present by aperture size, which restricts our ability to gather large numbers of photons from faint sources and image quality (e.g. Bedding, Minniti, Courbin, & Sams 1997, A&A, 326, 936). Because of their large collecting area and emphasis on achieving near diffraction-limited image quality, the 8-m Gemini Telescopes have the potential of opening new frontiers in the study of nearby galaxies. Studies of stars in nearby galaxies require wide-field surveys to obtain statistically significant samples which are needed to probe reliably changes in stellar properties such as age and/or metallicity. The characteristic angular dimensions of nearby systems are summarized in Table 4.1. The dimensions of these structures exceed the isoplanatic patch sizes delivered by traditional single-star adaptive optics systems, which typically are a few tens of arcsec.

Table 4.1. Characteristic dimension of nearby galaxy systems

Structure	**Angular size**
Galactic globular cluster ½ light radius	30 - 180 arcsec
Bulge scale length (Virgo)	5 - 30 arcsec
Disk scale length (Virgo)	50 - 300 arcsec
Scale length (Virgo E)	40 arcsec

Because of increase in field size, multiconjugate adaptive optics (MCAO) systems on 8-m telescopes offer an unprecedented means of studying nearby galaxies. In an effort to demonstrate

the scientific potential of an MCAO system on Gemini, we have constructed several sample science programs. The intent is not to assemble yet an exhaustive list of science targets; rather, we wish to examine a small number of projects that include targets ranging from the Milky Way to distances in excess of 10 Mpc. These programs share a similar theme, which is to probe the critical formation and evolution events in galaxies, when basic structural properties were imprinted. The ultimate goal is to distill a set of common requirements for these programs, which in turn will serve as the basis for detailed numerical simulations.

AO systems deliver diffraction-limited performance at near-infrared wavelengths, and this wavelength bias is reflected in the science programs. The near infrared domain is a critical portion of the spectrum for studying old and intermediate-age populations, as the coolest, most evolved stars in these systems; while being relatively faint in the visible part of the spectrum, they reach their peak brightness at wavelengths long ward of 1 micron. The near infrared is also of paramount importance for probing heavily obscured star forming regions in nearby galaxies. Finally, the near infrared is the prime portion of the spectrum for studying the lowest mass stars in the Galaxy, which have temperatures that position the peak of their spectral-energy distributions between 1 and 2.5 microns, and enhance strong absorption features that are robust temperature diagnostics.

The people who made substantial contributions to the nearby galaxies MCAO science cases are:

Taft Armandroff (NOAO, US)
Ivan Baldry (AAO)
Michael Bolte (UCSC, US)
Bernhard Brandl (Cornell, US)
Gary da Costa (Mount Stromlo, ANU, Australia)
Tim Davidge (HIA, Canada)
Rene Doyon (University of Montreal, Canada)
Doug Geisler (University of Conception, Chile)
Markus Kissler (ESO, Europe)
Chip Kobulnicky (University of Wisconsin, US)
Tod Lauer (NOAO, US)
Peter McGregor (Canberra, Australia)
Dante Minniti (Universitad Catolica, Chile)
Doug Richstone (University of Michigan, US)
Francois Rigaut (Gemini Observatory)
Basilio Santiago (UFRGS, Brasil)
Ethan Schreier (STScI, US)
Eric Steinbring (CfAO)
Thaisa Storchi-Bergmann (UFRGS)
Keith Taylor (Caltech, US)

Several others either passed through the room and contributed comments, or provided email input. On the proposals below, a few key people are listed as PI and collaborators, although all

present at the workshop provided feedback and often ideas. This chapter is based on contributions written by Tim Davidge, Gary Da Costa, Bob Schommer, Ted von Hippel, Ray Sharples, Francois Rigaut and Jean-Rene Roy.

4.2 Calibration of the Supernovae Ia Zeropoint – Bob Schommer (CTIO)

4.2.1 Scientific Background

The Type Ia supernovae peak magnitudes show a dispersion around a uniform Hubble flow of only ~$0^m.12$ in the nearby universe, when corrected for reddening and small luminosity differences (Riess et al. 1996; Phillips et al. 1999). This nearby SNe sample determines the Hubble diagram quite precisely, because distances to individual supernova can be measured to roughly 5% precision, permitting both the mapping of the local flow (Hamuy et al 1996; Riess et al 1996) and the geometry of the Universe (Perlmutter et al. 1997; Schmidt et al. 1998). While the measurement of the geometry of the Universe requires only relative magnitudes for nearby and distant objects (and thus can be expressed in a dimensionless manner), the determination of the Hubble constant with supernovae requires a calibration of the intrinsic luminosities of these objects.

Table 4.2. SNe Ia with HST Cepheid distances

Sne	**Host**	**Distance**	**Comment**
1937C	IC 4182	28.31	Old SN photometry
1972E	NGC 5253	27.92	Pec galaxy host
1981B	NGC 4536	31.10	Virgo member
1990N	NGC 4639	32.03	
1998bu	NGC 3368	30.37	Leo I group
1980N	NGC 1316	31.34	Fornax group Distance
1989B	NGC 3627	30.22	Leo group Distance
1992A	NGC 1380	31.34	Fornax group

The current determination of the supernova zeropoint rests on measurements of distances to the host galaxy of the supernovae via the use of the Cepheid period-luminosity relation. The calibration of the Cepheids is done in the Large Magellanic Cloud, and thus the true distance to the LMC is a vital part of this distance scale. The determination of the zeropoint of the observed Hubble diagram for the supernovae itself is relatively precise, with errors of only about $0^m.03$

(Hamuy et al. 1996), while the error in the distance to the LMC is driven by concerns about systematic errors and has a range of perhaps $0^m.4$(18.3-18.7, see Walker 1998). The distance to the host galaxies of supernova via the relative Cepheid distance modulii yields errors of $0^m.15$-$0^m.20$ per galaxy (e.g., Saha et al., 1997). This error, combined with the $0^m.12$ dispersion about the corrected Hubble diagram, yields a precision in the absolute magnitude of the supernovae of approximately $0^m.2/(n^{0.5})$, where n is the number of galaxy hosts included in the calibration.

Thus the dominant statistical error in the Hubble constant is due to the small number of Cepheid host distances. The requirements are the existence of the spiral host for a SN Ia within a distance of about 20-30 Mpc, i.e., to the Virgo cluster or slightly beyond. There are 5 such hosts known whose distances have been directly measured, and 3 SNe whose hosts are members of a group or cluster, as detailed in Table 4.2. Figure 4.1 shows these calibrators plotted on the peak magnitude-rate of decline relation from Phillips et al. (1999).

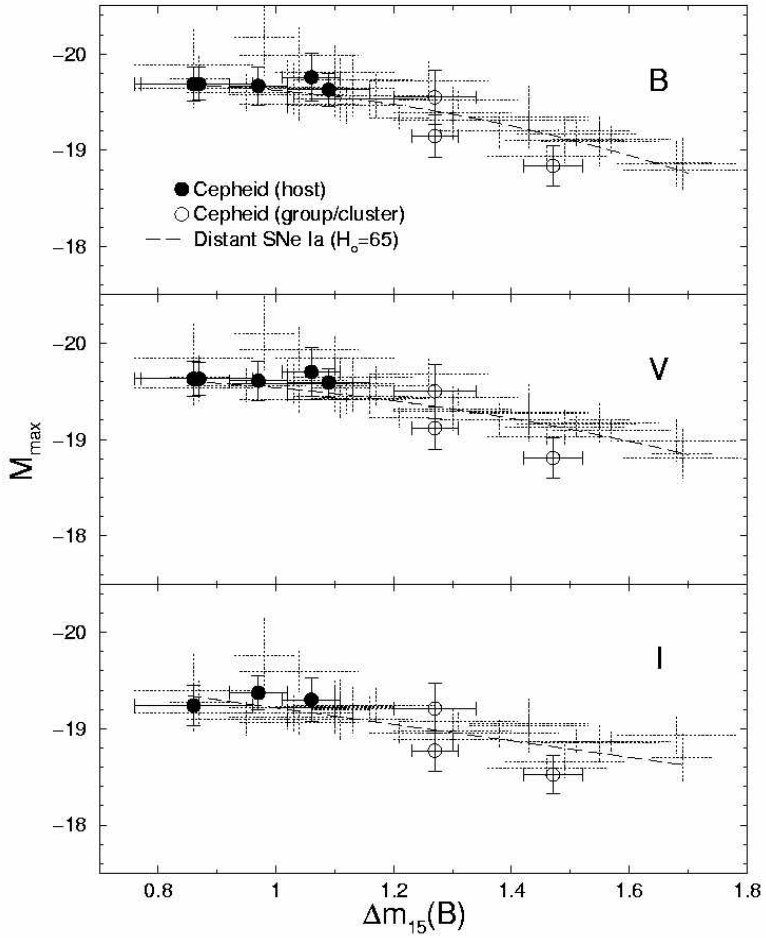

Fig. 4.1. The absolute magnitudes in BVI for Type Ia supernovae as a function of the Phillips (1993) parameter $Dm_{15}(B)$. The filled circles correspond to the five Sne which occurred in host galaxies with HST Cepheid distances. The open circles are Sne which are members of groups or clusters with at least one HST Cepheid distance available. The crosses are 35 Sne Ia in the Hubble flow with distances derived by assuming a value of H_o = 65 km s^{-1} Mpc^{-1}.The dashed lines show fits from Phillips et al. (1999). Figure from Suntzeff et al. (1999).

4.2.2 Proposed Observations

The number of Sne Ia calibrators can be doubled immediately with accurate distances to E/SO galaxy hosts. Measurements of the Red Giant Branch tip in these galaxies should be able to give

reliable distances. Table 4.3 shows the current set of nearby [(m-M)< 31.6] supernova with E and SO hosts. At absolute magnitude of –6.5 in K, these giant branch tips should be reachable with 10:1 S/N in <4 hours in K, even for the most distant systems, and yield distance accuracies ($0^m.15$-$0^m.2$) comparable to the Cepheid work with HST, in single epoch observations. The required observations would be J, K images of the host galaxies in order to produce K, J-K color magnitude diagrams and locate the giant branches in those CMDs. I band observations hold some additional potential for exploration of the colors and separations of possible metallicity effects, but this depends on the ability to deliver images with sufficiently small FWHM at these shorter wavelengths.

Because the decline rate of type Ia correlates with the properties of the host galaxies, the sample from early type host galaxies has the added attraction of extending the calibration to slower declines than the Cepheid samples (i.e, with $\Delta m_B(15)$> 1.2; see Figure 4.1). The observations will therefore allow exploration and calibration of the full range of supernovae luminosities.

Table 4.3. Supernovae with E or S0 host galaxies

SNe	Host	Est. DM	RGB Tip (K)	Comments
1980N	NGC 1316	~31.0	~24.5	Fornax
1981D	NGC 1316	~31.0	~24.5	Fornax
1986G	NGC 5128	~27.8	~21.3	Centaurus
1991bg	NGC 4374	~31.1	~24.6	Faint, anomalous SN
1992A	NGC 1380	~31.6	~25.1	Very distant
1994D	NGC 4526	~31.1	~24.6	Virgo
1937C	NGC 5253	~28.2	~21.7	Controversial SN
1996ai	NGC 5005	~30.4	~23.9	

4.2.3 MCAO vs CAO Comparison

These observations require accurate photometry of thousands of stars in very crowded fields in the host galaxies. The advantage of MCAO versus conventional AO for this work lies in the ability to extract accurate photometric measures over as wide a field as possible. Conventional AO measures may well be attempted to this purpose and will undoubtedly be tried for targets in the northern hemisphere. To this end multiple pointings would need to be used to produce CMDs with sufficient statistics to identify with clarity the RGB tip. The MCAO FOV would probably produce 10 times as many measures per pointing; a likely strategy for CAO would be to observe

a minimum of 3-4 pointings per galaxy, and thus the multiplex advantaged for MCAO is likely to be between 3 and 10 for this project.

4.3 Stellar Populations in Nearby Starburst Regions -- Bernhard Brandl (Cornell University), Rene Doyon (Universite de Montreal) and Jean-Rene Roy (Gemini Observatory)

Our aim is to investigate the stellar populations in massive star-forming regions located in nearby galaxies; in particular, we wish to investigate the interplay between high and low mass star formation and the processes and timescales for triggered star formation. This program requires a wide field of view and is mainly based on deep JHK broadband imaging to explore the stellar super-clusters of starburst regions in nearby galaxies.

4.3.1 Scientific Background

When and where do massive stars form relative to other stars in stellar clusters? In NGC 6611, the intermediate-mass stars formed both before and after the high-mass stars (Hillenbrand et al. 1993), while in NGC 3293, there may be a temporal progression with mass (Herbst & Miller 1982). What triggers star formation and regulates the overall efficiency? Is it, for example, protostellar outflows from low-mass stars (Nakano et al. 1995; Matzner & McKee 2000), or ionization and compression from high-mass stars (e.g., Brandner, et al. 2000; Walborn, et al. 1999; Hester et al. 1996; Oey & Massey 1995)? Or is the onset of star formation random, following local turbulent compression and gravitational collapse (Elmegreen 1993, 1997)? For example, random birth orders have been suggested for parts of the 30 Dor cluster (Selman et al. 1999), while other regions show a clear age gradient. Or is the process triggered by large-scale disturbances like interaction/merger or passing by galaxy satellites (Drissen et al. 2000; Whitmore et al. 1999). The super star clusters identified in nearby starburst galaxies by HST may be young globular clusters formed during galaxy mergers. The ages of these clusters can be inferred from near-infrared spectra and broad band images.

The stellar initial mass function (IMF) is a vital problem in understanding star formation, and very few measurements exist for a large range of stellar mass in a coeval cluster (e.g., Brandl et al. 2000). A main goal of this project is to better understand the processes that lead to the stellar mass spectrum in a variety of starburst regions close enough to detect their stars individually. Do low-mass stars really dominate the mass of starburst clusters as inferred from the extrapolation of their IMF slopes? Do most stellar members of a cluster form simultaneously, or do low- and high-mass stars form independently in time and space via different physical processes? Is there a universal IMF, and if so what does it look like? If not, how does it depend on environment (metallicity, galactic shear, gas pressure, temperature, total luminosity, total mass). This investigation is an extension to nearby galaxies of the science case for Milky Way young massive star clusters presented in the previous chapter.

The approach is based on studies of resolved stellar populations in the nearby galaxies and studies of the integrated properties of young stellar clusters in more distant galaxies like “The Antennae” or NGC 7252.

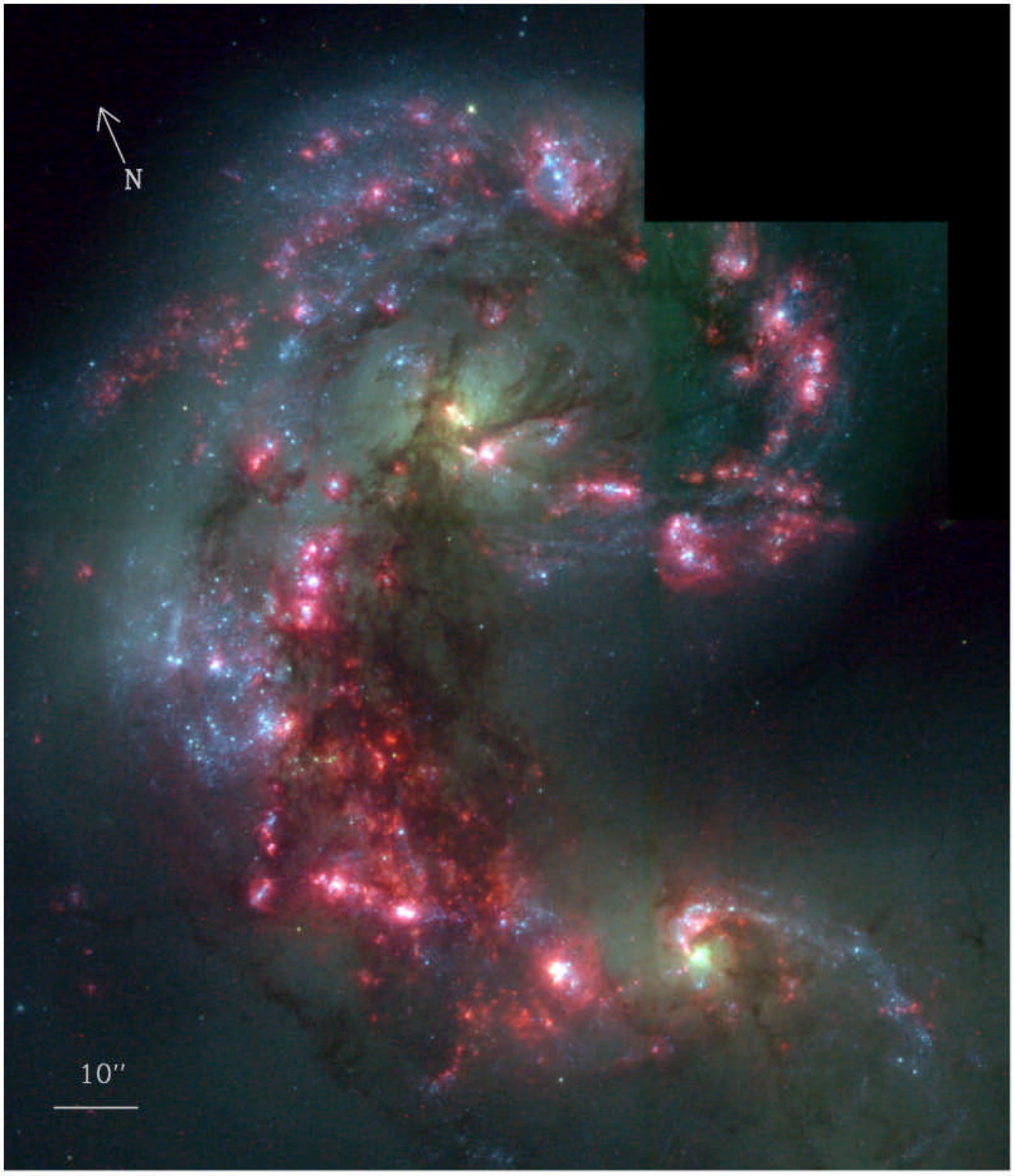

Fig. 4.2 Color image made from HST/WFPC2 UBV-Ha images of NGC 4038/4039, "The Antennae". At least 20 super stellar clusters could be observed with MCAO in this pair of merging galaxies (from Whitmore et al. 1999).

4.3.2 Target super stellar clusters in nearby galaxies

We propose to employ MCAO to obtain deep NIR broadband filter images in J, H, and K-band to determine the stellar contents from sensitive JHK photometry. In addition, thermal L and/or M band images (although probably not sensitive enough to detect disk emission from sub-solar mass stars) would reveal valuable information on embedded massive stars. The later images would come from a thermal infrared imager, not the MCAO imager which will not be sensitive beyond K band.

There are several potential targets in the nearest galaxies:

SMC: NGC 346, N88A, NGC 330, NGC 371

LMC: 30 Dor, NGC 2100, N113, N159, N160

M33: NGC 604, NGC 595, IC 133

The maximum resolution will not be sufficient to resolve stars in the starburst cores in M33 or more distant starbursts in nearby galaxies, but it will be enough for the Magellanic Clouds (see HST images of R136, taken with NICMOS (Brandl et al. 2000, Zinnecker et al. 1999). However, the star clusters in the Antennae (NGC 4038/4039) at 19.2 Mpc appear slightly resolved on HST/WFPC2 images, with median effective radii of 4 +/- 1 pc, similar to or perhaps slightly larger than those of globular clusters in our Galaxy (Whitmore et al. 1999). The Antennae merging pair is the archetype of merging pairs and it is also the closest. It has many hundreds star clusters (Whitmore & Schweizer 1995; Withmore et al. 1999), of which 50 can be considered SSCs. Nineteen of these have I < 19.0 mag which the NIFS team associate with the limit for obtaining reasonable S/N (10 per spectral pixel in 1800 s at Z = 18.5 mag). The youngest SSCs appear to be heavily obscured, so their optical brightness may not reflect their mid infrared brightness correctly. Velocity dispersion in SSCs can also be determined from near infrared spectra of their CO first-overtone absorption bands. Combining these velocities with the measured sizes, it will be possible to infer total masses of the SSCs and to derive the mass function of young globular clusters. This will provide a strong constraint on whether the numerous globular clusters associated with many elliptical galaxies are actually formed during galaxy mergers.

4.3.3 Proposed observations

We aim for the largest MCAO field of view as possible. The regions of interest are of the order of 5 arcmin in size. Multiple guide stars are likely to exist all across the region and the proposed MCAO field of view of 1.5 to 2 arcmin would typically require a 2 x 2 or 3 x 3 mosaics. We would exploit the highest strehl ratios that could be delivered by MCAO; a stable PSF across the MCAO field would be very advantageous. Gemini resolution at the diffraction limit at H band corresponds to the following separations:

LMC	SMC	M33	Antennae
0.013pc	0.016pc	0.163pc	1.6 pc

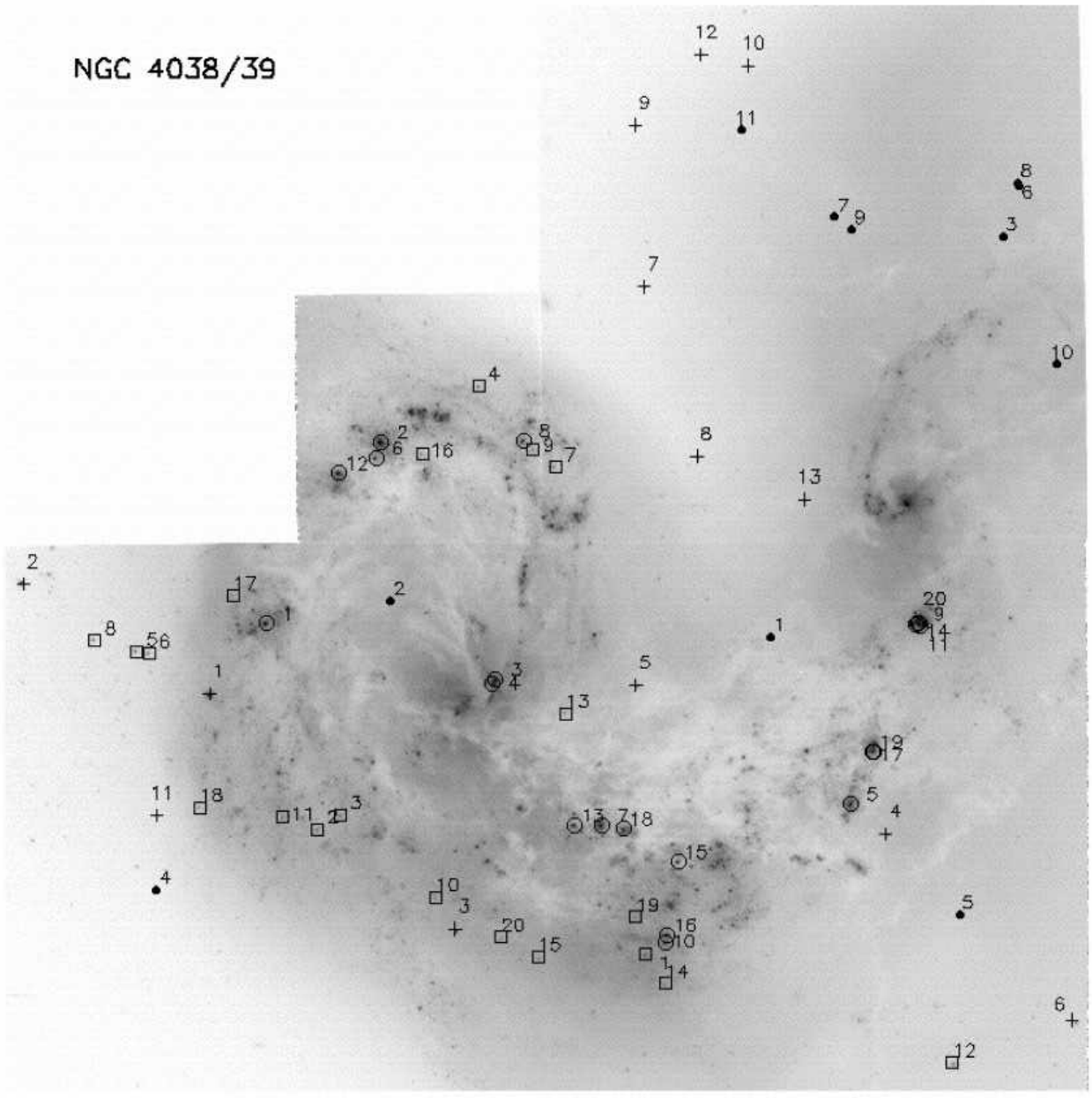

Fig. 4.4. The stellar clusters in "The Antennae" are identified by circles (< 30 Myr) and open squares (500 Myr);. Filled circles correspond to foreground stars (Whitmore et al. 1999).

The program will be based mainly on broadband filter imaging. JHK is mandatory, L-band and PAH features at 3.3 microns would be desirable. Narrowband (R~100) images (e.g, FeII, Br-γ, H2, CO-bh, PAH) are desirable but not mandatory.

Target Density

A handful of young massive star forming regions are well known in each LMC, SMC, M33 and in some local dwarf galaxies. Total is in the order of 20 but in very distinct regions in the sky. At larger distances, several starbursting galaxies (NGC 253, NGC 4038/4039 or "The Antennae", NGC 4214, NGC 5128, NGC 5253, NGC 7252, Henize 2-10) have numerous star forming regions within a 2 arcmin field of view.

For a young (1Myr) and moderately extincted (m_V = 5 mag) region, the observed K-band luminosity of an individual PMS star is as follows:

Mass	LMC	SMC	M33
0.4 $M_¤$	21.5	22.0	27.5
1.0 $M_¤$	21.0	21.5	26.5
2.0 $M_¤$	20.3	20.8	25.8
4.0 $M_¤$	19.2	19.7	25.2

Neglecting crowding and dynamical range, a sensitive Gemini imager would be able to observe individual young stars in the LMC/SMC down to well below half a solar mass, and all OB (possibly A) stars in M33.

The guide star availability for this program presents a two-fold problem: (i) in the LMC/SMC, many guide stars (V < 15) are available but several bright cores which may confuse the WFS; (ii) in M33 and several others objects, no nearby bright (V<15) guide stars available, thus we need LGS necessary, which is an intrinsic advantage of MCAO. Furthermore, large maps with highest spatial resolution and constant PSF are only possible with MCAO.

4.4 The evolution of dwarf irregular versus elliptical galaxies in different environments -- Gary Da Costa (ANU)

4.4.1 Scientific background

Small galaxies come under two species: dwarf ellipticals and dwarf irregulars. Not only their appearance, but some of their fundamental properties like their gas content, star formation history and M/L ratios are dramatically different. Does the environment play a role in governing

the star formation history of dwarf elliptical galaxies? Is there an evolutionary link between dwarf Elliptical and dwarf Irregulars.

The Milky Way companion dwarf ellipticals (called dwarf spheroidals for historical reasons) show a variety of star formation histories. These vary from “basically old” (age larger than about 10 Gyr) to “dominated by intermediate-age” (from 2 to about10 Gyr). The star formation histories also vary in their details. In some cases, they show obvious “episodes” of star formation separated by quiescent periods, while in other cases they behave more alike a continuous star formation process. At present there is little understanding of this diversity of star formation histories.

1. One important clue is that there is a "correlation" with the distance to the Milky Way: the dwarf ellipticals with larger intermediate-age fractions are generally at larger distances. This hints at the influence of parent galaxy/environment. Possible factors include tidal influence, Galactic winds, ram pressure stripping, high X-ray or UV-flux. In short, anything that might affect gas content evolution or conditions for early star formation.
2. In the M31 system, at least for the lower luminosity dwarf ellipticals (i.e. not 147/185/205), the situation is strikingly different. The intermediate-age population class objects are less obvious compared to the Galaxy’s companions, e.g. there is no system known around M31 to have any population younger than approximately 5 Gyr, whereas there are at least 3 Galactic companions with ~1-3 Gyr populations. Also, the system with the youngest intermediate-age population (~6-8 Gyr) is the most distant from M31.
3. There are low-luminosity galaxies, mostly dwarf irregulars or transition objects, in the Local Group that are not directly associated with the Galaxy or M31 (e.g. WLM, LGS3, and Phoenix). All contain young stars and varying amounts of HI. This again hints at some effect from the environment.
4. Two dwarf ellipticals in the M81 group, which is a much more compact environment than the local group, have been studied with HST. Both systems show strong upper-AGB populations - i.e. stars more luminous than those of the RGB tip. This by itself is an indication of significant intermediate-age population. The intermediate-age populations in Galactic dwarf ellipticals were actually first recognized via identification of the upper-AGB (carbon) stars.

4.4.2 Proposed Observations

The plan is to measure J, K magnitudes for these stars, which should give bolometric magnitudes which in turn yield age estimates (the luminosity of AGB-tip is brighter for younger ages). The near-IR wavelength domain is also an advantage for these studies since variability (all upper-AGB stars are variables at some level) is much less in the near-IR than in the optical. The current plan with NIRI is to survey other M81 group dwarf ellipticals for luminous upper-AGB stars. The detectivity limit with NIRI (and Flamingos-I/II) basically allows surveying dwarf ellipticals in the local group or nearby groups as the M31 group. However to go further requires access to fainter limiting magnitudes that only MCAO can provide. In the southern hemisphere, the dEs in the Centaurus group and in the most distant part of the Sculptor Group are prime targets. Going further in distance, there are the Leo I Group, the Fornax galaxy cluster and the loose association of galaxies that contain the Circinus Galaxy at a distance of 6-7 Mpc .

4.4.3 Why MCAO & advantage versus CAO

Basically, with MCAO one should be able to study dwarf ellipticals out to larger distances and thus in a larger variety of environments - from loose and low density groups to more compact denser groups. With MCAO it becomes possible to image (resolve) all dwarf ellipticals up to 10 Mpc.

M_{bol} has to be determined to ±0.2 mag, which translates into a S/N of about 10 or higher in both J and K. To reach K~23 and J~24 with S/N of 10 at 9 Mpc, about 3 hrs/galaxy are needed. It is thus certainly practical to survey 10 - 20 galaxies (or more) in a medium size program.

This program requires a stable PSF for accurate photometry over as wide a field as possible (1 arcmin is acceptable given the sizes of distant dwarf ellipticals) with appropriate pixel scale. Finding guide stars should not be a major issue. Given the claimed sky coverage of 10-50%, this should just be a matter of initially selecting the dwarf elliptical sample to be those with suitable guide stars.

It has to be noted that this program is not doable with classical AO, given the field and the PSF stability requirements. It is crucial to have an accurate photometry over the entire field-of-view (this requires a stable non-varying PSF) and a maximum field-of-view to fully sample the entire dwarf elliptical.

4.5 The Early Chemical Enrichment Histories of Nearby (r < 10 Mpc) Galaxy Spheroids --Tim Davidge (HIA)

The traditional view of galaxy formation is that spheroids, which here refer not only to elliptical galaxies, but also to the halo + bulge components of disk systems, formed during early epochs as the result of a rapid, dissipative, collapse. However, there is growing evidence that this picture is overly simplistic, and that hierarchal merging plays a key role in spheroid evolution, especially in low density environments. A further complication for bulges is that gas from the surrounding disk may be driven into the central regions of the galaxy, thereby triggering episodes of star formation well after basic morphological properties (e.g. M_B, ellipiticity, bulge to disk ratio etc) were imprinted. The metallicity distribution function (MDF), which is the histogram distribution of stellar metallicities, is a key diagnostic for probing the collapse history of galaxies. Simple monolithic collapse models predict well-defined MDFs, with total system mass being the prime parameter defining the chemical enrichment history of the system (e.g. Arimoto & Yoshii, A&A, 173, 23). On the other hand, low mass systems that experience independent chemical enrichment histories prior to merging to produce larger spheroidal systems will have MDFs that depart from the monolithic collapse predictions.

MDFs can be determined from stars evolving on the red giant branch (RGB). While spectroscopy is the prefered means for determining metallicities, this can only be applied to systems within a few Mpc given that stars near the RGB tip have $M_I \sim -4$. In any event, the strongest absorption features, such as the MgH bands at visible wavelengths or the near-infrared Ca triplet, only monitor the abundances of certain elements, and do not track mean metallicity. The photometric properties of giants provide another means of determining metallicities in stellar systems with ages < 3 Gyr, where the effects of age on RGB colors are minor, and this technique

can be applied out to distances in excess of 10 Mpc using AO-compensated data obtained with an 8 metre telescope.

The greatest sensitivity for photometric metallicity determinations occurs on the upper 1 mag of the RGB. A complicating factor is that this portion of the RGB contains the stars with the coolest effective temperatures, and if these have metallicities that are solar or higher then the spectral-energy distributions at visible wavelengths will be affected by line-blanketing, with the result that at wavelengths shortward of 1 micron these objects will be significantly fainter than more metal-poor giants with comparable ages. This introduces a bias against detecting the most metal-rich stars. The effects of line blanketing are much reduced at infrared wavelengths, and deep J and K images can be used to construct MDFs spanning the full range of metallicities.

HST has been used to investigate the MDF of galaxies as distant as Cen A (r ~ 3 Mpc, Harris et al. 1999, AJ, 117, 855). An intriguing result is that the MDF of this galaxy cannot be modelled by a simple one-zone chemical enrichment model. Rather, the MDF appears to require at least two enrichment events, which Harris et al. (1999) suggest are the result of two collapse episodes. The MDF of the Local Group compact elliptical galaxy M32, as constructed by Grillmair et al. (1996, AJ, 112, 1975), is remarkably similar to that of Cen A, despite obvious differences in environment and integrated system mass. These data suggest that the star forming histories of spheroidal systems may be very different from that predicted by traditional models.

With MCAO on Gemini it will be possible to obtain deep J and K images sampling the RGB-tips of spheroidal systems and spiral galaxy disks out to distances that include the Virgo cluster; hence, MDFs could be constructed for systems spanning a range of masses, environment, and morphologies. These observations require diffraction-limited image quality to obtain reliable photometric measurements of stars that are, by traditional standards, extremely faint, and also to resolve individual objects in very crowded environments. Field of view is also of great importance as large numbers of stars must be surveyed to properly sample the entire range of metallicities in a system, and a moderately stable PSF across the field is essential.

4.5.1 Program Summary:

Intrinsic brightness of sources:

M_K = -6.5 (RGB-tip)

Observables:

Deep J and K images, with 10-sigma accuracy at K = 24 (RGB-tip in the Virgo cluster)

Sample targets:

Maffei 1, NGC 3379, Virgo cluster ellipticals and spirals

Observing Requirements:

- diffraction limited resolution (a Strehl ratio in excess of 0.3)
- stable PSF over a field comparable to the scale lengths of bulges and ellipticals in the Virgo cluster (ie. 30 - 40 arcsec)

Key diagnostics:

K vs (J-K) color-magnitude diagrams.

4.6 Intergalactic Stars -- Ted von Hippel, Gemini Observatory

The formation of galaxy clusters involved interactions and mergers of galaxies, the injection of hot gas into the intergalactic medium via galactic winds, and the tidal ablation of stars from the mean gravitational shear of the cluster. It is likely that most of this activity occurred during the initial collapse phase of the cluster (Merritt 1984, ApJ, 276, 26), leaving stars floating freely in the overall cluster potential. Numerical simulations suggest that between 10% and 70% of the initial mass in galaxies is released into the intergalactic medium (Miller 1983, ApJ, 268, 495). Recently Ferguson, Tanvir, & von Hippel (1998, Nature, 391, 461) employed deep HST I-band observations to directly detect intergalactic red giant branch stars in the Virgo cluster. They found that 5 to 10% of the stars in the Virgo cluster are in the intergalactic component within the observed cluster radius. Observations of intergalactic planetary nebulae in both Virgo (Feldmeier et al. 1998, ApJ, 503, 109) and Fornax (Theuns & Warren 1996, MNRAS, in press) arrive at even more substantial intergalactic populations. Observations of intergalactic red giants and planetary nebulae offer exciting possibilities to a) probe galaxy cluster mass distributions via planetary nebulae radial velocities, b) determine the source of the intergalactic stars by measuring their metallicities, and c) determine the interplay of galaxy collisions versus violent relaxation of the cluster via the distribution of intergalactic stars throughout the cluster.

It is unlikely that the diffuse stellar component in galaxy clusters will be distributed uniformly. Low luminosity dwarf galaxies, like those surrounding the Milky Way, will appear as loose concentrations of stars, while fragments of relatively recent collisions may persist as coherent streams of material. Finally, galaxies passing through the diffuse sea of stars will presumably leave a wake.

Nothing is known about the metallicity distribution function (MDF) of the diffuse stellar population, and there are no published predictions. It can be anticipated that the stars should be relatively metal poor when compared with the mean luminosity-weighted metallicity for the visible galaxies, as tidal effects will tend to strip the most loosely bound objects, which are located in the outskirts of galaxies, and hence are metal-poor. A direct measurement of the MDF of the intergalactic population is a first step to understanding its relationship to the visible galaxies.

A more obvious prediction is that the MDF of the intergalactic population should be spatially uniform. The visible galaxies in Virgo constitute a uniform population, in the sense that metal-rich and metal-poor galaxies have roughly the same degree of central concentration. Hence, there should not be a radial gradient in the metallicity of the intergalactic stellar population. If one were found, it would have profound implications for understanding cluster evolution, since it could imply that the intergalactic stars formed in situ from, for example, the cluster cooling flow. The search for radial abundance gradients is relatively straightforward, since it relies only on a differential comparison of fields, rather than an absolute calibration of the photometric system.

While the ability to measure planetary nebulae radial velocities is just within reach of ground-based 8 and 10 meter telescopes with existing or planned optical spectrographs, efforts to fully probe the gravitational potential of the intergalactic stars must await much larger telescopes and/or wide-field AO (i.e. MCAO). The initial detection of the intergalactic population in Virgo required just over nine hours with HST in the I-band, and measurements at shorter wavelengths will be difficult to obtain given the cool temperatures of these stars. However, these objects are detectable in JHK, and photometric measurements at these wavelengths are required to measure the color of these stars, and thereby their metallicity. We expect the detection of the tip of the RGB in the near-infrared to take a few hours with MCAO on Gemini. Dozens of fields are required to measure the spatial profile of the intergalactic population, as well as to test for metallicity differences as a function of cluster position; consequently, studies of the intergalactic population are well-suited to MCAO.

4.6.1 Program Summary

Intrinsic brightness of sources:

M_K = -6.5 (RGB-tip)

Observables:

Deep J and K images, with 10-sigma accuracy at K = 24 (the RGB-tip in the Virgo cluster). Crowding is not a problem.

Sample targets:

Fields in Virgo cluster sampling a range of cluster positions. This same technique may also be applied to the Fornax cluster.

Observing Requirements:

- diffraction limited resolution (Strehl ratios in excess of 0.2 - 0.3 in K; superb imaging conditions will be required in J)
- a stable PSF over a field comparable to galaxy scale lengths in Virgo (i.e. on the order of arcminutes)
- control fields to measure the densities of foreground and background sources.

Key diagnostics:

K vs (J-K) color-magnitude diagrams.

4.7 Extragalactic Globular Clusters -- Ray Sharples (Durham University)

Globular clusters (GCs) are homogeneous stellar systems containing stars of a predominantly single age and metallicity. They are the brightest individual objects that can be resolved in early-type galaxies, and hence can be used to study the properties of these systems to larger distances than is possible with resolved stars. Although the relative efficiency of star formation in GCs with respect to the field is not fully understood, there is good evidence that GCs form during starburst activity, which might occur during the initial collapse of a protogalaxy, or during major

merger events; hence, GCs provide an important probe of critical episodes in the star formation and chemical enrichment history of their host galaxy.

A key development has been the discovery that the GC systems in many elliptical galaxies have bimodal color distributions. This indicates the presence of at least two distinct GC populations, with different ages and/or metallicities. The systematic properties of how the subpopulations vary with properties such as galaxy luminosity and environment are still poorly understood.

The comparison of GC subpopulation properties with model predictions (e.g. Ashman & Zepf 1992; Forbes et al. 1997) can help constrain and improve galaxy formation theories. The key to testing the different models is in determining the age, metallicity and kinematics of the GC subpopulations over a range of environments.

Spectroscopy provides the most direct method for determining cluster properties. However, obtaining these data can be a time consuming process, which is only feasible on 8-10m class telescopes for the closest ellipticals. On the other hand, imaging studies can sample a much larger number of GCs, while providing information on the spatial distribution and broad-band colours of clusters. An added benefit of imaging is that for nearby galaxies direct measurements of cluster tidal radii (r_t=0.6 arcsec at D=10 Mpc) and ellipticities can be made, which would allow constraints to be placed on the orbit eccentricities due to tidal truncation. Finally, with imaging data it will be possible to study the GC luminosity function, which will provide insight into the dynamical evolution of the GC system.

Contamination from foreground stars and background galaxies is a complicating factor for imaging studies, although stars and galaxies can be identified using the size and spatial distribution of sources. Luminous old GCs have half-light radii in the range 3-5pc. With HST/WFPC2, clean samples of GC candidates have been isolated on the basis of image parameters out to D=15 Mpc (r_e=0.04-0.07 arcsec; Gebhardt & Kissler-Patig 1999). The spatial distribution of GCs closely follows that of the parent galaxies, with typically half of the cluster population contained within 1-2 arcmin of the centre, which is well matched to the corrected field of MCAO.

So far, the discussion has focused on populations of old GCs. However, populations of apparently young GCs have been identified in recent merger remnants (e.g. Holtzman et al 1992; Zepf et al 1999). The most luminous of these are significantly brighter than the most luminous clusters in the Milky Way. Deep MCAO images would enable the structural parameters of these objects to be probed to determine if they will eventually evolve into a population with characteristics similar to old GCs. If a direct link can be established then studies of young GC systems may provide clues into conditions that prevailed during the early stages of galaxy formation.

4.7.1 Program Summary

Intrinsic brightness of sources:

M_H = -14 (brightest GCs), M_H = -10 (GCs at turn-over point in the LF)

Observables:

Deep I and H images will be needed. To observe GC systems in the Coma cluster (μ_0 = 35), and hence sample a range of extreme environments, it will be necessary to obtain photometry with 10-sigma accuracy at H = 25. These observations would be supported with deep optical imaging from the ground and with the HST + ACS.

Sample targets:

Early type galaxies in Virgo, Fornax, and Coma clusters. Merger remnants with μ_0 = 34 (N1275, N3256, N4038, N3597, N7252), and selected field galaxies.

Observing Requirements:

- diffraction-limited imaging in H, with S/N = 20 at H = 25 (and K?)
- stable PSF over 1 - 2 elliptical galaxy scale lengths in the Virgo cluster (i.e. 40 - 80 arcsec)
- natural tip-tilt star constellation must be able to cope with large extended objects (half-light radii ~1') in the field!

Key diagnostics:

(I-H) [and (J-K)?] colours

H [and K?] LF

Image concentration index to probe the structure of individual GCs in nearby (ie. r < 10 Mpc) systems

4.8 SIMULATIONS – Francois Rigaut (Gemini Observatory) and Tim Davidge (HIA)

In the following simulations, we have tried to quantify the gain (or absence thereof) brought by MCAO compared to CAO in various situations. The first simulation deals with crowded Galactic fields, an example of which is the Galactic Center or a typical globular cluster. The second simulation is directly linked to the determination of the RGB tip in galaxies at the distance of the Virgo cluster. The goal of the simulation was to determine whether the RGB tip was detectable and with what kind of accuracy. For both simulations, we have chosen a luminosity function (Galactic Center LF for case 1, LF of the RGB+AGB for case 2; for more details see the appropriate section below).

The fields were generated using field variant PSFs computed using the Monte-Carlo MCAO simulation code of FR. These PSFs include both the atmospheric residuals and all other sources of aberrations (static aberrations of the telescope, instrument, alignment errors according to a simple model), so these images represent what we expect will be the final MCAO product under median seeing conditions (r_0=16.5cm at 550nm).

4.8.1 Crowded Galactic field

To generate this field, we actually used a measured LF on the Gemini galactic center data set that we completed up to K=30 in an effort to take into account the continuous stellar background. This main stellar component was set to have a color H-K=0. In addition, we added a fake "horizontal branch" (that could also be seen as a red clump for the sake of this simulation) at K=17, with random color (H-K in the example reported here) uniformly distributed between –2 and +2. The net results are color-magnitude diagrams with a vertical component (H-K=0), plus an horizontal component (K=17, |H-K|<2). This simple scheme allows a determination of both the errors on the color and on the K magnitude in a single run. The figure 4.5 shows the K luminosity function used to generate these images.

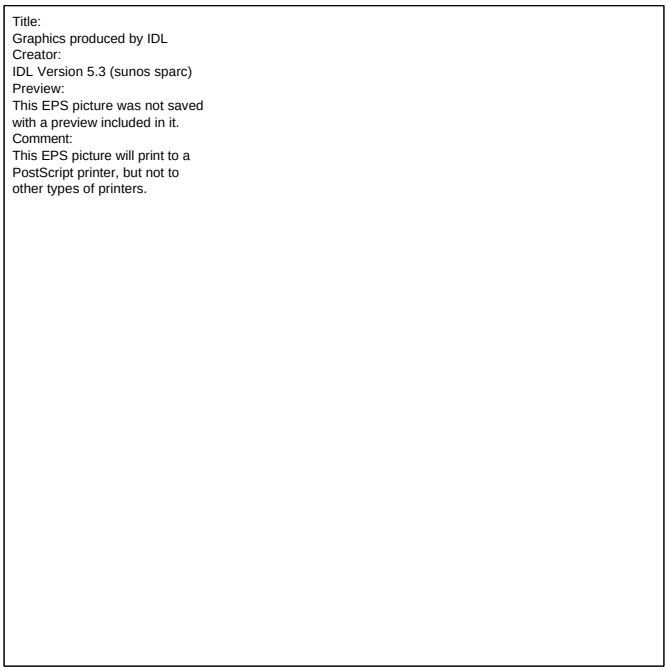

Figure4.5: K Luminosity Function used to generate the "galactic stellar field"

Both H and K images used here are representative of what could be expected on a 30x30 arcsec field with the guide star in a corner, i.e. it is roughly equivalent to one quadrant of the strawman MCAO imager (80x80 arcsec). Conditions are approximately equivalent to what was obtained on the Gemini Galactic center data, as shown in figures 4.6, 4.7 and 4.8: Figures 4.6 show the field used for the simulation reported here. In this image, the guide star was chosen to be at the center of the field. For this simulation, we used the lower left quandrant of this field. Figure 4.7 and 4.8 show images that were actually obtained during the demonstration science observations of the galactic center, in K band and H band. The field in the large image (upper right image in each figure) is 40 arcsec on a side. Although the Strehl ratio is lower in these images than the one in the MCAO simulated image, one can see similar anisoplanatic image quality loss in the simulated and actual images. Note that the conditions under which these images were obtained are quite severe (airmass~1.7). However, we are also considering the red end of the spectrum (bands H and K) for which the anisoplanatic effects are the less severe. Similar results are expected for shorter wavelengths (J) at smaller airmass (1.2-1.3). Each image was generated with space variant PSFs provided by the MCAO/CAO Monte-Carlo code written at Gemini by FR. The images are equivalent to one hour exposures. Photon and background noises were taken into account.

Figures 4.9 and 4.10 show the results of the photometric analysis of the H and K images. We have used the "Starfinder" package, which was developed at University of Bologna (Italy) exclusively for the photometric analysis of Adaptive Optics images. It is comparable to DAOPHOT, and has shown similar performance on test cases (Diolaiti et al, Proc SPIE 4007, p879, 2000). Each figure shows the reconstructed CMD and the H and K images from which the photometry was extracted. As seen in both CMDs, the detectivity limit is K~20-21, i.e. far from

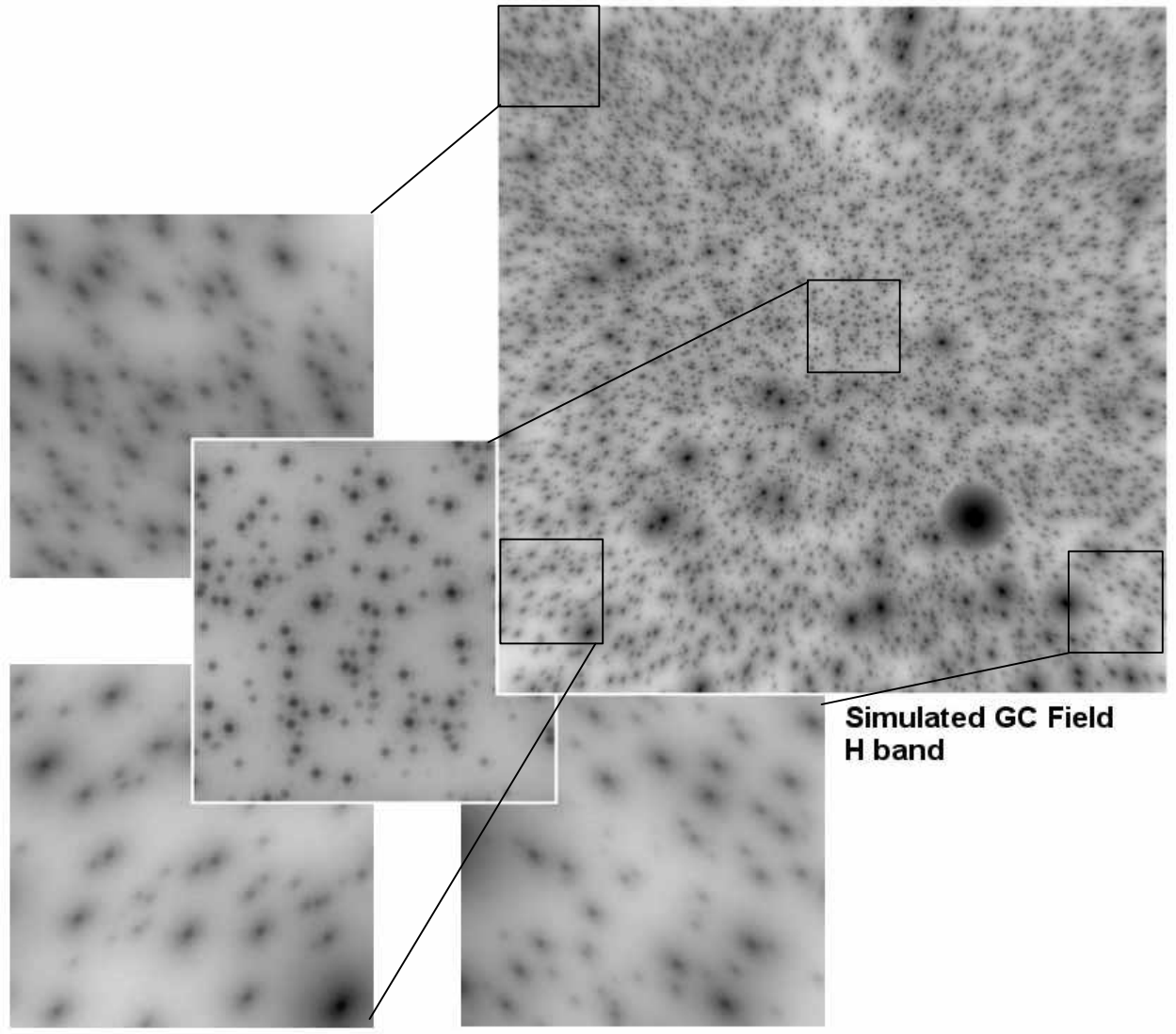

Figure 4.6: Example of classical AO field simulated for the galactic stellar field photometric analysis.

the limit reported in section 2.6. This is because the limit is imposed here by the crowding, not by the ultimate background noise.

The most striking effect in the CAO CMD (fig 4.10) is the very large scatter, both from the "horizontal branch" and the color. This dramatic effect is solely due to the PSF variation. It has to be noted that no effort was made in this simulation to take into account the PSF variation in the photometric processing. This is a rather extreme case. However, it is effectively very difficult in crowded field like this one to extract a valid PSF in the small sub-fields in which the PSF can be deemed to be constant. Indeed, in this example, the PSF varies significantly over *a few* PSF radii. Therefore it is difficult to get a large enough number of stars to extract a statistically significant PSF.

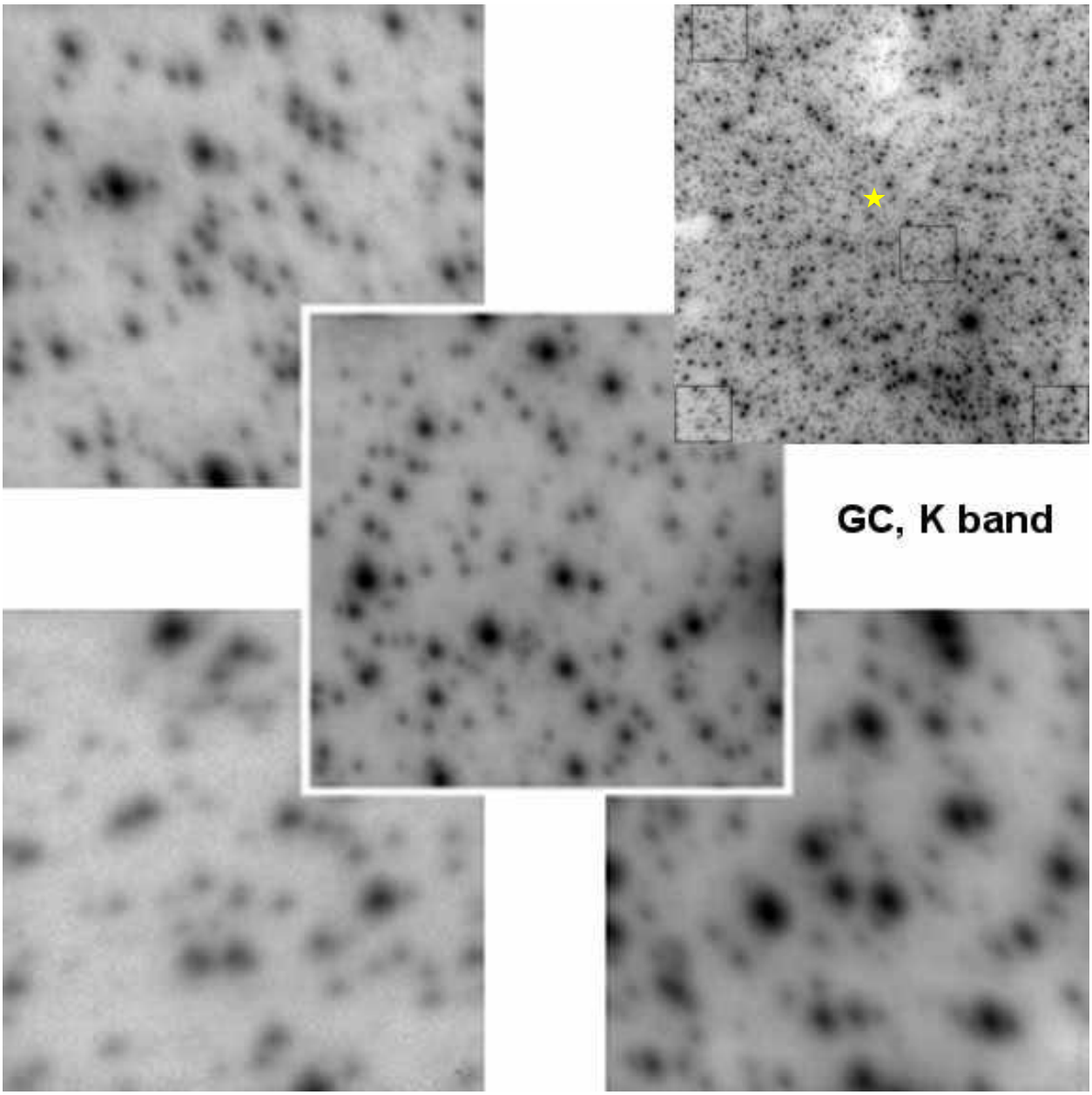

Figure 4.7: Example of anisoplanatic image quality degradation in an actual K band image from the galactic center obtained with Hokupa'a on Gemini during the demonstration science runs. The field shown in the upper right panel is 40 arcsec on the side. The 4 other images are subfields of 5x5 arcsec, as indicated by the squares in the upper right image. Their respective location in this figure is as in the upper right image (i.e. the center image is the center image in the large field). The guide star location is marked by the yellow star.

This point deserves some explanations: the AO PSF, as noted before, shows a very prominent bi-modal feature: a narrow core (roughly λ/D) on top of a broad halo (roughly the seeing size). The latter contains a significant fraction of the energy (roughly 1 minus the Strehl ratio), therefore can not be ignored. The PSF given to the photometry analysis code should therefore extend over an area which is several times the seeing, i.e. typically a few arcsec. But the isoplanatic patch in its strictest and more general sense -that is the area in which the PSF does not vary- is very small. If one tolerates a variation of only a few percent of the Strehl ratio, this isoplanatic patch is a few

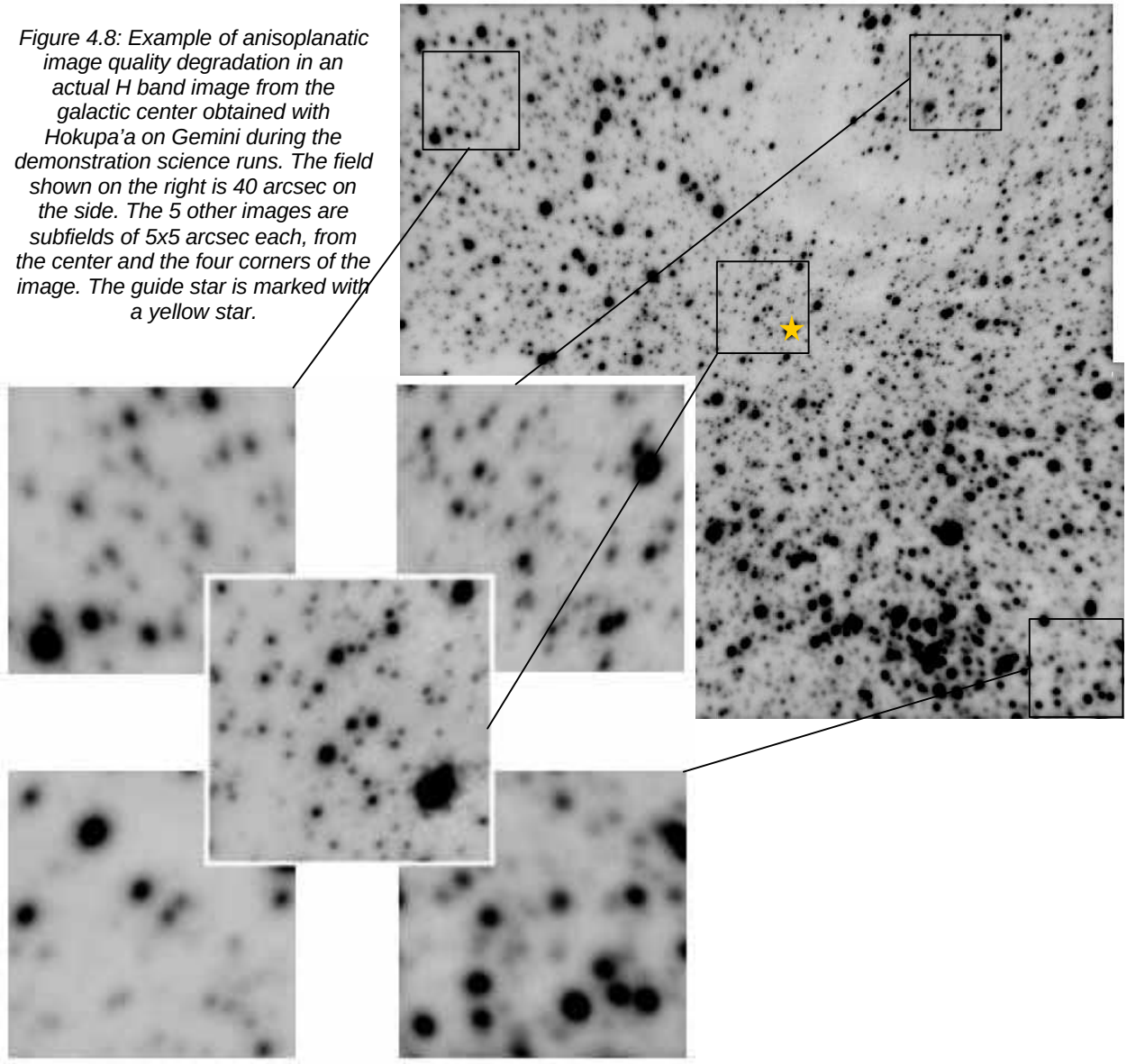

Figure 4.8: Example of anisoplanatic image quality degradation in an actual H band image from the galactic center obtained with Hokupa'a on Gemini during the demonstration science runs. The field shown on the right is 40 arcsec on the side. The 5 other images are subfields of 5x5 arcsec each, from the center and the four corners of the image. The guide star is marked with a yellow star.

arcsecs in J or H band. If one considers in addition that to extract a PSF from an image of a crowded field, many stars are usually needed, the problem is now obvious: How to find these "many" 3'' extended stars, preferably not overlapping too much, in a typically 10x10 arcsec area? The solution to this problem generally involves making assumption over the behavior of the PSF off-axis from the guide star. But these assumptions are usually rather approximate (unless one has a whole bank of turbulence sensors), and usually lead to at least 5-10% error on the photometry.

This effect is illustrated in the CAO CMDs (fig 4.10), which show an rms error on the K magnitude of approximately 0.2 (at the "horizontal branch"). In contrast, the MCAO CMD (fig 4.9) show a rather clean sequence, with no detectable bias, and rms errors on the color between 1% (K<16) and approximately 5% (K=20). The number of detected stars for the CAO and MCAO cases is similar (878 stars retained for CAO, 961 for MCAO).

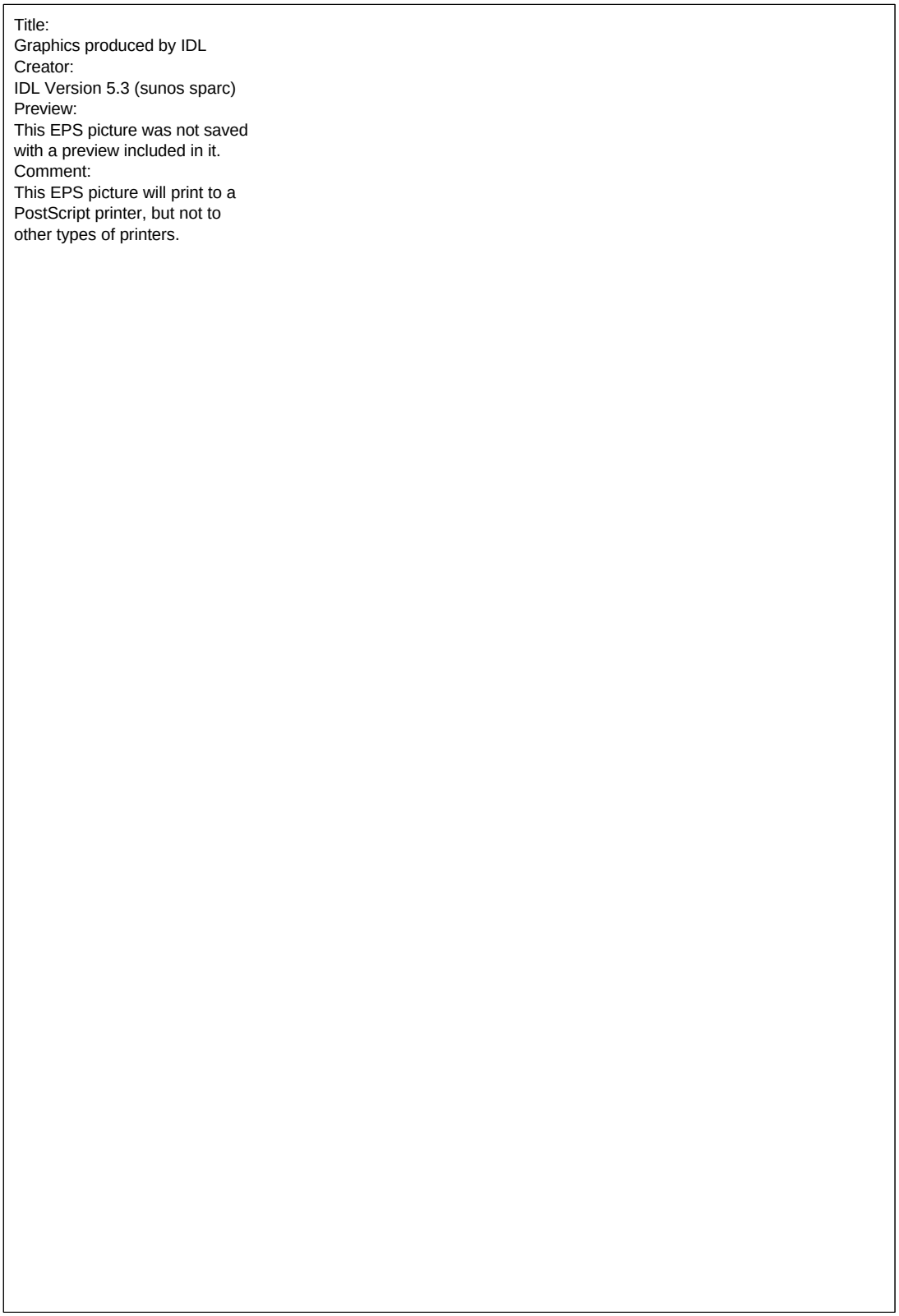

Figure 4.9: H,K CMD for the simulated galactic field observed with MCAO

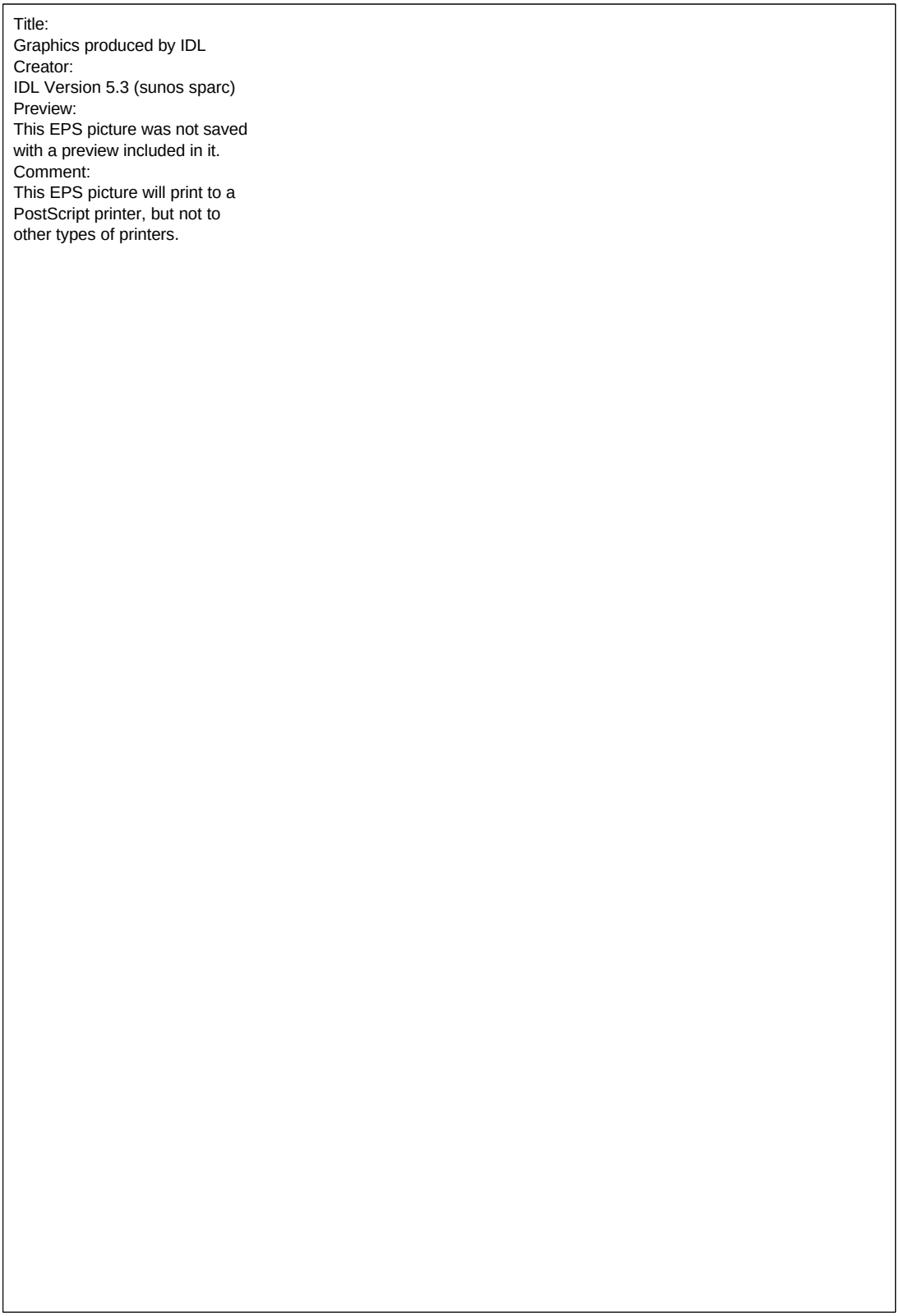

Figure 4.10: H,K CMD for the simulated galacic field observed with Classical AO

4.8.2 Very crowded Virgo Field

Models of crowded stellar fields have been used to assess the benefits of MCAO with respect to conventional single-star AO. Model images corresponding to those produced by a conventional single star AO system and an MCAO are presented in Fig.4.11. The models include the effects of anisoplanicity appropriate for conventional AO and MCAO. The simulated stellar fields contain 10,000 stars between K = 24 and K = 25 distributed over a 1 square arcmin. This brightness range was selected because it corresponds to the magnitude of the top of the giant branch at the distance of the Virgo cluster. A population of fainter stars, extending to K = 26.5, in numbers that follow a power-law LF with exponent 0.3 and which holds throughout the upper portions of the Galactic bulge (Davidge 2000, submitted to AJ), was also added to form a background. Stars between K = 23.5 and 24 were also added, in numbers that correspond to 25% of those between K = 24 and 24.5, to represent an AGB component. All stars have J-K = 1, which is a roughly appropriate for a metal-rich population. Noise that corresponded to an integration time of 6 hours on Gemini was included.

The brightness of individual stars was then measured using the PSF-fitting routine ALLSTAR. The PSF is a critical element of this analysis. For conventional AO it is clearly desirable to construct a PSF that is variable across the field, to correct the effects of anisoplanicity. However, it is very difficult to construct a variable PSF in crowded fields using current photometry routines, since the effects of crowding and PSF variability cannot be decoupled unless a large number of very bright objects are present (same argument as in the previous section). Given this difficulty, a single PSF was constructed for each filter + field combination.

Observations of globular clusters with the CFHT AOB indicates that a single PSF introduces photometric errors of only a few hundredths of a magnitude (Davidge & Courteau 1999, AJ, 117, 1297; Davidge 2000, ApJS, 126, 105) in (K, J-K) CMDs over a 30 arcsec field of view centered on the guide star during median seeing conditions. Given the inability to track PSF variations, the analysis was restricted here to a 15 x 15 arcsec field in an effort to present a comparison that is most favorable for conventional AO.

The CMDs constructed from the most crowded case images are compared in Fig.4.12; the results for the “on-axis” image –i.e. centered on the guide star in the CAO case- are shown in the top row. The bottom row show the results obtained on the off-axis field, in the corner of the 1’x1’ MCAO field of view. The input CMD is shown on the left. The results obtained using the classical AO images are in the middle, while the right CMDs are from the MCAO images. The difference is striking. While the CAO and MCAO CMDs from the on-axis images are similar – althought the MCAO CMD goes slightly deeper and shows marginally less scatter- the off-axis CMDs demonstrate a clear advantage for MCAO, with which many more object are detected. The gain is larger than 1 magnitude and the scatter is significantly less. MCAO has therefore a distinct advantage with respect to conventional AO for photometric programs that utilize the current generation of photometric tools (i.e. that are best suited for constructing a single PSF). If extended to data covering an even larger field of view the differences between results generated with MCAO and conventional AO will become even larger.

The noise in these CMDs is dominated by crowding and by photon/background noise, and is not a feature of AO compensation.

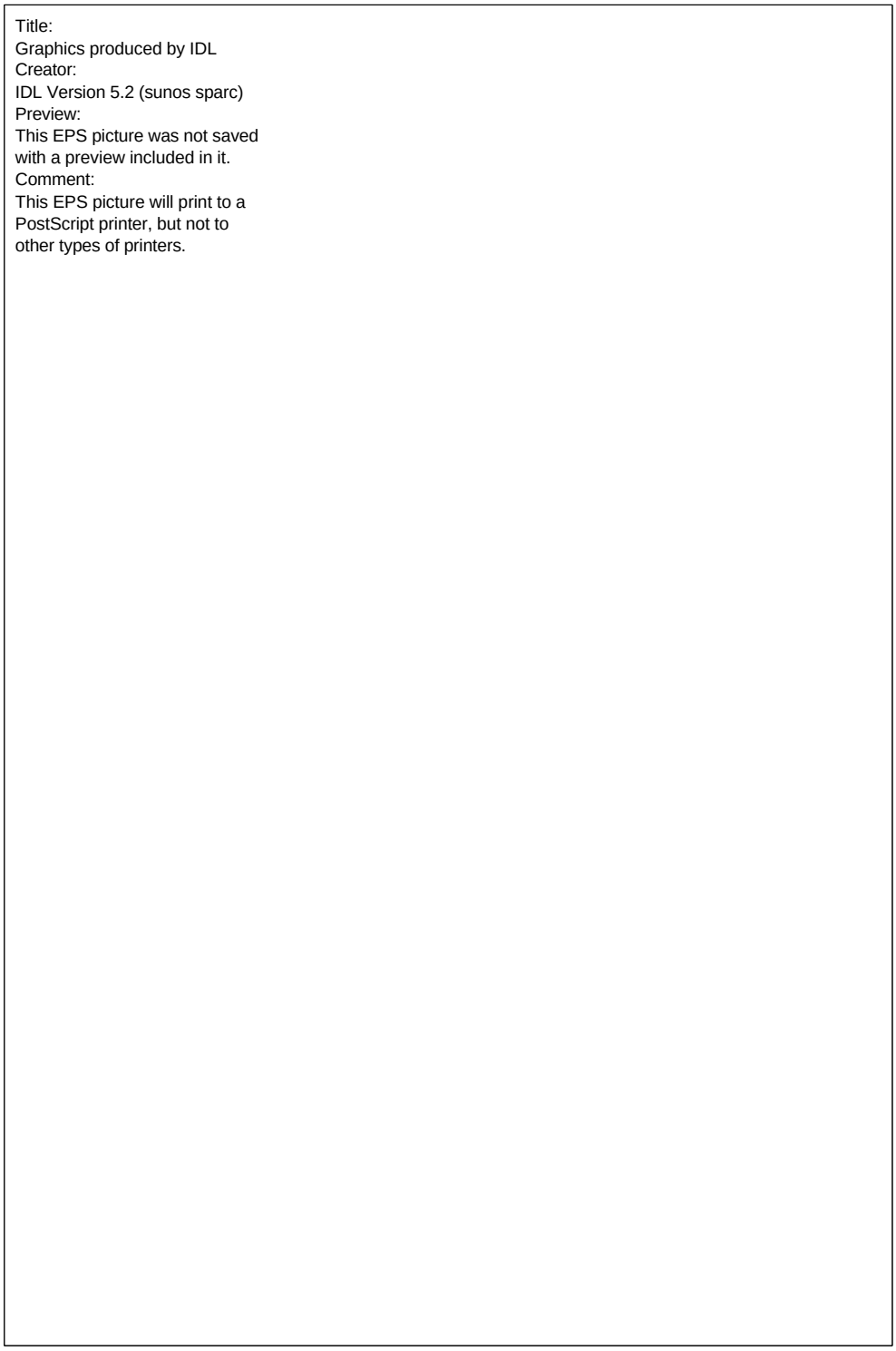

Figure 4.11: Images generated for the analysis. Each image is 11"x11" (full images are 15"x15"). "On-axis" refers to images centered on the AO guide star or in the MCAO field. "Off-axis" images shown here are centered on a point 35" away from the AO guide star / MCAO field center, in a corner of the 1'x1' MCAO field. Not shown is the seeing limited J band image (very similar to the K seeing image) and the On-axis K band image, which is very similar to the off-axis MCAO K band image. The On-axis J and K band MCAO images are basically identical to their off-axis counterpart, and are not shown.

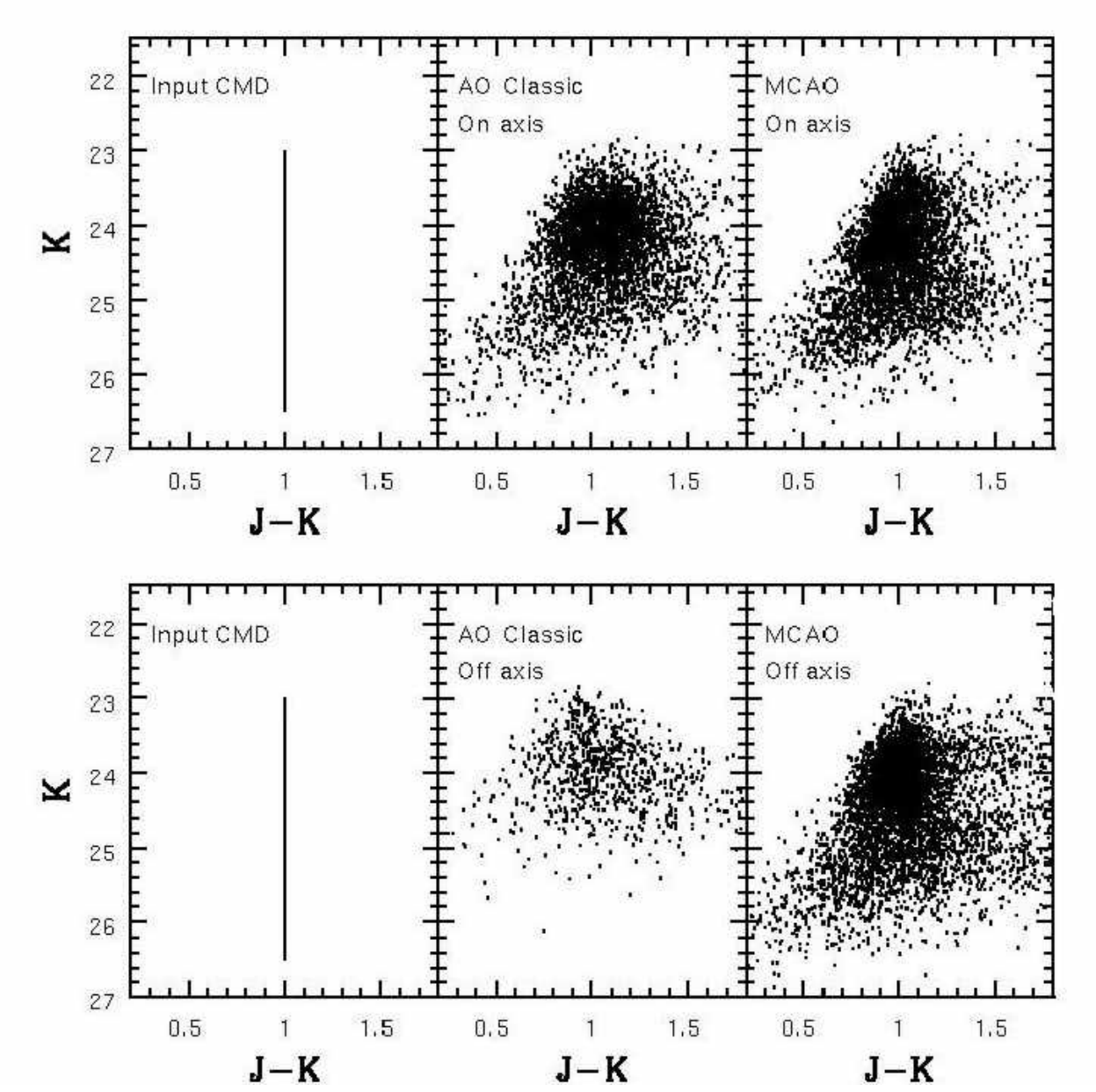

Figure 4.12: CMDs for the on-axis and off-axis Virgo fields. Input CMD (left). CMD found with Classical AO images (center) and with the MCAO images (right).

4.9 Instrument Requirements

The following basic requirements can be drawn from the science cases described above:

1. The MCAO system shoud be fitted with an imager of the largest field possible. The proposed 80x80 arcsec is adequate. Proper samplign is very important, but the compromise proposed in the strawman imager is acceptable.

2. PSF uniformity is of the utmost importance for accurate stellar photometry and should be one of the main priority with high Strehl and large field of view.

3. The MCAO system must be capable of delivering a moderately high Strehl ratio. It is the experience of a few of us (e.g. Davidge & Rigaut) that significant improvements in photometric performance occur when the Strehl ratio exceeds a few tenths.

4. The MCAO system must be capable of exploiting the best imaging conditions. This is of particular importance for the J band, as even modest Strehl ratios near 1.3 microns require superb imaging conditions. This means that the MCAO system must be deployable on a short time scale so that rare seeing opportunities can be exploited.

5. The integration times for some of the programs described above are lengthy (on the order of a night), and so the MCAO system must be capable of working for long periods of time. This means that the system should be insensitive to changes in sky background (which will vary with the phase of the moon, and may effect the ability to use faint guide stars), and sky transparency (e.g. if clouds are present).

Finally, studies of globular clusters with the CFHT AOB indicate that the typical atmospheric conditions on Mauna Kea are such that good photometric performance (i.e. errors in photometric brightness of a few percent) can be achieved over the 30 x 30 arcsec field of the KIR imager (e.g. Davidge & Courteau 1999, AJ, 117, 1297, Davidge 2000, ApJS, 126, 105). To be worthwhile, the Gemini MCAO must be capable of significantly improving upon this observing efficiency. This is not simply a matter of enhancing the field of view, since if the Strehl ratio is degraded markedly then there will be a loss in efficiency.

References

Hamuy, M., Phillips, M. M., Schommer, R. A., Suntzeff, N.B., Maza, J., & Aviles, R. 1996a, Astron. J., **112**, 2391

Perlmutter, S., Gabi, S., Goldhaber, G., Goobar, A., Groom, D. E., Hook, I. M., Kim, A. G., Kim, M. Y., Lee, J. C., Pain, R., Pennypacker, C. R., Small, I. A., Ellis, R. S., McMahon, R. G., Boyle, B. J., Bunclark, P. S., Carter, D., Irwin, M. J., Glazebrook, K., Newberg, H. J. M., Filippenko, A. V., Matheson, T., Dopita, M., & Couch, W. J. 1997, Astrophys. J., **483**, 565.

Phillips, M. M. 1993, Astrophys. J. (Letters), **413**, L105

Phillips, M. M., Lira, P., Suntzeff, N. B., Schommer, R. A., Hamuy, M., \& Maza, J. 1999, Astron. J., **118**, 1766

Riess, A., Press, W. H., & Kirshner, R. P. 1996, Astrophys. J, **473**, 88

Saha, A., Sandage, A., Labhardt, L.,Tammann, G. A., Macchetto, F. D., & Panagia, N. 1997, Astrophys. J., **486**, 1

Schmidt, B. P., Suntzeff,N. B., Phillips, M. M., Schommer, R. A., Clocchiatti,A., Kirshner,R. P., Garnavich, P., Challis, P., Leibundgut, B., Spyromilio, J.,Riess, A. G., Filippenko, A. V., Hamuy, M., Smith, R. C., Hogan, C.,Stubbs, C., Diercks, A., Reiss, D., Gilliland, R., Tonry, J., Maza,J., Dressler, A., Walsh, J., & Ciardullo, R. 1998, Astrophys. J., **507,** 46

Suntzeff, Nicholas B., Phillips, M. M.;Covarrubias, R.,Navarrete, M., Pérez, J. J., Guerra, A.; Acevedo, M. T., Doyle, Laurance R., Harrison, Thomas,Kane, Stephen, Long, Knox S., Maza, José, Miller, Scott, Piatti, Andrés E., Clariá, Juan J., Ahumada, Andrea V., Pritzl, Barton, Winkler, P. Frank, 1999, Astron. J., **117**, 1175

CHAPTER 5

STAR FORMATION AND HISTORY OF DISTANT GALAXIES

5.1 Introduction

It is now realized that most classes of extragalactic objects change with cosmic epoch. Counts surveys since the 1960s have revealed that many more of these classes of objects, in particular radio sources and quasars, existed at early epochs as compared with their number at present. During the 1980s, the first deep counts of galaxies showed a large excess of blue galaxies at faint apparent magnitudes; these studies culminated in the remarkable findings of the Hubble Deep Field-North (Ferguson, Dickinson and Williams, 2000, ARAA, 38, 667).

During the past decade, considerable effort has been dedicated to studies of galaxies at intermediate and high redshifts ($z = 0.4$ to > 2) with the main goal to study directly galaxy evolution and even seeing galaxy formation. Such studies have often been limited to the bulk properties of these objects, limiting our physical insight. MCAO with the increased light gathering of the Gemini South Telescope will allow astronomers to study individual systems with high spatial resolution, and therefore, to determine the spatial distribution and dynamics of star forming material and stellar populations. The goal is to get to the physics of evolving individual galaxy and to understand how they evolve on their own and as a function of environment.

The big questions we wish to address with the proposed MCAO imager and spectrograph are

- How to reconcile the range of observations of galaxies between $0 < z < 5$ with an overall consistent scenario of galaxy formation and evolution?
- How did mass assembly of galaxy constituents proceed?
    - What is the origin of rotation of galaxies?
- When did the massive galaxies form the bulk of their stellar population?
    - How and when did abundance gradients appear in galaxies?
- What is the history of galaxy clustering?

The distant galaxy science cases that were considered in some detail and that are reported in this chapter are:

- Evolution of galaxies in the field
    - Broad band imaging => Spatially resolved spectral energy distributions
    - Metallicity and ionization gradients at ‘magic’ redshifts

  - Spatially resolved Hα kinematics
- Evolution of galaxies in clusters
  - Broad band imaging (HST ACS+MCAO), IFU spectroscopy => spatially resolved metallicity and dynamics
- Chemical evolution of galaxy disks
- Galaxy formation: the masses of galaxies at z = 2
- Gravitational lensing as a tool to do 30m science on a few lucky galaxies

It remains to be seen which of the most promising scenarios for the origin and evolution of galaxies can be established convincingly by observations. There exists the possibility that new physical processes not yet established by laboratory experiments may need to be invoked. MCAO will certainly bring us to new frontiers of extragalactic research undreamt by our pioneers Hubble, Humason, Zwicky, Shapley, Sandage and de Vaucouleurs.

The people who made substantial contributions to the distant galaxies MCAO science cases are:

Ivan Baldry (AAO)
Elizabeth Barton (DAO/HIA/NRC)
Mark Chun (Gemini Observatory)
Roger Davies (Durham University)
Mike Edmunds (Cardiff University)
Inger Jorgensen (Gemini Observatory)
Chip Kobulnicky (U. of Wisconsin)
David Koo (Lick)
Peter McGregor (ANU)
Simon Morris (DAO/HIA/NRC – now Durham University)
Francois Rigaut (Gemini Observatory)
David Schade (DAO/HIA/NRC)
Ray Sharples (Durham University)
Eric Steinbring (CfAO)
Thaisa Storchi-Bergmann (UFRGS)
Howard Yee (U. of Toronto)

Several others either passed through the room and contributed comments, or provided email input. On the proposals below, a few key people are listed as PI and collaborators, although all present at the workshop provided feedback and often ideas.

The intent with the above structure is to show in some detail the science goals for field galaxies, and then summarize the cluster situation more succinctly, focusing on explaining where cluster science may differ from the field. Almost all of the science projects for field galaxies carry over to cluster galaxies. The lensing case is separated out, as it seemed a particularly strong case for MCAO and is a place where exciting results could be obtained quickly; this is something one

might do as 'demonstration science'. It was decided that the above covered well both the range of distant galaxies science, and also most of the high priority science cases for MCAO.Several other science cases were considered and thought attractive, but were not included in this document for reasons of space. These included:

- $z \geq 2$ clusters (high z Radio galaxies – a detailed proposal is available in this area)
- Origin and evolution of the Fundamental Plane (needs more modeling of spectroscopic performance of MCAO)
- A Blank field survey (36", 9 dithers)
- Identification of Sunyaev-Zeldovich Cluster Candidates
- High z Supernovae

5.2 Field Galaxy Imaging -- David Schade (DAO/HIA/NRC), David Koo (Lick) and Inger Jorgensen (IGPO)

Abstract

An invaluable capability of the Hubble Space Telescope (HST) is to image galaxies to redshift z ~ 1 at a spatial resolution that shows the large-scale morphology in similar terms to those we are accustomed to for local galaxies. It is possible to visually classify galaxies, see the bulge and disk as separate components, and observe spiral and barred structures in massive galaxies. It is also possible to make reasonably accurate measurements of bulge-to-disk ratios, sizes and surface brightnesses, and colors of bulge and disk components individually. (See the example of modeling the stellar populations of the bulge and disk separately from Bunker et al. 1999 astro-ph/0004348). At redshifts greater than one, the angular diameter *vs* redshift relation is nearly flat so that increased resolution is not the key to extending morphological studies of massive galaxies out to higher redshifts. The real key is to observe at the same rest-frame wavelength as we are observing in nearby objects while preserving spatial resolution of ~0.1 arcsec or better. In order to obtain measurements of morphology, size, surface brightness, and symmetry that are directly comparable to those obtained for lower redshift galaxies, it is fundamentally important to make these measurements at the same rest-frame wavelengths. Hence the need for adaptive optics in the infrared on a large aperture, infrared-optimized telescope. We believe that MCAO on Gemini South will fulfill this goal; this is what we demonstrate.

5.2.1 Background Science

The following sections outline areas where the analysis of luminosity profiles is of scientific interest. Specifically, we address those areas where two-dimensional profile fitting of galaxy images is useful. The two-dimensional fitting is used to extract the relative luminosities of the disk and bulge as well as the sizes, the surface brightness and the colors of the components. Hierarchical clustering models and monolithic collapse models for the formation of early-type galaxies result in different predictions for the relative disk luminosities of the products. The mergers in the hierarchical clustering models in most cases are expected to destroy the disks

present in the galaxies prior to the merging. Thus, measuring the relative luminosities of the disks in early-type galaxies can shed light on the importance of merging.

I. Existence of elliptical galaxies at high redshift

An important thrust of present searches for extremely red objects (EROs) is to determine the number density of large elliptical galaxies at redshifts greater than one. The use of morphology rather than colors to identify candidate high redshift ellipticals offers in a far more robust test of whether most of the mass of elliptical galaxies is assembled in one piece at high redshift versus scenarios involving the recent hierarchical accumulation of mass.

Analysis of the luminosity profiles (for example by two-dimensional modeling) is required in order to separate true de Vaucouleurs profiles from galaxies of other types. Fairly large sample sizes (tens to hundreds) are needed to provide statistical significance. Gemini can do this reliably to roughly K = 21 in one hour; it is an estimate only at this point, but simulations by Jorgensen further in the text will illustrate this possibility. However, on a pessimistic note, we remark that the low surface density of high redshift ellipticals (that we estimate at one every few square arcmin) may make this difficult for field sizes of 1-2 arcmin unless clustering helps us out.

II. Fundamental Plane

Strong correlations exist between various properties of elliptical galaxies, specifically their luminosities, their sizes, their central velocity dispersions, the abundance of heavy elements and so on. The Fundamental Plane is a relation between the half-light radius, the surface brightness and the velocity dispersion. The relation is linear in the logarithmic space. Thus it can be viewed as a plane in the 3-dimensional parameter space. The physical origin of the Fundamental Plane and the other scaling relations are not yet understood. However, the Fundamental Plane has a very low scatter making it possible to detect changes in the mass-to-light ratios of the galaxies of about 5% when samples of 20-30 galaxies are used. This makes the Fundamental Plane the most powerful tool for studying galaxy evolution at distances beyond the local universe. This is feasible beyond z = 1 with an 8-meter telescope. The studies can be done in clusters or in the field. The first step in the study of the fundamental plane at moderate-to-high redshifts is to discriminate between early and late type galaxies. This requires accurate measurements of half-light radius and effective surface brightness from the luminosity profiles. The multiplexing advantage provided by a MCAO imager applies if one is observing clusters, because the density of field ellipticals is low; only one field elliptical every few arcminutes (estimate only at this time) is expected.

III. Evolution of disk galaxies

The most direct way to study the evolution processes of disk galaxies is to isolate large samples of disk galaxies over a range in redshift and to examine their color, size, and surface brightness distributions. Estimates of mass can be made via modeling of the stellar populations. Infrared observations are particularly powerful since they have reduced dependence on young stellar populations compared to optical pass bands. This project can and should be done in both clusters and the field. Multiplexing advantages can be exploited in clusters. In the field, only a few galaxies per square arcmin.

IV. Evolution of bulges

It will be important to find out whether bulges are mini-ellipticals which form at high redshift (if indeed this is what ellipticals do) as opposed to forming at later times by mergers or by secular processes in disks. The bulge components need to be separable from their disks; this argues for high spatial resolution. This evolution can be studied in both clusters and the field and the same remarks apply as in III above.

Some considerations are generic to all these science cases:

1. The ability to effectively measure individual components and to discriminate between bulges and disks always involves a trade-off between resolution and signal-to-noise. If the size of the point-spread-function (PSF) is larger than the characteristic galaxy size, then more integration time is needed than if the spatial resolution element (FWHM of the PSF) is smaller that the galaxy size. The errors on the measured parameters go approximately as the square root of the integration time and the inverse square of the FWHM.
2. The surface density of field galaxies to K=20 is a few objects per square arcminute. The typical scale sizes of galaxies at K=20 is 0.2-0.4 arcsec.
3. The surface density of field galaxies is very near the critical point where the multiplex advantage of MCAO can be fully exploited. This is true only if EVERY galaxy in the field is a high-priority target. If only a subset (by redshift, morphological type, etc) of the galaxies is of interest (this will certainly be true for kinematic studies) then the multiplex advantage will not be fully exploited for field galaxies. The surface density is too low.
4. Galaxy properties (e.g. size, surface brightness, color) have broad distributions; this drives the requirement for large sample sizes. It also argues that sample size takes precedence over single measurement precision in many cases; the fundamental plane may be an exception. If the surface density of objects is low, MCAO increases the precision of individual measurements dramatically, but yields no advantage in sample size (except that it reduces the integration time required to reach a specific level of measurement precision).
5. For this kind of programs, a good knowledge of the PSF as a function of position can enable effective science as much as a uniform PSF over the field. However, it is difficult to predict the how the PSF varies over the field unless the vertical profile of turbulence during the time of the science exposure is known, which would imply having site testing instrument on site. A pre or post science exposure calibration on a stellar cluster is also possible, but does not provide a calibration better than typical 5-10% of the isoplanatic angle, as the atmosphere varies quite rapidly. MCAO does not eliminate *all* the PSF variation (especially if faint tip-tilt guide stars are used), but – as discussed in chapter 2 -, it reduces it dramatically. Also, it has to be noted that image quality degradation due to image motion only are much simpler to model (2 parameters) than high order phase decorrelation.
6. For some science cases and especially for faint galaxies down to K = 20, it may be advantageous (if possible) to get only low-order correction in order to achieve spatial resolutions of FWHM ~0.15 arcsec, instead of ~ 0.07 arcsec. Such a low-order correction, if over a wide field, could constitute an advantageous approach for several science cases.

5.2.2 Proposed observations : requirements and other constraints

This program will require deep imaging in J, H, and K. Extensive mosaicing will be needed to observe the corresponding sky area covered with instruments such as Gemini/GMOS and Keck/DEIMOS, or even with the HST ACS (which will be used for the optical/UV imaging data).

The strawman imager described in the introduction of this document provides the minimum field of view required for this project.

As a simulation, we have included an image of the NICMOS observations of the HDF-S (Figure); this is roughly equivalent to a 1 hour integration with Gemini in the K band, at least in term of the signal-to-noise ratio for galaxies within an aperture of 2 arcsec. The field size is roughly one arcmin and it includes seven sources to K = 20 (2" radius aperture).

The surface density of field galaxies to K=20 is a few objects per square arcmin. Exposures time will be approximately 1 hour per broad band colour. Fields will be chosen to include suitable density of guide tip/tilt stars; if necessary, we will select a field at a lower galactic latitude.

5.2.3 MCAO vs CAO for this program: a detailed comparison

In the MCAO Conceptual Design Document, Jorgensen and Rigaut demonstrated the gains from MCAO for science cases involving galaxy morphology. We reproduce some of this discussion here.

We constructed a simulated galaxy field in which the galaxy sizes and luminosities match observed properties of galaxies at z = 0.6. The projected density of galaxies is higher than found in rich clusters, the main purpose being to simulate a large enough number of galaxies to quantify what MCAO allows us to achieve, rather than simulate real looking galaxy clusters. The galaxy field covers 65" x 65". The galaxies have either $r^{1/4}$ or exponential luminosity profiles, and none is a combination of the two types.

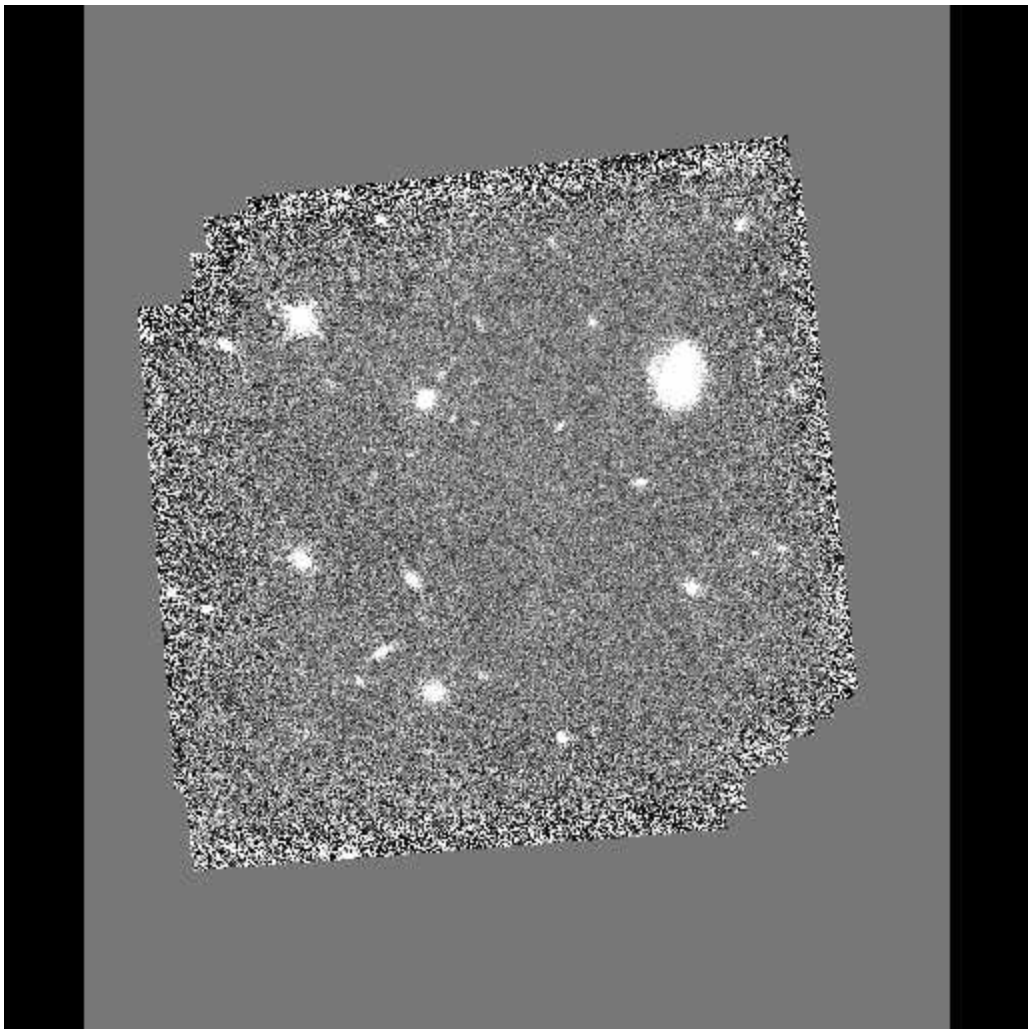

Figure 5.1: Image of the NICMOS observations of the HDF-S. This is roughly equivalent to a 1 hour integration with Gemini in the K band, at least in terms of the signal-to-noise ratio for galaxies within an aperture of 2 arcsec.

We concentrate on two subfields, each 16.25" x 16.25". The central subfield covers from -4" to 12.25" relative to the optical axis, while the outer subfields covers from 13.65" to 29.9". Thus, the outer-most corner is 42.3" from the optical axis. Each subfield contains three stars. Simulations were made for the classical AO with one 17 mag natural guide star and one laser guide star, both located in the center of the field. For the baseline MCAO system, we used five laser guide stars and three 17 mag natural guide stars. Sky background and noise were added equivalent to an exposure time of 6 hours in the H-band.

Figure 5.2 shows the simulated fields for the seeing limited case, for classical AO and for MCAO. In Figure 5.3, a smaller area of the outer field located approximately 30" from the optical axis illustrate the gains in resolution for MCAO compared to classical AO.

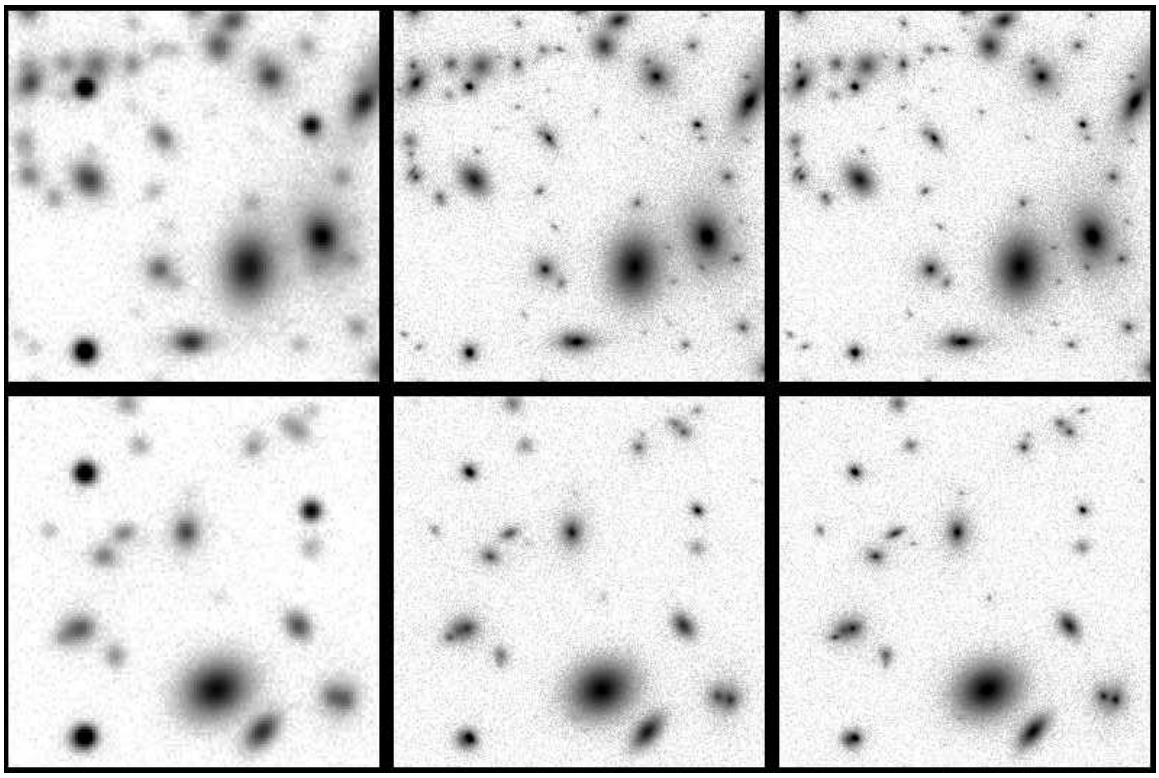

Figure 5.2: Simulated galaxy field at z = 0.6. Top row – central subfield; bottom row – outer subfield. Left – Seeing limited case, FWHM = 0.5 arcsec; center – classical AO; right – MCAO. The subfields cover 16.25" x 16.25". The pixel size for the seeing limited case is 8 times as large as for the AO and MCAO simulations. This larger pixel size matches the typical pixel scale for non-AO imagers.

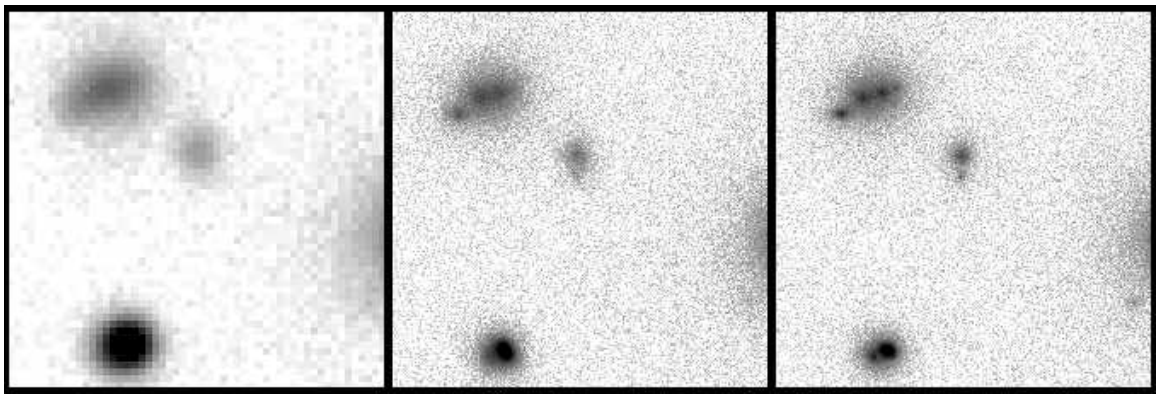

Figure 5.3: A 7" x 7" subfield of the simulation, approximately 30" from the optical axis. Left – seeing limited case; center – classical AO; right – MCAO. The subfield contains eight faint galaxies, one close to the bright star in the lower left. All eight galaxies can easily be identified in the MCAO simulation, while in the simulation of classical AO only five of the galaxies can be identified due to the degradation of the PSF away from the optical axis.

The simulated images were analyzed in a way similar to what one would do with real high spatial resolution images of intermediate redshift galaxies, e.g. HST images. The galaxies brighter than 22 mag in the H band were fitted with 2-dimensional models convolved with a 2-dimensional point-spread-function (PSF). Each simulated galaxy was fitted twice, first with an

$r^{1/4}$ and then with an exponential profile. The output of this process consists of the half-light radii, the total magnitudes, the ellipticities and the position angles for the best fitting models. Furthermore, the goodness of the fit is derived as $\chi^2/N_{pix,}$ where N_{pix} is the number of pixels within the fitting radius, where $\chi^2 = \Sigma\ (n_i - n_{i,model})^2/\sigma_i^2$ with the sum over all the pixels within the fitting radius. The three stars in the fields were fitted by scaling the constructed PSF. All objects in a field are fitted simultaneously. Pixels containing signal from the objects that are not fitted are omitted from the fit. The use of a residual image with the fitted models subtracted is employed for the evaluation of the quality of the derived fits.

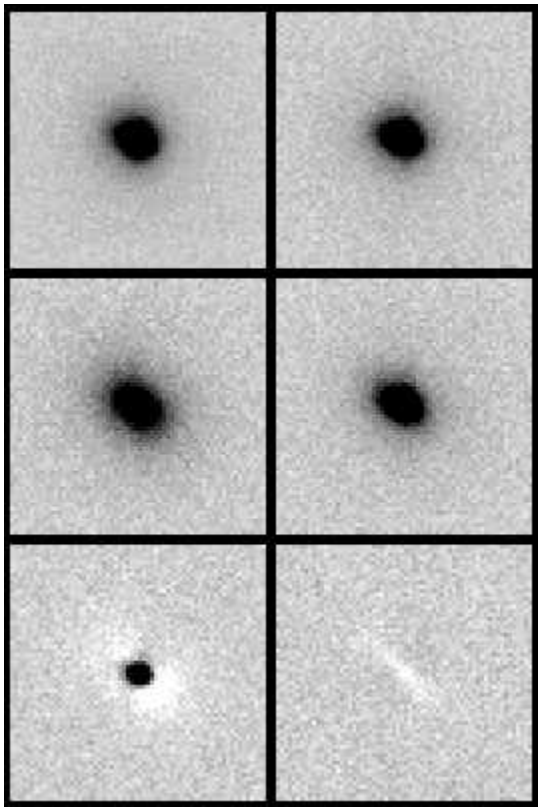

Figure 5.4: The point-spread-functions used for the simulations. Left column – classical AO; right column – MCAO. Top row – PSF for the central subfield; center row – PSF for the outer subfield; bottom row – difference between the PSF for the central subfield and the outer subfield. For the classical AO, the peak signal in the (normalized) PSF for the outer field is only 40% of the peak signal in the PSF for the central field. The difference between the two PSFs for the MCAO is only about 3 per cent.

The PSFs were constructed from two or three stars in each simulated field. Figure 5.4 shows the PSFs as well as the difference between the PSFs for the central and the outer fields. The large PSF variation with distance from the center of the field is obvious for the classical AO case. For real observations stars may not be conveniently located in the field. In order to illustrate the worst case scenario, we mismatched the PSFs, fitting the outer field using the PSF for the central field and visa versa.

In order to assess whether it is possible to recover the input profile types, we use the goodness of the fit, χ^2/N_{pix}. Figure 5.5 shows χ^2/N_{pix} as a function of the input total magnitude. In Fig.5.5a

and c we have used the correct PSF derived from the same field as the field fitted. For galaxies brighter than about 20.5 mag, fitting the incorrect profile, e.g. an exponential to an input $r^{1/4}$ profile, results in a significantly worse fit than when the correct profile is fitted. Thus, the input profile type can be recovered. In the case of a mismatched PSF (Fig5.5b and d), the input profile type can be recovered to the same magnitude for the MCAO simulations, while for the simulations of the classical AO the fits become indistinguishable at about 20 mag and fainter. This is an expected from the PSF variation over the field in the case classical AO and illustrates a very clear advantage of MCAO.

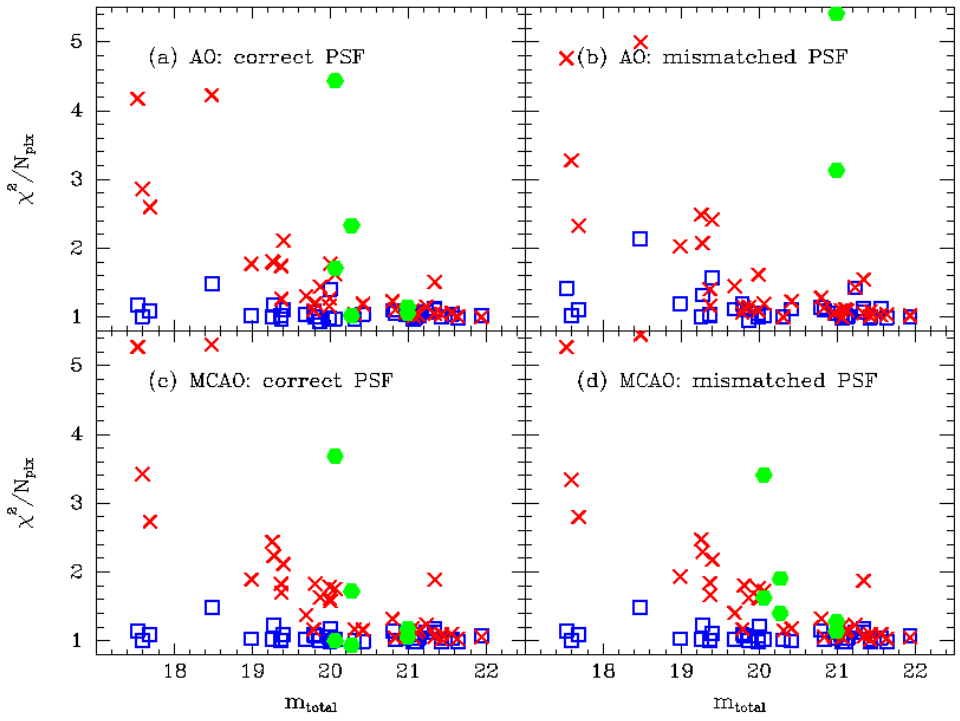

Figure 5.5: The goodness of the fits, c^2/N_{pix}, as a function of input total magnitude. (a) and (c): The correct PSFs were used. (b) and (d): The fits were performed with the mismatched PSFs. Boxes (blue) – the galaxies were fitted with the correct profile type; crosses (red) – the galaxies were fitted with the incorrect profile type. Grey (green) hexagons – results for the stars. In panel (a) and (c) the one star with large c^2/N_{pix} is located very close to a faint galaxy. This star was not included in the determination of the PSF. In panel (b) four of the six stars have c^2/N_{pix} larger than 5.5.

In addition to the goodness of the fits, we can inspect the residual images in order to judge if the correct profiles can be recovered. In Figures 5.6 and 5.7, we show the residual images for the fits with $r^{1/4}$ and exponential profiles. For the brighter galaxies, the residuals show very clearly which of the two profile types is correct; we can reliably recover the input profile type. Figure 5.6 also shows the significant PSF variation over the subfields that we are analyzing. The residuals from the stars (marked with black circles) reflect the systematic PSF variations.

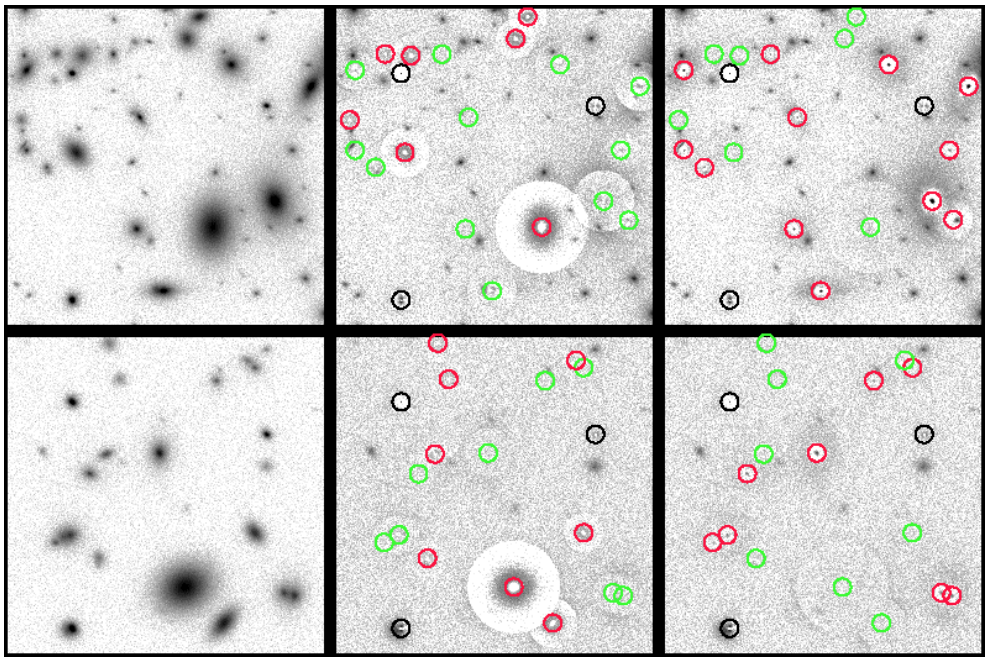

Figure 5.6: Residual images for the simulation of classical AO. Top – central field; bottom – outer field. Left – input simulated image; center – residuals after fitting with $r^{1/4}$ profiles; right – residuals after fitting with exponential profiles. In the residual images galaxies fitted with the same profile type as the input profile are marked with light grey (green) circles, while galaxies fitted with the incorrect profile type are marked with dark grey (red) circles. The three stars in each field are indicated by black rings.

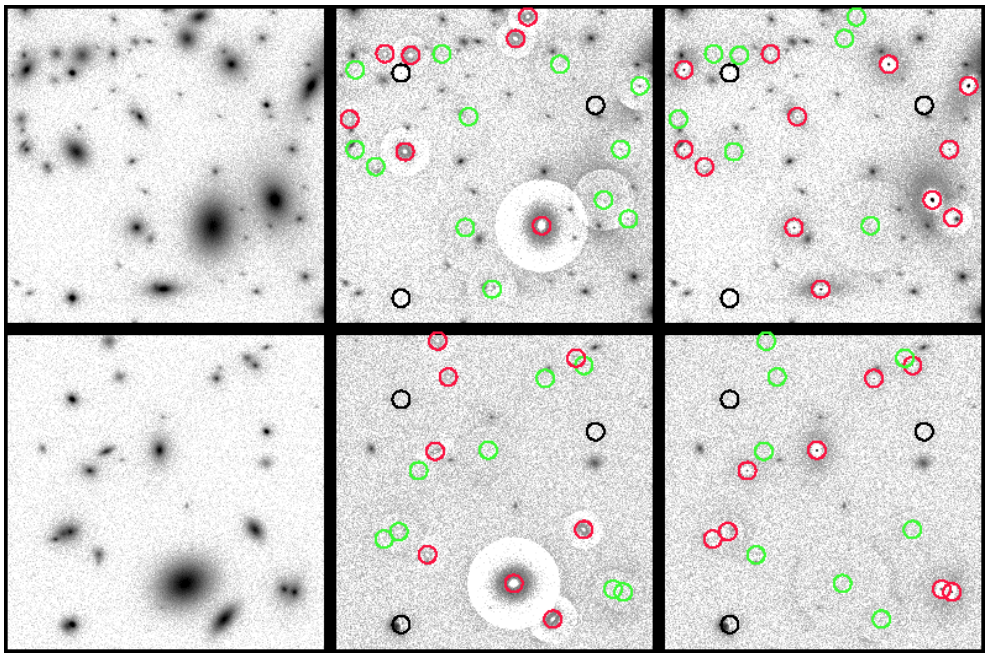

Figure 5.7: Residual images for the simulation of MCAO. Top – central field; bottom – outer field. Left – input simulated image; center – residuals after fitting with $r^{1/4}$ profiles; right – residuals after fitting with exponential profiles. In the residual images galaxies fitted with the same profile type as the input profile are marked with light grey (green) circles, while galaxies fitted with the incorrect profile type are marked with dark grey (red) circles. The three stars in each field are indicated by black rings.

Before discussing the results for the total magnitudes and the half-light radii, it is worth noting that even for nearby bright galaxies - e.g. galaxies in the Coma cluster - the typical random uncertainties on the total magnitudes are of the order 0.1 mag, while the uncertainties on the half-light radii are about 10%. These uncertainties are due to the large angular extent of galaxies which means that the total magnitudes and half-light radii must be measured by fitting models to the brighter parts of the galaxies; alternatively, we attempt to estimate the parameters from the asymptotic behavior of the enclosed luminosity as a function of aperture size.

Figure 5.8 and 5.9 show the results from the fitting versus the input parameters for the total magnitudes and the half-light radii, respectively. We show the results from fitting the correct profiles, as well as fitting the incorrect profiles. For real data the best fitting profile type would have to be decided on by judging the values of χ^2/N_{pix}.

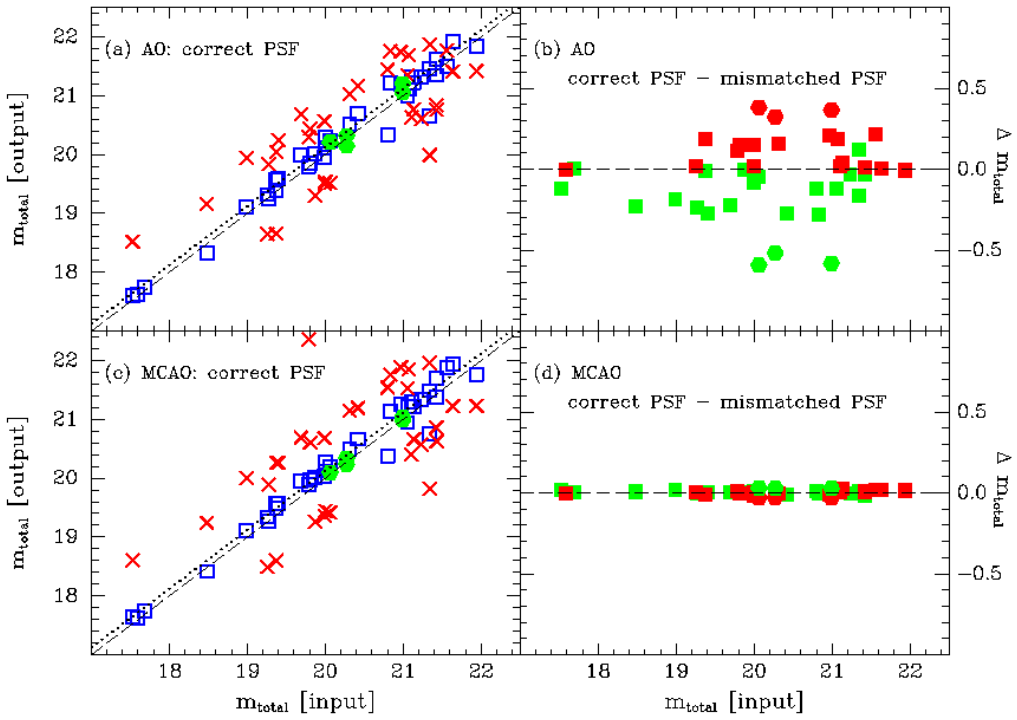

Figure 5.8: Total magnitudes of galaxies and stars. (a) and (c): The correct PSFs were used. Boxes (blue) – the galaxies were fitted with the correct profile type; crosses (red) – the galaxies were fitted with the incorrect profile type. Grey (green) hexagons – results for the stars. The dashed lines are the one-to-one relations, the dotted lines are the expected relations due to the limited size of the PSF used in the fitting, see text. (b) and (d): The difference between the result when the correct PSF is used and when the mismatched PSF is used. Dark grey (red) – the outer field; light grey (green) – the central field. Boxes – galaxies; hexagons – stars, at +0.4mag and –0.5mag in panel (c). The mismatched PSFs result for the classical AO in systematic errors in the total magnitudes of 0.2-0.3 mag for the galaxies (and 0.4-0.5 mag for the stars).

The small offsets between the one-to-one relations on Figures 5.7a,c and 5.8a,c and the location of most of the points are due to the limited size of the PSFs used for the fitting. The PSFs include about 88% of the total signal in the stars. The fit cannot be done with larger PSFs, due to the low signal-to-noise of the stars. For real observations this is a common problem if the available stars

in a field are as faint as those included in the present simulations. The small size of the PSFs causes the magnitudes of the galaxies to be determined too faint by 0.12 mag, and correspondingly the derived half-light radii is too small. For $r^{1/4}$ and exponential profiles, an offset of 0.12 mag in the total magnitude corresponds to an offset in the logarithm of the half-light radius of about 0.075. The dotted lines on Figures 5.7a,c and 5.8a,c show the expected relations when the systematics due to the small PSF size are taken into account. The derived total magnitudes and half-light radii follow these expected relations, with some scatter as expected.

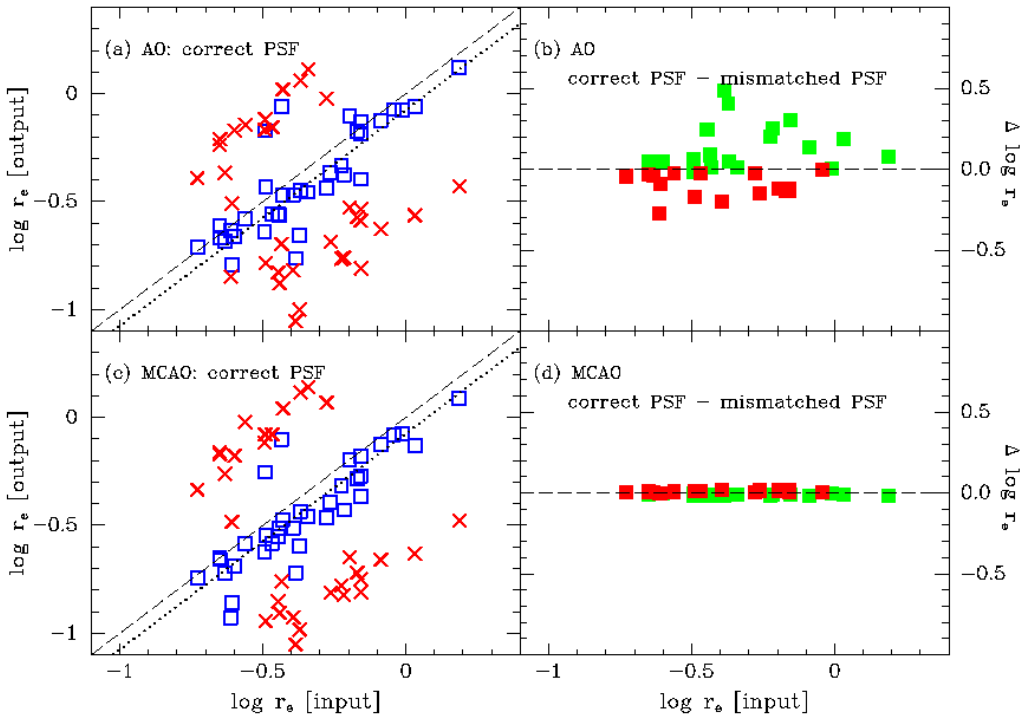

Figure 5.9: The half-light radii of the galaxies. (a) and (c): The correct PSFs were used. Boxes (blue) – the galaxies were fitted with the correct profile type; crosses (red) – the galaxies were fitted with the incorrect profile type. The dashed lines are the one-to-one relations, the dotted lines are the expected relations due to the limited size of the PSF used in the fitting, see text. (b) and (d): The difference between the result when the correct PSF is used and when the mismatched PSF is used. Dark grey (red) – the outer field; light grey (green) – the central field. The mismatched PSFs result for the classical AO in systmatic errors in the half-light radii of 25-50 per cent (0.1-0.2 in log r_e).

For the classical AO, the PSF variation over the field will in general not be fully mapped. It can easily be the case that the PSF is known only from the central NGS. Figures 5.8b,d and 5.9b,d show the effect of using the mismatched PSFs. For the classical AO, this results in systematic errors in the total magnitudes of 0.2-0.3 mag for the galaxies (and 0.4-0.5 mag for the stars), and systematic errors in the half-light radii of 25-50 per cent. For the MCAO simulation no systematic effects result from mismatching the PSFs.

Classical AO can only be used successfully for reliable measurements of half-light radii and total magnitudes of distant galaxies if the PSF is known as a function of position in the field. Any given field of view of 1' x 1' at high Galactic latitude (where we are most likely to pursue studies

of high redshift galaxies) will contain less than five stars bright enough to use for reconstruction of the PSF variation over the field. Thus, in most cases, we will have insufficient knowledge of the PSF variation over the field of view. ***The very small variation of the PSF over the field that a MCAO system will deliver is essential for the ability to measure half-light radii and total magnitudes of distant galaxies. The presented simulations show that without MCAO, we cannot study galaxy morphology with quantitative methods over field of view (1 'x 1' or larger) that are absolutely necessary for pursuing the science cases outlined in this proposal***.

5.3 Chemical Evolution of Galaxy Disks -- Chip Kobulnicky (University of Wisconsin), Simon Morris (DAO/HIA/NRC), Ivan Baldry (AAO), Eric Steinbring (CfAO) and David Koo (Lick)

Abstract

We propose to use the MCAO and a multi-IFU spectrograph to measure the chemical abundances in galaxies in the two magic redshift ranges of $1.29 < z < 1.64$ and $2.09 < z < 2.57$. We will measure the Hβ, [O III] 5007, Hα, [N II] 6584, and [SII] 6717 line strengths which provide estimates of the extinction due to dust, and of the oxygen, nitrogen and sulphur abundances among these same galaxies to study the disk metallicity-luminosity-linewidth relations at various look back times and as a function of the local environment.

5.3.1 Background Science

Research programs in galaxy evolution have traditionally followed one of two approaches; these may be summarized as “Effects of Nature” and “Effects of Nurture”. The former research programs focus on understanding how galaxies evolve as a function of cosmic time by observing galaxies at increasingly higher redshifts. The later types of programs seek to understand the role of local environment by comparing galaxies in the field to those in dense clusters. The extent to which “Nature” and “Nurture” both shape the development of galaxies is a subject of ongoing debate. *The MCAO spectroscopic observations proposed here will begin to untangle the effects of redshift (or age) from the effects of environment, by studying fundamental galaxy scaling relations in a range of environments at redshifts of z =1.3 to z = 2.5.*

The universe, as a whole, appears to show a higher rate of star formation, more frequent merger activity, and a higher fraction of galaxies with blue, irregular morphologies at $z > 1$ (e.g., Butcher & Oemler 1984ApJ...285..426). Significant changes in the star formation rate and populations of galaxies appear to happen in the redshift interval $z = 1$ to 2, which makes this an important interval for understanding galaxy evolution. It also seems likely that this is the interval where large galactic scale disks are formed. However, theoretical work points to formation at a later time ($z < 1$), while observational clues suggest early disk formation times ($z > 2$). Within galaxy clusters, it is well established that a strong correlation exists between galaxy type and local density, with high-density regions being dominated by earlier type galaxies (Dressler 1980ApJS...42..565). The average oxygen abundance per unit luminosity is also higher for disk galaxies in denser environments (Skillman et al. 1996ApJ...462..147). The average star formation rate increases for galaxies on the periphery of dense environments. A natural explanation for these correlations is that ram pressure from hot intra-cluster gas helps trigger star

formation in gas-rich galaxies and strips gas from the tenuous outer regions of spiral disks (Fujita & Nagashima 1999ApJ...516..619).

Furthermore, the overall history of star formation in galaxies is very closely related to the rate at which chemical build-up in stars and the interstellar medium of galaxies has taken place. The total amount of chemical elements and star formation drives the intensity of the isotropic background radiation in the optical, infrared and sub-millimeter wavebands. Also the abundance levels in the absorption line systems need to be coupled to those measured in the luminous parts of galaxies for a consistent view of the chemical build-up at various cosmic epochs. Measurements of chemical abundances, star formation and dust contents are necessary for "putting it all together" in a global picture such as the Equations of Cosmic Chemical Evolution of Pei and Fall (1995ApJ...454...69P). The objective of the Equations is to relate the absorption history, which provides a series of snapshots of the values of the various cosmology density parameters at different epochs, to the emission history, which provides information about the rates of formation of stars and heavy elements.

5.3.2 Proposed observations : requirements and other constraints

We will obtain MCAO spectra of 20 to 40 galaxies in each of 4 fields for specific redshift bins between z = 1.3 and 2.5. The galaxies will have all of the above emission lines visible in one of the J, H or K bands. Fields will be pre-selected using photometric redshifts to ensure a significant sample of candidate objects within a MCAO field. If possible, fields will also be chosen to allow sampling of a range of galaxy densities, although obviously biased towards regions of higher densities to obtain more efficient multiplexing.

Low-resolution R ~ 1500 observations will be obtained to measure the ratios of strong Balmer and [OIII] emission lines which indicate the gas-phase metallicity (Edmunds & Pagel 1984MNRAS.211..507).

Star forming spiral and irregular galaxies at z~1 have angular sizes of 1 to 2 arcsec. The low density of target galaxies (see Kobulnicky et al. on galaxy densities in Appendix II of this document) means that the largest possible field of view will offer the most efficient means of selecting interesting galaxies and multiplexing the spectroscopic observations.

A typical luminous HII region with an Hα luminosity of 10^{40} erg/s will have a flux of 1.50×10^{-18} erg/s/cm^2 at z = 1. The linear size of 100 pc will have an angular size of 0.01" at z = 1, so, even though individual HII regions will be unresolved, there is a substantial reduction of sky noise achieved by AO with the smallest possible pixel sizes. Typical starburst galaxies have Hα luminosities of few x 10^{41} erg/s or fluxes of a few $\times 10^{-17}$ erg/cm^2/s at z = 1.

Derivations of chemical abundances require flux measurements at S/N better than 10:1 in Hβ and [O III], but velocity resolution is not required; consequently, 3-4 hour exposure times will be sufficient to measure the line ratios with adequate S/N. Ideally weaker lines like [N II] (typically 0.05 of Hα low abundance systems) and [S II] will also be measured as they provide important density and nitrogen abundance diagnostics. These goals require optimal S/N, but not necessarily the excellent spatial resolution achievable with AO. Coarser fibers and/or larger pixels would suffice. Detailed S/N calculations have not yet been performed for the high z end of

the redshift range proposed here. It is likely that such observations will require a prohibitive amount of time or will need to wait for the next generation of 30-50 m extremely large telescopes. If the observing time turns out to be prohibitive, the program could be scaled back to just include the first redshift window.

5.3.3 MCAO vs CAO for this program

MCAO provides a time saving of ~10 over conventional AO because of the ability to observe 10-20 galaxies simultaneously. Single galaxies could be studied with conventional AO (e.g. NIFS), but MCAO provides a multiplexing advantage by a factor of 10-20. Uniform PSF is not absolutely required, but uniform image quality will greatly improve the ability to search for metallicity gradients in the galaxies and compare different galaxies, e.g. determine the slope of the gradients for various galaxy types/masses.

5.4 Galaxy Formation: The Masses of galaxies at z = 2, Simon Morris, (DAO/HIA/NRC), Chip Kobulnicky (U. Wisc), Ivan Baldry (AAO), Eric Steinbring (CfAO), Elizabeth Barton (DAO/HIA/NRC) and Ray Sharples (U. Durham)

Abstract

Using the MCAO system with GIRMOS and multiple IFUs, we will use resolved emission line kinematics to measure the masses of galaxies from z = 1.3 to 2.7.

5.4.1 Background Science

Understanding the assembly of galaxies requires measurement of the masses of the luminous building blocks as a function of redshift (Benson et al. 2000, MNRAS, 311, 793). This can be done in a number ways. Galaxy-galaxy lensing is a promising technique which deserves attention (see previous science case). Another route is via measurement of the stellar absorption line or gas emission line kinematics. Both of these approaches have challenges associated with them. Stellar absorption line work is likely to be restricted to the highest surface brightness regions of galaxies (e.g. centers of elliptical galaxies), and even then will probably not probe redshifts much beyond 1 with 8m telescope collecting areas (see modeling presented in Appendix I and II). Gas emission line work can push out to much larger redshifts, but carries with it the concerns that the gas kinematics might not be dominated by gravity, and even if it is, that the motion might not be yet in virial equilibrium.

Despite these concerns, several papers have been published using the integrated line widths of high redshift emission line galaxies as a diagnostic for their masses (Moorwood et al. 2000, astro-ph/0009010, Pettini et al. 1998, ApJ, 508, 539, Guzman et al. 1997, ApJ, 489, 559). Identification of those objects where the gas kinematics is dominated by winds or outflows will be enormously helped by spatially resolved spectroscopy such as MCAO equipped with a multi-object spectrograph will enable.

5.4.2 Proposed observations : requirements and other constraints

Candidate objects will be selected using photometric redshift observations over a field of at least 100 square arcmin. The photometric redshift technique simultaneously will deliver a redshift and also a galaxy SED which will allow us to concentrate on galaxies most likely to be both in the correct redshift range and also most likely to show emission lines. Narrow band filter surveys already indicate that the density of objects with Hα in the H-band ($1.3 < z < 1.8$) will be 1-3 per square arcmin, with a slightly larger number in the K-band ($2.0 < z < 2.7$). Assuming that the GIRMOS IFUs can patrol the full 2 arcmin diameter circular regions passed by the ISS AO feed, and that GIRMOS will also permit some IFUs to observe in the H band while others observe in the K band at the same time, then one could expect to observe around 12 objects at one time.

We note that the surface density of Lyman α emitting galaxies with a flux in Ly-α+continuum of $>2.6 \times 10^{-17}$ ergs/cm^2/s at $z = 4.5$ is one per square arcmin per Δz of 1 (Rhoads et al. 2000, astro-ph/0003465). Lyman α enters the J band at $z = 7$, and it would be very exciting (albeit risky) to put any spare IFUs onto objects identified by photometric redshifts as candidate objects at these redshifts. Observations of these objects could be considered an essentially free bonus addition to the above program. IFU observations will allow optimal extraction of any detection after the event, thereby decreasing the limiting flux threshold. However slitlets may allow a more accurate background sky subtraction.

We would prefer the full 2 arcmin diameter field of view in order to increase the multiplex gain. The key AO parameter for these observations is the slit coupling to a 0.1 arcsec slitlet. Thus the highest possible image quality is not needed. That said, it is likely that the star formation and hence emission line morphology of these objects will be very lumpy, and so significant S/N gains can be made by using AO.

A spectral resolution of FWHM<=100 km/s (> or = 3000) is needed for the science (assuming one can measure a velocity of an emission line to 1/10 of the spectra resolution). For this project, one is helped by the (1+z) broadening of the lines, so an observed frame FWHM of 100 km/s corresponds to a rest frame resolution of 30 km/s. Measuring the velocity dispersion of individual lumps in the galaxy would be a secondary goal should the S/N permit.

For the science case above, one would like to be able to select on an IFU by IFU basis whether one observed within the H or K bands. For each object, the wavelength range to be covered is around 0.2 micron to compensate the three sigma of the expected photometric redshift uncertainties.

We also note that for the majority of the targets in this science case, one would not need a 3 x 3 arcsec FOV. IFUs with 1.5 to 2 arcsec FOV would suffice (see Figure 5.10). The fiducial 0.1 arcsec sampling corresponds to around 800 kpc at these redshifts. Finer sampling is almost certainly not useful due to the faint surface brightness expected

Sample selection will aim at identifying objects with fluxes similar to those in Moorwood et al 2000, astro-ph/0009010, i.e. with integrated line fluxes of $>8 \times 10^{-17}$ ergs/cm^2/s in Hα. It is expected that this flux will be spread over between 5 to 20 IFU resolution elements (each 0.1 x

0.1 arcsec). After the observations, these spectra will be optimally combined if necessary in order to increase the S/N. (See Figure 5.10 for some object morphologies in the rest frame UV)

Moorwood et al. 2000 (astro-ph/0009010) have presented a narrow band survey to find Hα emitters in the K band. They found 10 objects in 100 square arcmin with a filter width of about 0.03 in Δz. They were sensitive to a 3 sigma flux of about $8x10^{-17}$ ergs/cm^2/s, and found objects with equivalent widths between 50 and 700A (rest frame) or star formation rate of 20-30 M_{sun}/yr. They also show VLT ISAAC spectra of the objects which required an hour each of exposure time with a slit wide enough to get all the flux, and summed all that flux up along the slit to produce fairly convincing looking spectroscopic line detections (see Figure 5.11).

The Hα line is in the K-band filter for a Δz of about 0.7, and in the H-band for a Δz of about 0.5. From this, we calculate that if we could do objects as faint as they did, expanding the exposure time by a factor 4-8, but also spreading the light into 5-20 spatial elements), we will get 0.1 per sq arcmin * 0.5 / 0.03 in the H band and 0.1 * 0.7 / 0.03 in the K band - i.e. between 1 and 3 per square arcmin. If we can use the full 2 arcmin diameter AO field of view, we get π^2 arcmin to look in, or between 3 and 9 objects per band that we could in principle put IFUs on. In an ideal world, one would be able to choose which band one used on an IFU by IFU basis, in which case one could in principle expect around 12 objects doable with an IFU per pointing if one has the full 2 arcmin diameter field of view to patrol.

We note that there is a minor correction to these surface densities: we have not counted the objects where the Hα line lies on top of a strong sky OH line. At the proposed spectral resolution of around 3000, we expect this to affect around 1/5 of the target objects (see NIFS CoDR document).

Detailed S/N calculations are being performed, but we expect that exposure times of the order of 4-8 hours per field will be needed. An example of a closely related S/N calculation is in the draft GIRMOS OCDD, where it is shown that in a 1 hour exposure on a z = 1 galaxy observed at Hα in the J band, there will be a significant (>20) number of IFU elements with a S/N of greater than 10 for an integrated SFR of 10 M_{sun}/yr.

Calculations by Barton indicate that if the 8 x 10^{-17} ergs/cm^2/s Hα flux quoted above is spread over 5 IFU elements (i.e. 0.2 x 0.2 arcsec), then a S/N of >10 can be obtained in less than 1 hour. Alternatively, if the emission were spread into 5 discrete lumps, then a S/N>10 can be obtained for the central IFU pixel for each lump in 1.8 hours. At a radius of 1 arcmin from the center for classical AO, this time goes up to 3.5 hours. Twenty equal flux lumps would take 28 hours with MCAO and 56 hours with classical AO.

5.4.3 MCAO vs CAO for this program

The MCAO gain is entirely in multiplex advantage (i.e. NIFS + Altair +LGS versus GIRMOS + MCAO). As described above, this is likely to result in a multiplex advantage of around 10. We also could allow some of the 'spare' IFUs to be used at no extra observing time cost on possible very high redshift objects. This will be impossible with the NIFS+Altair+LGS combination.

The study described requires substantial samples of objects (>=100) in order to probe a range of redshifts and galaxy continuum luminosities. The time to do this one object at a time is likely to be prohibitive and so one can state that this project is enabled by MCAO.

For NGST to compete for this science case it will need to have an IFU spectrograph and also a R>1000 capability. It is not clear at the moment that it will have either of those.This science case is very close to some of the key ALMA science. ALMA is expected to produce CO (2-1 or 3-2 around 100 GHz observed) velocity maps of z = 1-3 galaxies very rapidly. Detections should be possible in a few minutes, presumably maps will take somewhat longer. ALMA will have comparable or slightly better spatial resolutions. It will be good however to obtain data on both the molecular and the ionized gas in these galaxies. Using MCAO in combination with ALMA would allow us to map out the fractions of these two components as a function of both position and velocity across high z galaxies.

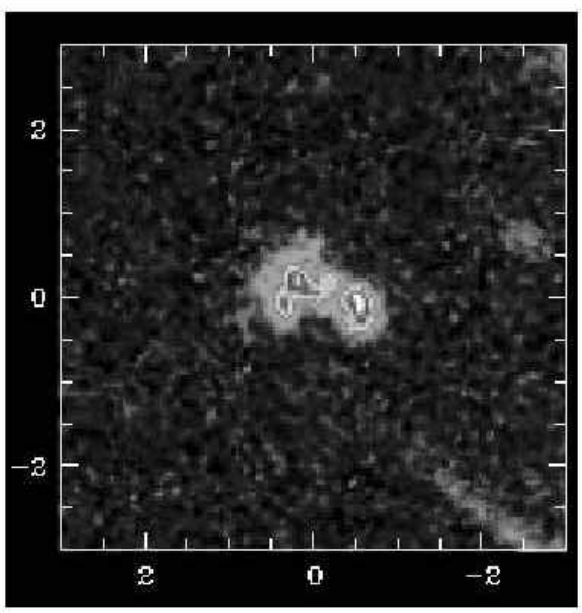

Fig. 5. WFPC2 HDFS flanking field F814W image of 338.287-60.555. Scale is in arcsec..

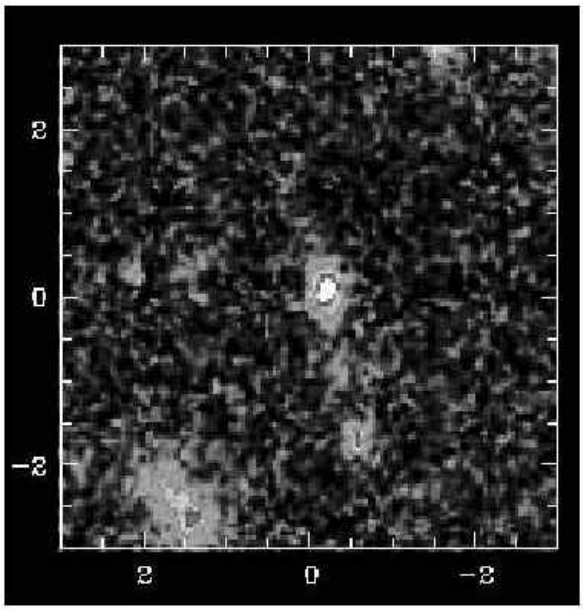

Fig. 6. WFPC2 HDFS flanking field F814W image of 338.288-60.577. Scale is in arcsec..

Figure 5.10 – Morphology in rest frame ultraviolet waveband of two z = 2 Hα emitting objects (Moorwood et al. 2000)

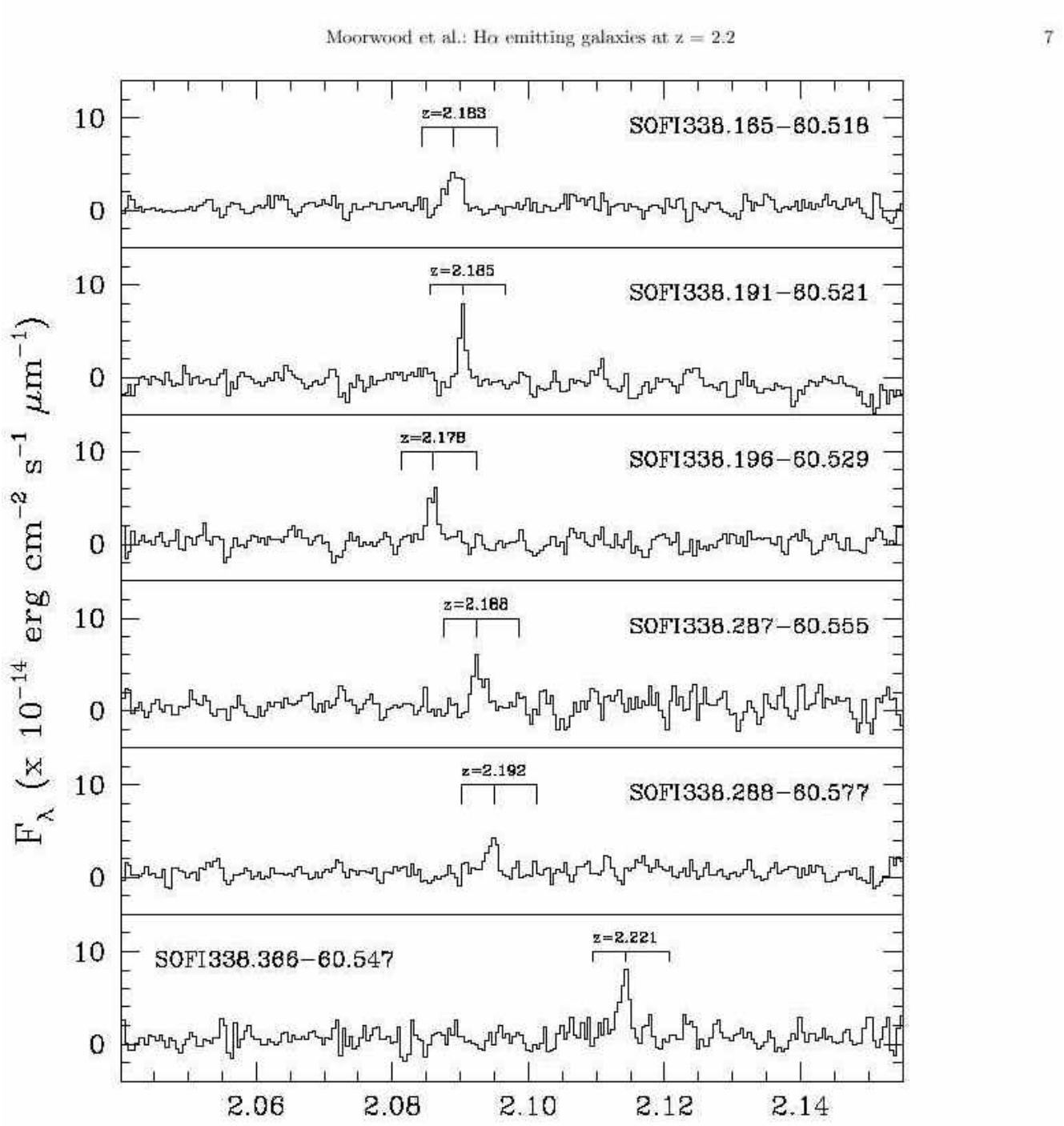

Fig. 7. ISAAC spectra of Hα emitting galaxies. The tick marks under the redshift labels show the expected positions of the [NII](6548,6584Å) lines assuming the detected line is Hα.

Figure 5.11 – VLT/ISAAC spectra for 6 Hα emitting galaxies at z = 2 (Moorwood et al. 2000)

5.5 Galaxy Formation in Clusters -- H. Yee (U. Toronto)

Abstract

We will use the excellent imaging and spectroscopic capabilities of MCAO to study the formation of bulges and disks in cluster environments over the redshift range z = 0.6 to 1.4. In many models, this is the redshift range where clusters are assembled, as galaxies fall into the cluster potential for the first time. Multi-color imaging will reveal the spatially resolved star formation histories of cluster galaxies on 250 pc scales. Hα spectroscopy (R = 3000) will allow us to measure the spatially resolved rotation curves, masses, and star formation rates within galaxies as a function of cluster radius.

5.5.1 Background Science

The formation of galaxy clusters signifies a turning point in the evolution of the universe where local mass overcomes the dispersing effect of cosmic expansion. The epoch when clusters form depends on the standard key cosmological parameters. Clusters also provide exquisite laboratories for studying many aspect of galactic evolution within a well-defined environment.

Within galaxy clusters, it is well established that a strong correlation exists between galaxy type and local density, with high-density regions being dominated by earlier type galaxies. The average star formation rate increases for galaxies on the periphery of dense environments. A natural explanation for these correlations is that ram pressure from hot intra-cluster gas helps trigger star formation in gas-rich galaxies and strips gas from the tenuous outer regions of spiral disks (Fujita & Nagashima 1999ApJ...516..619). However, the extent to which the cluster galaxies evolution differs from field galaxies at similar redshift is not yet established.

We propose a program to understand the formation of clusters by observing their growth over the redshift range z = 0.6 - 1.4. How does the distribution of galaxy types within clusters change from 8 Gyr to 5 Gyr ago? How does the average cluster richness change over this cosmic timescale? How does the distribution of galaxy masses vary both as a function of redshift and radial distance within the cluster? How do the mean bulges and disks within clusters compare to field galaxies at similar redshift? We believe MCAO is capable to provide robust answers to several of this questions.

5.5.2 Proposed observations : requirements and other constraints

Imaging surveys are now detecting large numbers of high redshift clusters out to z = 1.4. In the next few years, catalogs of hundreds of photometrically selected, and spectroscopically confirmed cluster members will be available from which we will be able to select target fields. Of the estimated 200 high redshift clusters that will be cataloged, about 50 will have nearby guide stars suitable for MCAO. Targets will be selected by previous slitlet (non IFU) spectroscopy (FLAMINGOS or GMOS) to have emission lines in a region of the spectral bandpass free from night sky lines.

We will image 10 clusters at redshifts 0.6-1.4 in the K band (rest frame 1.1 μm) and J band (rest frame 6000 A) at 0.05" resolution (250 pc) to measure morphological parameters and colors. Using the 80" MCAO imaging field, a 2 x 2 mosaic will be performed to cover the typical cluster dimensions near z = 1; 160" corresponds to 1 Mpc. The mosaiced 2 x 2 fields will cover 160", comparable to the HST/ ACS field of 202". An example of a target MCAO cluster is shown in the image below.

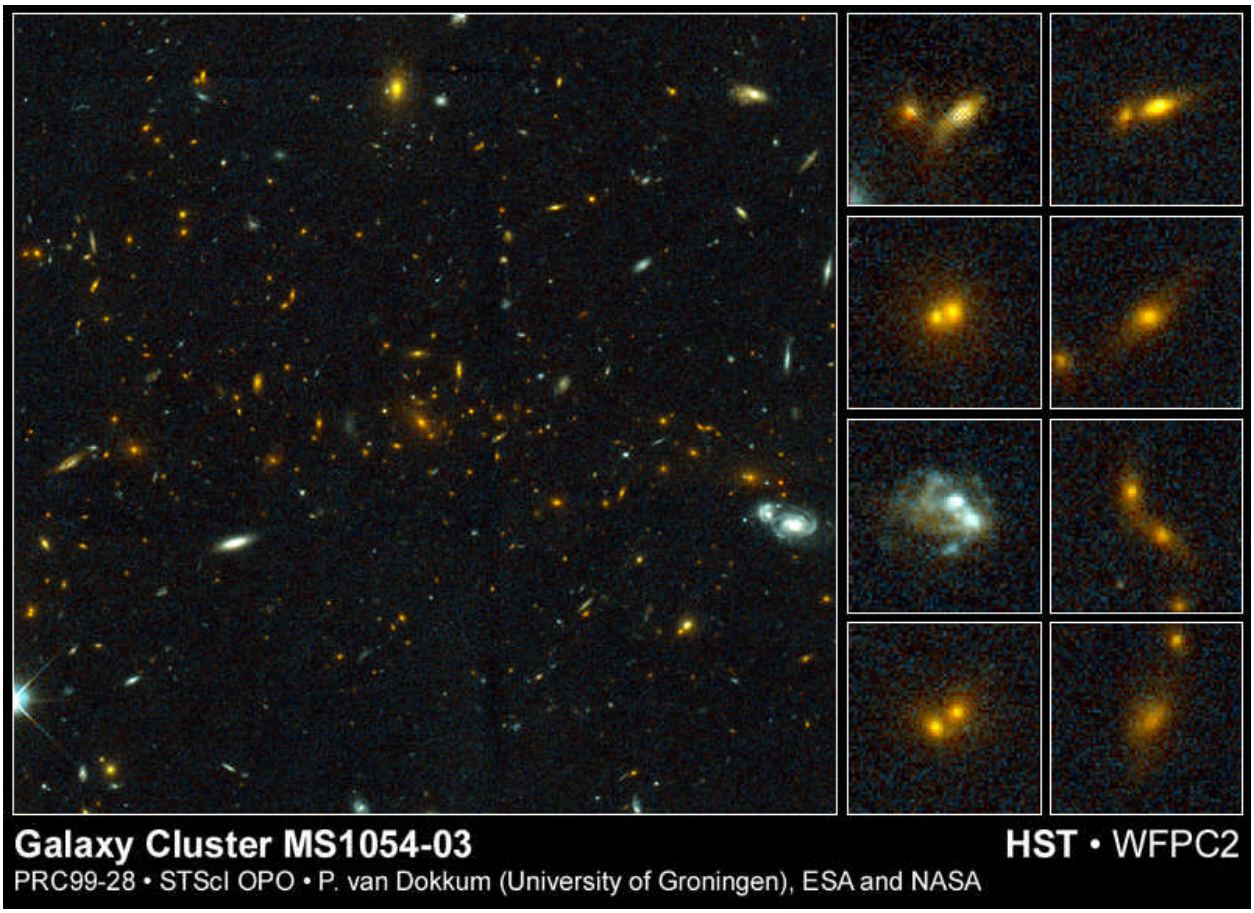

Figure 5.12 - Example of a MCAO target cluster at z = 0.8

We will combine these data with HST/ACS V-band and I-band (rest-frame 3000 - 4000A) images which have comparable field of view and pixel scale (0.05") to measure the full spectral energy distributions (SEDs), from the rest-frame ultraviolet through near infrared. These SEDs will be used to make a pixel-by-pixel star formation history of each galaxy on a 250 pc scales. From this 4-color imaging, we will proceed to do disk-bulge de-convolutions to reconstruct the formation histories of bulges and disks as a function of radius within the cluster.

In the second phase of the program, we will obtain R = 3000 integral field spectroscopy of the Hα line for late-type cluster galaxies. Over our selected redshift range, Hα appears in the J band window. These data will be used to derive galaxy masses from spatially resolved rotation curves. We will also study the star formation rates within galaxies, and as a function of cluster radius to determine whether (and how) ram pressure from the intracluster medium is responsible for triggering star formation as galaxies fall into the cluster potential for the first time.

The basic imager with 80" field of view is acceptable, although we will require a 2 x 2 mosaic to cover a field comparable to the HST/ACS measurements at bluer wavelengths. The MCAO pixel size of 0.05" compares well with the ACS 0.05" pixels. The 0.05" pixels are sufficient to isolate the largest star forming regions at z = 1, where 0.05" corresponds to 250 pc.

For spectroscopy, an aperture size of 0.1" (0.5 kpc) will be large enough to obtain good S/N while allowing at least 10 spatial resolution elements across a typical 5 kpc galaxy disk. An IFU with 1.5"-2" diameter (10 kpc) will be sufficient to cover the line-emitting SF regions of most galaxies out to the radii where rotation curves plateau.

The spectral resolutions of R = 3000-5000 are optimal in order to minimize the deleterious effects of OH sky lines, while permitting good velocity resolution (<80 km/s). While higher resolving powers may be useful for further reducing the impact of night sky lines and improving the S/N of intrinsically narrow lined galaxies, the S/N per resolution element will degrade if the lines are over-resolved.

For imaging, we require integration times of 2 hours to reach a 3 sigma surface brightness sensitivity of XX mag/arcsec^2 in the K band. In the continuum we require exposures of 2 hrs each in J and K to reach XX mag below L* (where L* is M_K = -22? for H_0 = 70).

A star-forming galaxy with a SFR of 0.4 M_{sun}/yr/kpc^2 will be detectable in Hα with a S/N of 10 per spectral and spatial resolution element in 4 hr. This is the minimum S/N needed to measure rotation curves and galaxy masses.

In the 80" MCAO imaging field of view, we will image 50-100 objects per cluster down to 0.XX L*. A typical cluster will contain 10-20 late types galaxies with emission lines per MCAO field of view; this is estimate is robust and is based on imaging of intermediate z clusters and observed morphological fractions which indicate ~35% of late type objects.

At least one guide star will be available per MCAO field for 50 of the target clusters. A smaller number, perhaps 15, will have 3 guide stars for the full 2 x 2 mosaic.

5.5.3 MCAO vs CAO for this program

MCAO makes this program possible by providing high resolution imaging in the *rest frame* I-band and near IR for z = 0.6 - 1.4 galaxies. The pixel scales and field sizes are comparable to images that HST/ACS will provide in the rest frame ultraviolet/blue. MCAO is required because 250 pc linear scales are needed to resolve internal structure of galaxies like giant star forming regions and to perform accurate disk-bulge de-convolutions. The 80" MCAO field is well matched to the cluster angular sizes at z ~ 1. *MCAO enables the measurement of up to 32 rotation curves simultaneously!* The pixel scale and sensitivity MCAO will be superior to the upgraded HST/ACS, especially in the K-band which is most crucial for measuring the morphology and luminosity of bulges and the old stellar populations.

For studying the populations within clusters, dozens of object need to be observed per cluster at a range of cluster radii. This can only be done by increasing the field size to a size comparable to the clusters themselves, i.e. 2'. MCAO will enable the study of 8 times the number of objects

compared to conventional AO (30") field. Although this program could be done with conventional AO (e.g. NIFS), MCAO represents an impressive multiplexing gain of 8 for imaging, and as much as a factor of 32 for spectroscopy using the movable IFUs. In addition, the stable PSF will result in a dramatic increase of the accuracy of the measurements of galaxy sizes, etc.

5.6 Gravitational Lensing Studies of High Redshift Galaxies -- Mike Edmunds (Cardiff) and Ray Sharples (U. Durham)

Abstract

Using the MCAO system for imaging and spectroscopy, we are able to exploit the amplification due to gravitaional lensing by intermediate redshift clusters to bring the study of the properties of high redshift galaxies within the grasp of Gemini. We examine three specific cases in detail: (i) spatially resolved element abundance studies; (ii) resolved kinematics to study gas flows and galaxy masses; (iii) spatially resolved studies of the rate and morphology of star formation.

5.6.1 Background Science

Gravitational lensing by clusters of galaxies has opened up a powerful new approach to the study of galaxies in the high redshift universe. Because the probability distribution for gravitational lensing by cluster-size masses peaks for clusters at intermediate (z = 0.5 - 1.0) redshifts, there is a natural scale for strong lensing (~0.25 Mpc) which is well matched to the MCAO field of view. The majority of lensed background galaxies will also lie at redshifts z ~ 1 to 2, which is where independent evidence (Madau et al. 1996MNRAS.283.1388) suggests that much of the assembly of large galaxies is occurring.

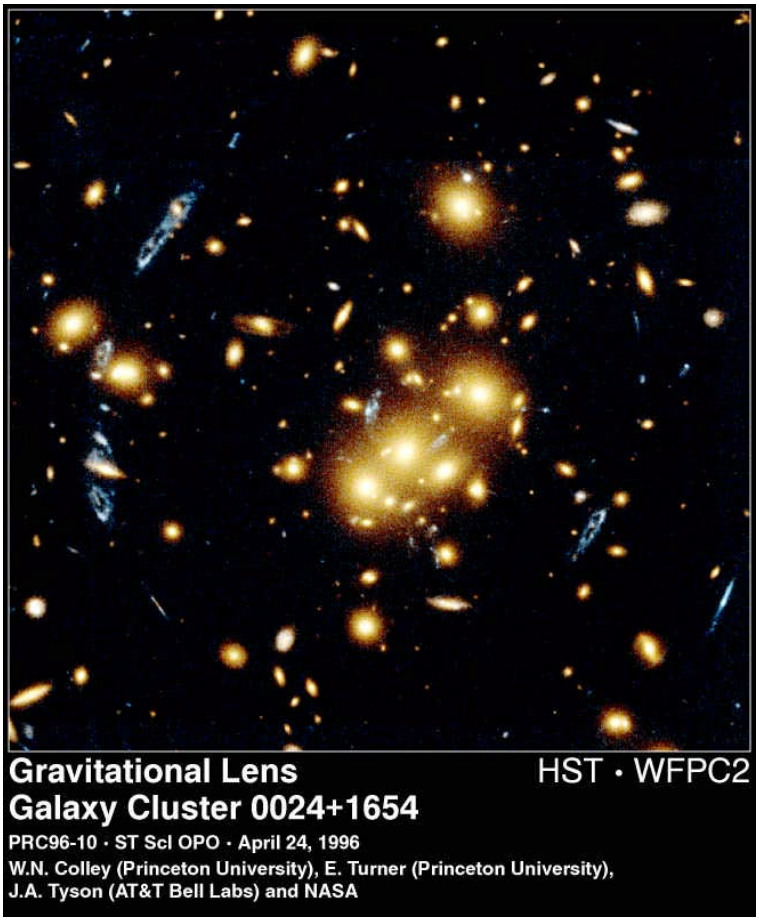

Figure 5.13: Example of multiple images of a background ring galaxy lensed by the cluster gravitational field.

The goals of our study are to examine the chemical properties of galaxies in formation and constrain the importance of early strong inflows and outflows on their global structural and chemical properties. Using resolved spectroscopic studies we can link these to information on

their mass distribution, morphology and star formation rate.

By limiting our study to clusters with well-constrained lens models, we will maximise our ability to reconstruct galaxy images on the source plane and hence obtain gas phase chemical abundances and kinematics as a function of position within the galaxy. Using GIRMOS IFUs with MCAO (0.1 arcsec/pixel) on a galaxy with an amplification by a factor of 10, will allow us to probe scale lengths of 100 pc in galaxies at redshifts z ~ 2. ***This is the only foreseeable way of probing chemistry and kinematics on such scales until the advent of diffraction-limited 30-50 m telescopes.*** The spatial resolution achieved by MCAO+lensing clusters is also well-matched to the sizes of the giant-HII emission-line regions expected from studies of local galaxies.

5.6.2 Proposed observations: requirements and other constraints

The cluster sample will be selected using ground-based surveys to select clusters with well-constrained lens models and suitable giant gravitational arcs. We assume that initial redshift estimates for giant arcs will be obtained using GMOS spectroscopy to identify the redshifted [O II] 3727 ($z < 2$) and MgII ($2.0 < z < 2.5$) lines. This will allow selection of the appropriate GIRMOS band in which to measure the redshifted [OII]3727, Hβ, [OIII]5007 lines and the Hα/N[II] diagnostic emission line ratio for metallicity estimates.

On average, we only expect one or two strongly lensed systems in each cluster, but these will usually be multiply-imaged with 3-5 images per source. *The uniform corrected field of MCAO will be crucial in maintaining uniform sampling of each image in a single exposure and in allowing simultaneous spectroscopy of all available arcs.* This makes possible the study of a statistically significant sample of reconstructed background galaxies in a reasonable time.

We expect that the active star formation regions will contain outflows, the characterization of which are an essential ingredient into physical models of galaxy formation (Edmunds….).

Line	$\lambda_0(\mu m)$	J	H	K
Hα/[NII]	0.6563	0.5-1.1	1.3-1.8	2.0-2.7
[OIII]5007	0.5007	1.0-1.8	2.0-2.7	3.0-3.9
Hβ	0.4861	1.1-1.9	2.1-2.8	3.1-4.0
[OII]3727	0.3727	1.7-2.8	3.0-3.9	4.4-5.5

Table 5.1: Redshift ranges in which the common UV/optical emission lines are observable in the J, H and K windows.

We require a minimum field of view of 1 arcmin in order to view simultaneously the multiply-imaged sources.

The key AO parameter for these observations is the ability to obtain two-dimensional spatially resolved spectra at high angular resolution. Giant HII regions in nearby galaxies can reach up to sizes of 300 pc. At z ~ 2, with no lensing amplification, this corresponds to angular scales of 0.03 arcsec or less and Hα/Hβ fluxes ~ $2x10^{-18}$ ergs/cm^2/sec. With current instrumentation these lines would only be visible in exceptionally violent star formation events, rather than the more quiescent HII regions which probably characterize the evolution of normal spiral galaxies at most epochs. By concentrating on strongly amplified sources, *and* using adaptive optics, we can obtain the spatially resolved information critical to understanding the evolution of normal galaxies.

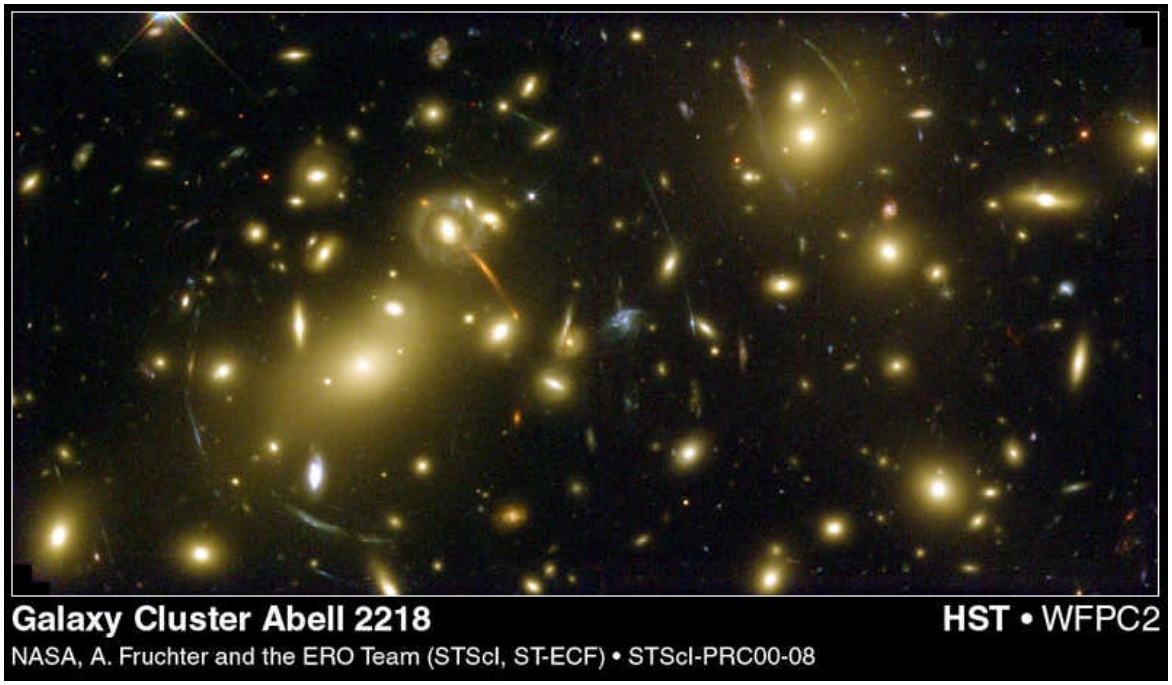

Figure 5.14: Another cluster with highly lensed background galaxies which will be a prime target for MCAO multi-object spectroscopy.

The expected outflow velocities and rotational velocity fields are ~ few hundred km/sec and will be easily detectable and mapped. Assuming one can measure a velocity from an emission line to 1/10 of the spectra resolution (if S/N > 10), this argues that the spectral resolution R~3000 required for OH rejection is adequate for this science case.

In order to obtain spectra for lensed galaxies with a range of potential redshifts, it is desirable, but not essential, to be able to select on an IFU by IFU basis whether one observes in the J, H or K bands. For each object, observations in at least the J+H bands or H+K bands are required to cover the appropriate diagnostic lines (Table 5.1). It would obviously be desirable to have the capability to obtain this wavelength coverage simultaneously.

In many cases, the arcs will be extended over scales > 3 arcsec. In this case the ability to close pack the IFUs to cover the full spatial (curved) extent of the arcs will be important.

Based on observations and theoretical models of giant HII regions in nearby galaxies, we would expect an Hβ flux of ~10^{-17} ergs/cm^2/s, assuming a lens magnification by a factor of 10. This is almost certainly an underestimate, because the generally higher star formation rates observed at high redshifts could easily increase the observed flux by a factor ~10. The limiting sensitivities are defined by the requirement to be able observe other diagnostic lines (e.g. [OIII] and [NII]) to strengths ~1/10 of the intensity of Hβ.

Kneib et al. 1996 and Franx et al. 1997 (astro-ph/9704090) find a surface density of ~10 strong arcs per cluster, each of which may require more than one IFU. Any unused IFUs could be deployed on star-forming cluster galaxies which, although not lensed, suffer from less $(1+z)^4$ cosmological dimming.

Detailed S/N calculations are being performed, but we expect that exposure times of the order of 4-8 hours per field will be needed. Assuming the above line strengths we estimate that a S/N of 5 can be obtained on the faintest diagnostic lines (1/10 Hβ) in exposure times of ~2hrs in the J, H or K bands. The S/N for kinematics and star formation rate diagnostics (e.g. Hα, Hβ) will be ~10x greater.

We anticipate that in the next few years sufficient numbers of massive intermediate redshift clusters will be obtained from photometric surveys (e.g. VISTA, X-ray selection –XMM, and Sunyaev-Zeldovich signatures) that the availability of MCAO guide stars will not be a problem in finding a sample of ~15-20 suitable clusters.

5.6.3 MCAO vs CAO for this program

Apart from a few exceptionally favorable cases, it will generally not be possible to obtain spatially resolved spectroscopy of all the multiple arc systems in a given cluster with classical AO. Even in the most favorable cases, the multiple integrations would require an extensive observing program.

In order to optimally reconstruct the kinematics and chemical gradients in the source plane, it is necessary to spectroscopically sample most/all of the arcs. In this sense this program is enabled by MCAO.

None of the instruments currently foreseen for NGST would be well suited to carrying out this program. Because of the achromatic nature of gravitational lensing, these sources will be an obvious target for ALMA observations, which will provide complementary information of the interstellar medium and dust properties of these galaxies.

Other images of the lensed galaxy at z = 4.92 are marked (A and D). The reconstructions of the images A-C are displayed at the bottom at a highly expanded scale. These images may be compared with the lens geometry and lens models. The bright know is unresolved in the wide-field reconstruction of C and is only marginally resolved in the reconstructed PC image shown on the right. The inset at the top right displays at enhanced contrast a second galaxy, G2, that was found serendipitously 37'' west of the arc (Franx et al. 1997).

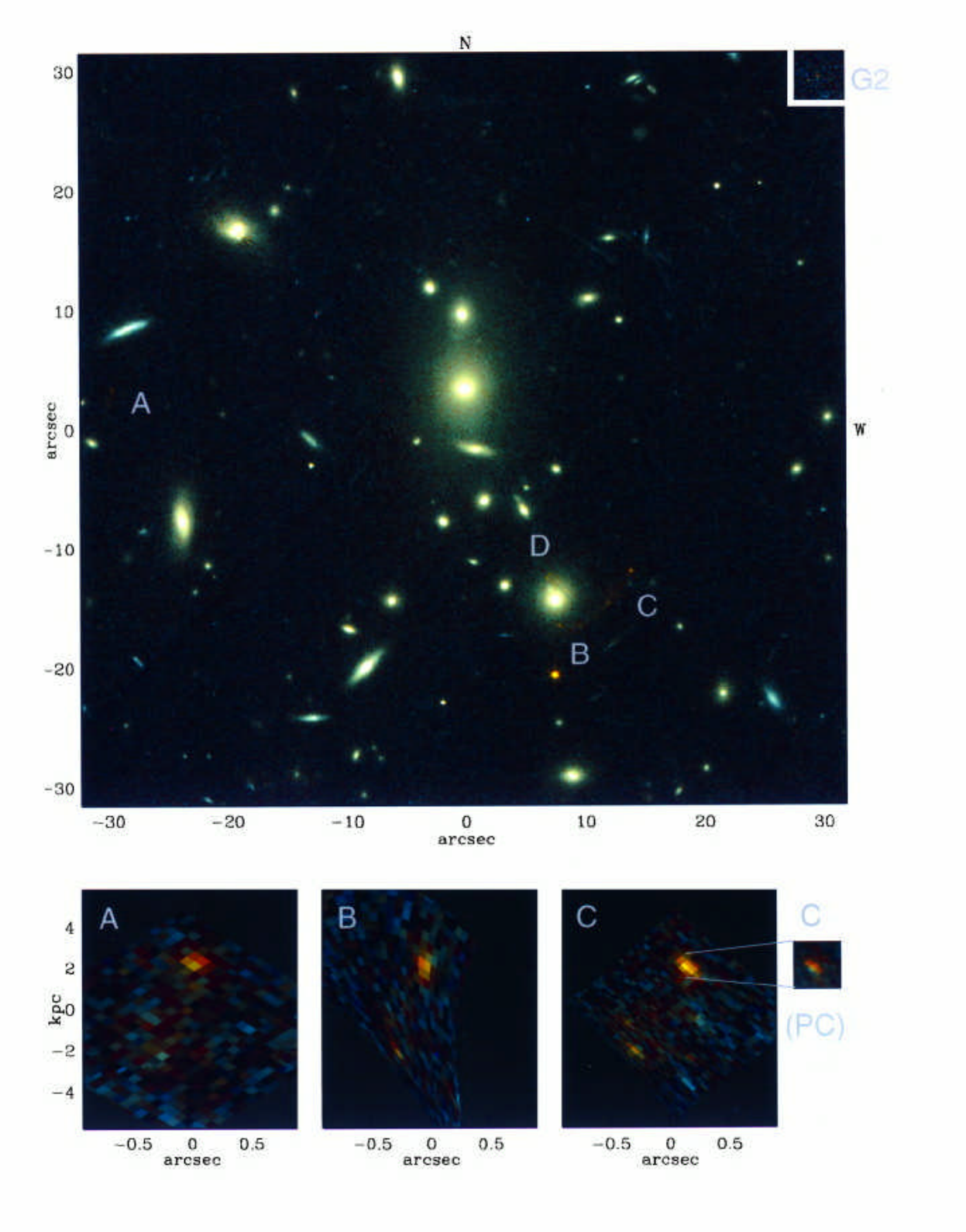

Figure 5.15 – HST images of the center of the cluster CL 1358+62 at z = 0.33. The cluster was imaged in the F606W and F814W passbands. The red arc is conspicuous and is marked B and C.

5.7 Some generic considerations on multi-object spectroscopy with MCAO: The case of GIRMOS -- Ray Sharples (Durham)

There is no doubt that AO fed spectrographs will deliver exciting astrophysical results as we have seen from several science cases presented in this document. However, the multiplexing advantage is not always clear, or when it is, one frequently faces sets of objects in a given field with a range of brightness, with the fainter tail becoming rapidly photon starved at sampling of 1/10 arcsec and spectral resolution of a few 1000s. We wish to address these limitations and consider them in the perspective of the GIRMOS concept presented at the MCAO Science Case Workshop.

5.7.1 A perspective on feasibility and limitations

The value of the science case for any multi-object spectrograph can be gained by examining the consequences of the three fundamental angular scales defining the spectrograph specification. These are the *patrol field* of the pickoffs, the *field of view* of a single IFU and the *pixel sampling* scale. The first of these defines a typical scale length over which targets must be clustered in order to use the multiplex advantage effectively. The second defines the typical size of an object of interest. The third defines the scale over which variations of physical properties within an object can be resolved. Table 5.2 shows how these scales map onto different physical scales for a range of classes of possible targets at increasing distances (we assume a standard cosmology with h=0.75, Ω_m=0.3, Ω_Λ=0.7). In the intermediate and high-redshift universe (z > 0.5 or look back time >5 Gyr), a multi-IFU spectrograph will enable the study of the internal structure of objects with the typical sizes of present day galaxies (20 kpc), which are clustered on scales ~1 Mpc, at a spatial resolution of 0.5 - 1kpc, i.e. the size of giant HII regions.

Class	**Distance**	**Patrol Field**	**IFU FoV**	**Pixel Samp.**
Star formation region (Orion)	500 pc	0.2 pc	1500 AU	50 AU
Galactic centre	8 kpc	5 pc	0.1 pc	800 AU
Starburst galaxy (NGC 4458)	10 Mpc	6 kpc	150 pc	5 pc
Galaxy cluster (Abell 2218)	z=0.2	0.25 Mpc	6 kpc	0.2 kpc
Hubble Deep Field spirals	z=0.5	0.7 Mpc	18 kpc	0.6 kpc
Lyman-dropout galaxies	z=3	0.9 Mpc	25 kpc	0.8 kpc

Table 5.2: Physical scale sizes which correspond to the baseline GIRMOS *parameters for the re-imaged focal plane (2' diameter), IFU field of view (3"x3") and IFU sampling (0".1 x 0".1).*

The core science programs which will fully exploit the capabilities of a multi-IFU spectrograph are those which (i) require the uniform AO-corrected PSF delivered by MCAO, (ii) are best undertaken using spectroscopy in the z, J, H and K near-infrared windows, (iii) and can make effective use of the available multiplex advantage (32 science pickoff apertures). Other potential targets include those requiring integrated measurements (e.g. total Hα flux) at intermediate spectral resolution, even though these do not fully exploit the AO capability. Likewise, it may be necessary to combine targets from different programs in some cases where the surface density for a particular program is insufficient to utilize the full multiplex advantage.

The primary scientific drivers for AO spectroscopy are not the S/N gains: in principle, this ensues from being able to use smaller entrance apertures to reduce the signal background when working close to the diffraction limit. Unfortunately, the use of an AO system in front of an astronomical spectrograph introduces its own difficulties in the form of transmission/scattering losses, due to the extra optical surfaces and correcting mirrors, and the unavoidable (without the use of cryogenically cooled AO systems) additional system emissivity. Diffraction losses at entrance slits with sizes approaching λ/D_{tel} are another potential loss of throughput, although these can be largely ameliorated by appropriate oversizing of spectrograph optics.

Any potential S/N gains from using small apertures are further reduced if the astrophysical targets of interest are not point sources. Although HST has shown that the physical scale size of faint galaxies does decrease beyond z~1 (the angular diameter-distance relation for a *fixed* physical scale length is essentially flat for z = 1-5 in most cosmological models), the measured angular sizes are not insignificant compared to the diffraction limit of an 8-metre telescope at infrared wavelengths (Gardner & Satyapal 2000).

Effective exploitation of the MCAO corrected images for spectroscopy will therefore primarily be devoted to targets which are extended and/or show complex structure on scales comparable with the IFU field of view. Although the direct S/N gains for compact sources are seen to be marginal (and within the uncertainties of the assumptions underlying these simulations), one clear advantage of AO spectroscopy is that is possible to achieve higher spectral resolutions for a given beam size by the use of very small entrance slits (c.f Gee et al. 1998) . This advantage is used in the *GIRMOS* concept to achieve the intermediate resolutions (R > 3000) required for effective software OH suppression with relatively compact spectrographs (beam size of 35-50mm), which can then be multiplexed into a single cryostat.

5.8 Surface density of targets and the redshift windowing

An important criterion in defining the specification for any multi-object spectrograph is the surface density of accessible targets. As discussed in the *GIRMOS* Development Studies report, the arrangement of the 32 pickoffs in four layers gives excellent geometrical access to the field. For a random distribution of objects, each layer of 8 pickoffs vignettes roughly 10% of the available field and all 4 layers vignette approximately 75% of the field. The mean surface density required to use all 32 arms of the proposed *GIRMOS* is therefore 32/0.75 per MCAO field or 15 objects per square arcminute. Table 5.3 gives some representative surface densities of possible *GIRMOS* targets; these figures apply to any type of multi-object spectrograph, IFU or slitlet based.

Object Class	Surface density (per ')	Reference
All galaxies (K<20)	10	Broadhurst et al (1992)
HDF Irregulars (z=0.5-1)	5-6	Fernandez-Soto et al (1996)
Lyman-break gals (R<25)	3	Lowenthal et al (1997)
Gravitational arcs in A2218	10	Kneib et al (1996)
SSCs (B<23) in NGC725	10	Schweizer & Seitzer (1998)
Orion stars (M>0.1M_{Sun})	2	?
T-Tauri stars	0.1	?

Table 5.3: Estimates surface densities of an example set of GIRMOS *target objects*

As well as considering surface densities of field galaxies, one must also consider the range of accessible redshifts for which spectral features will lie in the selected wavelength range. Fig.5.16 shows estimates of the surface density of emission-line galaxies from Bunker (1999) and indicates that the surface density of bright ($L > L^*$) star-forming galaxies with Hα falling in the K-band window (z = 2.0 - 2.7) is approximately 2 per square armin!

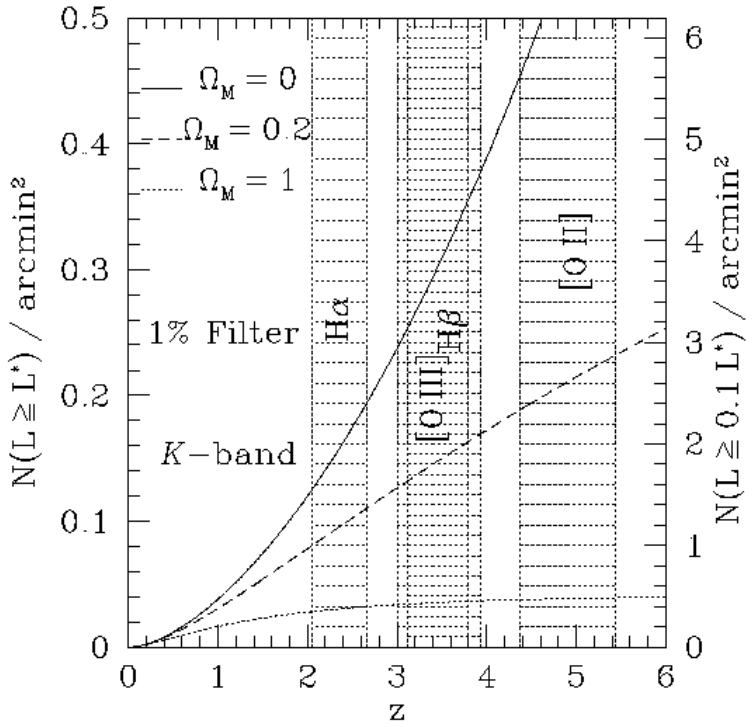

Figure 5.16: Predictions (dashed line) for number densities of field galaxies normalized to a 1% band pass filter. The effective band pass for GIRMOS *observations is approximately 20% at R=3000 and 5% at R=10000 (from Bunker 1999).*

5.9 A study case: star-formation in high-z galaxies

As repeated several times throughout this document, one of the lasting legacies of the Hubble Space Telescope (HST) is the realization that the universe displays a remarkable variety of complex structures on scales of less than one arcsec which are inaccessible to conventional (non-AO) ground-based imaging and spectroscopy. Some of the most dramatic examples of this are in the superlative images of galaxy morphologies as exemplified by deep extragalactic surveys such as the Hubble Deep Field (Williams et al 1996). HST imaging has shown that the Hubble sequence of galaxies, with its grand design spirals and large spheroidal systems, was probably put in place at redshifts around z = 1 - 2. In addition, however, HST has demonstrated that there exists a strongly evolving population of very blue galaxies at lower redshifts, many of which have peculiar morphologies and are actively forming stars (Fig. 5.17). Understanding the star formation history of these galaxies, and the reason for their decline over the past few Gyr, is an important goal of modern cosmology. Because of their complex morphologies, resolved spectroscopy (Figure 5.18) is essential to make any meaningful comparison with broad-band optical and infrared imaging. At redshifts z > 1, the most useful optical diagnostic lines (e.g. Hβ, O[III], Hα) are shifted into the infrared spectral region (Table 5.4).

Line	$\lambda_0(\mu m)$	J	H	K
Hα	0.6563	0.5-1.1	1.3-1.8	2.0-2.7
[OIII]5007	0.5007	1.0-1.8	2.0-2.7	3.0-3.9
Hβ	0.4861	1.1-1.9	2.1-2.8	3.1-4.0
[OII]3727	0.3727	1.7-2.8	3.0-3.9	4.4-5.5
Lyα	0.1215	7.2-10	11-14	15-19

Table 5.4: Redshift ranges in which the common UV/optical emission lines are observable in the J, H and K windows.

As a feasibility test of observing a sample of such galaxies with *GIRMOS*, we have resampled the original HDF F814W image (i.e. rest-frame B-band) into a 30 x 30 grid of 0'.1 pixels and estimated a global Hα flux based on the Kennicutt (1983) relation assuming star formation rates of 5, 10 and 20 M_{sun}/yr. We have then assumed that the Hα flux is distributed in the same way as the B-band light and used the emission-line S/N estimates from the GIRMOS OCDD to estimate the S/N in the line for each pixel. Since the enclosed energy curves for the drizzled HDF images (based on the measured PSF) are close to those predicted for MCAO, we have not included any explicit convolution with the AO PSF.

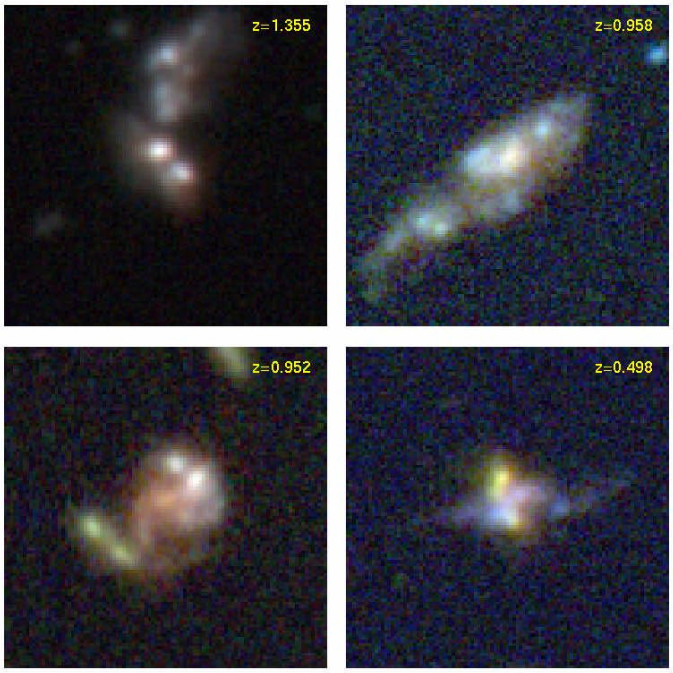

Figure 5.17: Irregular star forming galaxies in the Hubble Deep field. The box size in each case is 4"x 4". Understanding the star formation histories and kinematics of galaxies with these complex morphologies is well-matched to multiple IFU spectroscopy with a field of view of 3"x 3" and pixel sampling of 0".1 x 0".1.

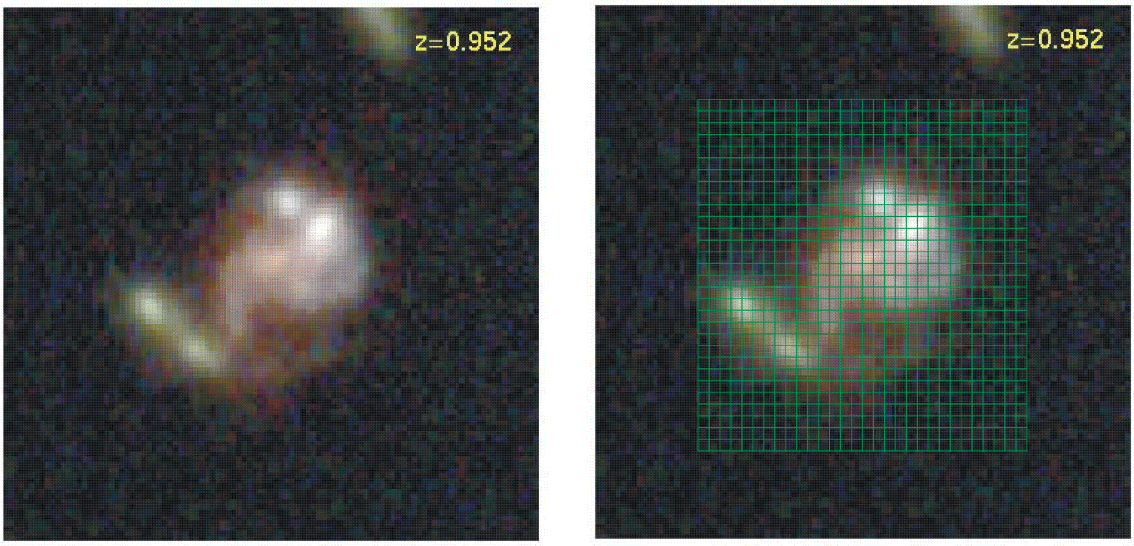

Figure 5.18: The irregular star-forming galaxy HDF3-222.1 (Williams et al 1996). This galaxy has a spectroscopic redshift of z = 0.952, for which Hα is shifted into the J-band at l=1.275 μm and I_{KC}=22.2. The right-hand figure shows a default GIRMOS *IFU (30 x 30 pixels @ 0".1 sampling) overlaid.*

Figure 5.19 shows that, provided the effective global star-formation rate measured by Hα is >10 M_{sun}/year for galaxies at this redshift, then there are a significant number of IFU pixels with

S/N>10 in a 3600 sec exposure. Note that these simulations do not explicitly include the underlying continuum, and exposures of 2-4 hours are probably more realistic for this kind of observation. With a S/N of >10 per IFU element it will be possible to study the variations in star formation rate (to 10% accuracy) and measure the kinematics (to ~30 km/sec) of the gas in different "hot" spots.

To estimate the surface density of such targets, we use the HDF photometric redshifts and morphological type catalogue of Fernandez-Soto et al (1998) who find 29 galaxies classed as 'irregulars' with $21 < I < 24$ and $0.5 < z_{photo} < 1.1$ (to get Hα in the J-band) or a surface density of 5.5 per square arcmin (~15 per *GIRMOS* field). Increasing the range of acceptible redshifts (to include z = 1.5-1.8 (where Hα lies in the H-band) would increase the surface density of targets to 6.3 per square arcmin (~20 per *GIRMOS* field).

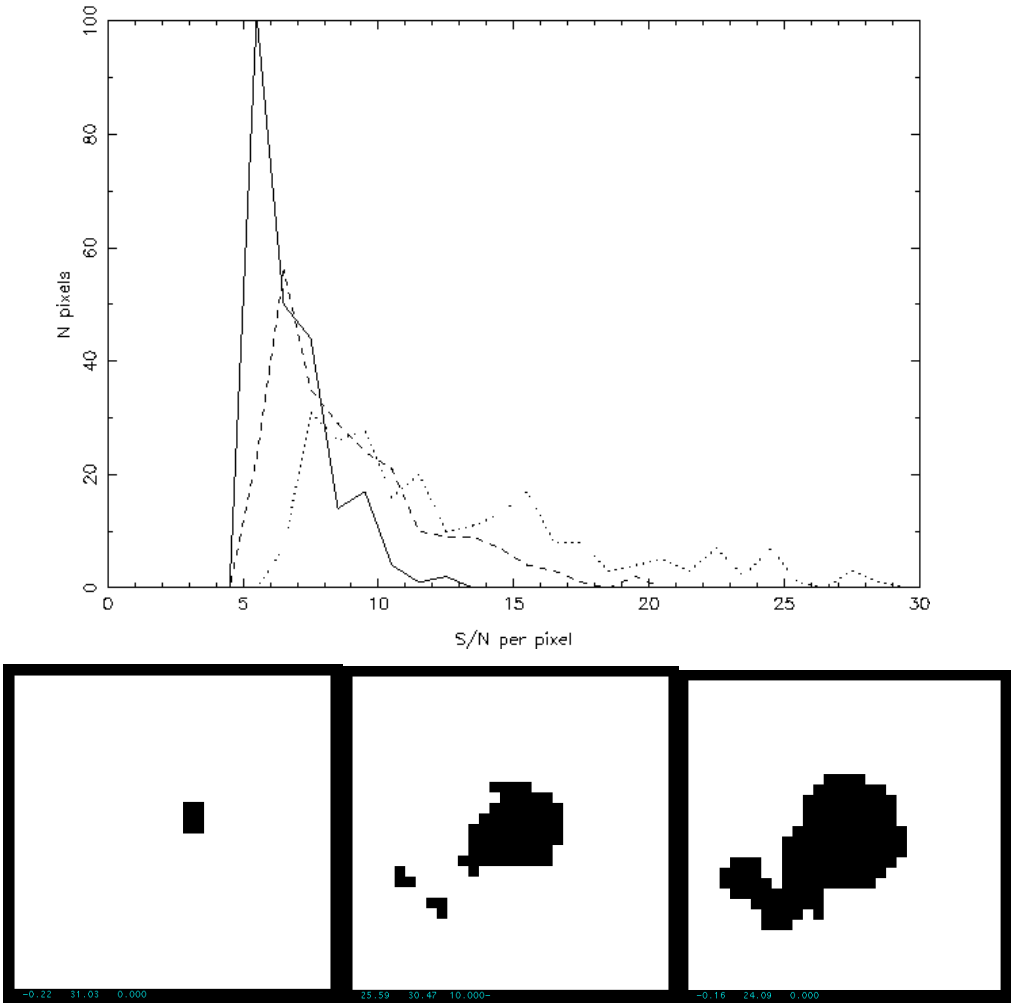

Figure 5.19: Spatial maps of the distribution of IFU pixels with S/N>10 in a simulated 3600 sec exposure of Ha emission from the HDF3-221.1, assuming global star formation rates of 5, 10 and 20 M_{Sun}/year respectively. The histogram shows the number of pixels in each image versus the estimated S/N in the line (solid line 5 M_{Sun}/year, dashed 10 M_{Sun}/year, dotted 20 M_{Sun}/year).

5.10 Program Summary

Table 5.5 gives an overview of the observing program parameters, in term of target density, exposure time and guide star availability.

Table 5.5: Distant galaxies observing program parameters

Subject	***Spectro***	***Imaging***	***Target density***	***Exposure time***	***Guide star***
Field galaxy imaging		I	Few arcmin^{-2} down to K=20	1 hr (J,H,K)	Suitable or lower b latitudes
Chemical evolution	S	I	Few per arcmin^{-2}	3-4 hrs (J,H,K)	Suitable or lower b latitudes
Cluster galaxy formation	S	I	>50 per fov	2hrs (J,K)	~15 clusters with 3 guide stars
Lensing of distant galaxies	S		~10 per fov	4-8 hours	15-20 clusters with 3 guide stars
Masses of galaxies	S		3-9 per fov	>10 hours	Fields chosen with suitable stars

Table 5.6 summarizes the gain of MCAo vs CAO for the distant galaxy programs, and the scientific complementarity of MCAO with other major future facilities.

Table 5.6: Distant galaxies. Gain of MCAO compared to CAO.

	CAO	***MCAO***	***Uniform PSF***	***Gain in resolution***	***Gain in sensitivity***	***ALMA***	***NGST***	***ACS***
Field galaxies	No	Yes	Yes	✓				✓
Chemical evolution	Yes	10 x	Helps	✓	✓			✓
Cluster: galaxy formation	No	8 x	Helps	✓	✓			
Lensing: distant galaxies	No	Yes	Yes	✓		✓	✓	
Masses of galaxies	In part	10 x	Yes	✓	✓	✓	✓	

5.11 Instrument requirements

While developing the above distant galaxies science cases, we considered the requirements they placed on future Gemini MCAO instrumentation. For the field galaxy imaging case, and also the imaging within the cluster and lensing cases, the strawman imager described in the introduction was considered adequate, although as always with imagers, a bigger field would be better. The situation for a spectrograph was more complex. The table below tries to summarize which science cases drive which spectrograph requirement. Due to the time available at the workshop and also the range of opinions of those present, these conclusions are somewhat subjective. That said, the proposals and the table below seem to indicate that a very strong scientific case could be made for an infrared multi-object type spectrograph with 10-15 deployable IFUs patrolling a 2 arcmin diameter MCAO corrected FOV. This case would be made even stronger if the NGST instrument complement either does not include IFU capability or only includes a rather limited single IFU.

	Field Galaxies				
	Imaging	**Metallicity**	**Kinematics**	**Clusters**	**Lensed galaxies**
IFUs Priority	na	High	High	High	V High
Slits Priority	na	Medium	Low	Medium	Low/Medium
How many IFUs[a]	na	5-10	10-30	10-20	5-15
Spatial fields of an IFU	na	1-3”	1-3”	3”	5-10”
Spatial sampling of an IFU	na	0.1”	0.1”	0.1”	0.1”
Spectral resolution	na	3000	3-5000	3-5000	3000
Different bands in different IFUs Priority	na	High	Medium	Low	High
Simultaneous J+H or H+K Priority	na	High	Low	High	High
Pushing to sub-micron Priority	na	High	Medium	Medium	Medium

[a] Estimated assuming a 2 arcmin diameter circular patrol field

References:

Benson, A. J., Cole, S., Frenk, C. S., Baugh, C. M., & Lacey, C. G., 2000, MNRAS, 311, 793

Butcher, H. & Oemler, A. 1984, ApJ, 285, 426

Dressler, A. 1980, ApJS, 42, 565

Ferguson, H. C., Dickinson, M., & Williams, R. 2000, ARA&A, 38, 667

Franx, M., Illingworth, G. D., Kelson, D. D., van Dokkum, P. G., & Tran, K.-V. 1997, ApJ, 486L, 75

Fujita, Y., & Nagashima, M. 1999, ApJ, 516, 619

Guzman, R., Gallego, J., Koo, D. C., Phillips, A. C., Lowenthal, J. D., Faber, S. M., Illingworth, G. D., & Vogt, N. P. 1997, ApJ, 489, 559

Kennicutt, R. C., 1983, ApJ, 472, 54

Kneib, J.-P., Ellis, R. S., Smail, I., Couch, W. J., & Sharples, R. M., 1996, ApJ, 471, 643

Madau, P., Ferguson, H. C., Dickinson, M., Giavalisco, M., Steidel, C. C., & Fruchter, A. 1996, MNRAS, 283, 1388

Moorwood, A. F. M., van der Werf, P. P., Cuby, J.-G., & Oliva, E., 2000, A&A, 362, 9

Pettini, M., Kellogg, M., Steidel, C. C., Dickinson, M., Adelberger, K. L., & Giavalisco, M. 1998, ApJ, 508, 539

Skillman, E. D., Kennicutt, R. C., Shields, G. A., & Zaritsky, D. 1996, ApJ, 462, 147